AD_____

Award Number: W81XWH-05-1-0110

TITLE: Prostate Expression Databases: Gene Expression Resources for Comparative Studies of Prostate Carcinogenesis

PRINCIPAL INVESTIGATOR: Peter S. Nelson, M.D.

CONTRACTING ORGANIZATION: Fred Hutchinson Cancer Research Center
Seattle, Washington 98109-1024

REPORT DATE: January 2008

TYPE OF REPORT: Final

PREPARED FOR: U.S. Army Medical Research and Materiel Command
Fort Detrick, Maryland 21702-5012

REPORT DOCUMENTATION PAGE

Form Approved
OMB No. 0704-0188

1. REPORT DATE	2. REPORT TYPE	3. DATES COVERED
05-01-2008	Final	6 DEC 2004 - 5 DEC 2007

4. TITLE AND SUBTITLE
Prostate Expression Databases: Gene Expression Resources for Comparative Studies of Prostate Carcinogenesis

5a. CONTRACT NUMBER

5b. GRANT NUMBER
W81XWH-05-1-0110

5c. PROGRAM ELEMENT NUMBER

6. AUTHOR(S)
Peter S. Nelson, M.D.

Email: pnelson@fhcrc.org

5d. PROJECT NUMBER

5e. TASK NUMBER

5f. WORK UNIT NUMBER

7. PERFORMING ORGANIZATION NAME(S) AND ADDRESS(ES)

Fred Hutchinson Cancer Research Center
Seattle, Washington 98109-1024

8. PERFORMING ORGANIZATION REPORT NUMBER

9. SPONSORING / MONITORING AGENCY NAME(S) AND ADDRESS(ES)
U.S. Army Medical Research and Materiel Command
Fort Detrick, Maryland 21702-5012

10. SPONSOR/MONITOR'S ACRONYM(S)

11. SPONSOR/MONITOR'S REPORT NUMBER(S)

12. DISTRIBUTION / AVAILABILITY STATEMENT
Approved for Public Release; Distribution Unlimited

13. SUPPLEMENTARY NOTES

14. ABSTRACT

This proposal aims to test the hypothesis that integrating observations derived from mouse model systems with observations from human prostate cancers will define relevant and consistent molecular alterations critical to the development and progression of prostate carcinoma. The research accomplished to date has: 1) assembled the requisite mouse models to enable the generation of tumor gene expression data; 2) produced a second-generation mouse prostate microarray that will allow for deeper profiling of mouse prostate gene expression; 3) identified a specific gene (osteopontin) commonly associated with multiple mouse prostate cancer models; 4) developed the methods/techniques that will enable precise dissection of mouse prostate epithelium; 5) expanded the Prostate Expression Database to archive microarray data; 6) determined strain-specific gene expression differences in the mouse prostate that could contribute to phenotypic differences on prostate cancer development and progression; and 7) identified developmental pathways altered in the Pten-/- prostate cancer model that could contribute to the process of carcinogenesis.

15. SUBJECT TERMS

Database, mouse model, gene expression, microarray, transcript, proteomics

16. SECURITY CLASSIFICATION OF:			17. LIMITATION OF ABSTRACT	18. NUMBER OF PAGES	19a. NAME OF RESPONSIBLE PERSON
a. REPORT	b. ABSTRACT	c. THIS PAGE			19b. TELEPHONE NUMBER *(include area code)*
U	U	U	UU	61	USAMRMC

Table of Contents

INTRODUCTION

This overall aim of this proposal was to test the hypothesis that *integrating observations derived from mouse model systems with observations from human prostate cancers will define relevant and consistent molecular alterations critical to the development and progression of prostate carcinoma*. Ultimately, the longer term objective of the studies are to identify those mouse models most accurately reflecting *in vivo* human prostate cancer, and prioritize those genes in human prostate cancer that are most relevant for therapeutic intervention.

The aims of the proposal remained unchanged for the duration of the project period. They were: (1) To determine transcript expression profiles of neoplastic lesions from mouse models of prostate carcinoma. (2) To stratify mouse models of prostate carcinoma through comparative analyses with clinical human prostate carcinomas. (3) To extend the utility of the Prostate Expression Database to facilitate comparative studies of mouse and human prostate carcinoma. (4) Write final report. (Note the *original Aim 2* involving proteomic studies was deleted due to recommendations by the reviewers).

Disease relevance: Model systems represent critical resources supporting essentially all facets of research involving prostate cancer including studies focused on disease etiology, disease progression, diagnostics, dietary factors, immune modulation, imaging, and pharmacologic intervention. Mouse models offer opportunities for testing hypotheses that would be difficult or impossible to evaluate in humans. Similarly, databases of sequence, gene expression, and disease model information also greatly facilitate scientific work in an extremely cost- and time-effective manner. There is a crucial need to develop interactive resources that generate, compile, and distribute relevant data correlating mouse prostate cancer models directly with phenotypes and genotypes of human prostate carcinoma so as to interpret experimental findings in the appropriate context, determine disease relevance, and prioritize model systems for appropriate pre-clinical studies. This proposal aims to address these needs.

BODY

The following summarizes the technical objectives for the proposal and the work accomplished during the 36-month interval between project initiation (12/06/04) and this report (12/31/07).

Technical objective 1: To determine transcript expression profiles of neoplastic lesions from mouse models of prostate carcinogenesis (Months 1-24).

Objective 1a. Microdissect specific epithelial populations of cells at discrete stages of prostate carcinogenesis: PIN, invasive carcinoma, metastasis.

Task 1: Breed and microdissect PIN models (months 1-12). We have obtained and bred mouse prostate cancer models of the following genotypes: Nkx3.1-/-, and acquired prostates with PIN lesions from the PB-RXR-/- mouse. The FGF8 mouse is no longer available (Dr. Roy-Burman, personal communication). Thus we used the expression profile from the Akt-/- mouse developed by Dr. William Sellers as an alternative. We have acquired gene expression data from prostates of these mice which develop PIN (these mice do not develop invasive cancer). We have now microdissected PIN lesions from the Nkx3.1-/- prostates. Objective completed.

Task 2: Breed and microdissect PIN and progression models (months 12-24. We have acquired, bred, and harvested prostates at the PIN and invasive cancer stages from the PB-PTEN-/- and TRAMP models. Microdissection of these lesions is complete as well as comparable wild-type controls. We extended the studies to include an AR mutant mouse model developed by our colleague Norm Greenberg and a compound mutant model involving TRAMP and a targeted deletion of the TMPRSS2 serine protease. Metastatic tumors from these animals were also dissected. Objective completed.

Objective 1b. Measure transcript levels in specific epithelial populations of cells at discrete stages of prostate carcinogenesis: PIN, invasive carcinoma, metastasis.

*Task 3: Construct microarrays (months 1-6).*We have constructed a 3rd generation mouse prostate microarray that now comprises ~44,000 oligonucleotides/genes. This array has been quality checked for reproducibility. Experiments using microdissected cancerous mouse prostate epithelium demonstrated high quality hybridization results. Objective completed.

Task 4: Amplify RNA from microdissected mouse prostate tissue (months 6-24). We have microdissected normal and neoplastic mouse prostate epithelium from the PB-PTEN, AR TRAMP, and TRAMP/TMPRSS2 models, amplified the RNA, verified the quality of the aRNA using the Agilent bioanalyzer. Objective completed.

Task 5: Hybridize mouse prostate cDNA probes to microarrays (months 6-24). We have hybridized amplified RNA from cancerous and benign mouse prostate epithelium in a comparative manner. The analysis of the PTEN-/- and TRAMP experiments identified ~600 genes differentially expressed between benign and neoplastic cells, with both lobe-specific and tumor-type specific differences. We have also compared the TRAMP vs TRAMP/TMPRSS2 tumors, Analyses of these data show striking differences that associate with the original initiating lesion at the PIN stage, with a general convergence to a more uniform dedifferentiated state later in the disease course. We have verified alterations in the expression of 10 genes by qRT-PCR. A manuscript detailing these results is in preparation for submission (Mecham *et al*; in preparation).

We have finalized a study evaluating strain-specific differences on mouse prostate gene expression that may identify host differences accounting for different cancer penetrance rates. The manuscript was published *Genome Biology* (Bianchi-Frias et al 2007 *Genome Biology*). We have also identified pathways of normal mouse prostate development that are re-activated in the setting of neoplasia and determined that several genes involved in normal prostate development exhibit altered expression in human prostate cancer and correlate with clinical outcomes. A study detailing these findings has been submitted for publication (Pritchard et al). The mechanistic analysis of one gene we found to be altered in multiple prostate cancer models, osteopontin, was published in with our collaborator Dr. Pradip Roy-Burman (Ani C et al 2006 *Cancer Research*). Objective completed with additional studies ongoing.

Objective 1c. Identify expression alterations that are common to specific stages of neoplastic growth.

Task 6: Format and QC microarray data (months 18-24). Data acquired. QC complete. Very good quality and reproducibility across biological and technical replicates. Objective completed.

Task 7: Statistical analyses of microarray data (months 18-24). Data acquired and analysed. Objective Completed.

Technical objective 2: Stratify mouse models of prostate carcinoma through comparative analyses with clinical human prostate carcinomas (months 18-34).

Objective 2a *Determine transcript alterations that statistically-associate with specific models of mouse prostate neoplasia (e.g. $NKX^{-/-}$ vs $Pten^{-/-}$)*

Task 8: Analyze mouse model transcript profiles using SAM and ANOVA to identify gene expression changes associating with specific genotypes and histology (months 18-30). The data has been acquired for the Nkx, Pten, and TRAMP models at all stages. The statistical analyses have identified >600 transcript alterations. Eight genes have been evaluated by other methods and confirmed. Objective completed. Additional studies with other models are in progress.

Objective 2b Categorize human prostate tumors into classes based upon expression profile similarities to mouse models (e.g. Pten$^{\downarrow}$-like vs Myc$^{\uparrow}$-like);

Task 9: Acquire human prostate cancer microarray profiles (in-house and from data repositories on the www), and format for analyses (months 30-32). We have acquired human microarray datasets from 4 published studies: LaPointe et al, Singh et al, Stephenson et al and Yu et al. In the course of generating these data, we analyzed gene expression in different human prostate cancer grades. A manuscript detailing these results was published (True *et al* PNAS 2007). Objective completed.

Task 10. Normalize mouse prostate cancer model expression microarray data with human normal prostate and cancer expression arrays (months 30-33). The datasets have been normalized and orthologs across array platforms and species have been mapped. Objective complete.

Task 11: Compare mouse prostate cancer expression microarray data with human normal prostate and cancer expression arrays using the methods of Golub *et al* for class predictors (months 30-34). Objective completed.

Task 12: Create a list of alterations in prostate carcinoma that can be used to stratify prostate cancers in a clinical setting (months 32-35). Objective completed.

Objective 2c *Categorize human prostate tumors into classes based upon the expression levels of specific gene(s)* (e.g. over expression of *Myc*);

Task 13: Repeat tasks 11-12 using specific gene expression levels as discriminators (months 30-34). Objective completed. A manuscript detailing these results is in preparation (Mecham *et al In Preparation*).

.

Technical objective 3: To extend the utility of the Prostate Expression Database (PEDB) for comparative gene expression studies of mouse and human prostate carcinoma. (months 10-34)

Objective 3a. Construct an interactive repository for microarray information that integrates multi-dimensional data (tissue type, quantitative and temporal gene expression measurements) for independent analyses.

Task 14: Determine a server configuration for a microarray database server (month 10). We have selected a server configuration using the opensource Bioconductor platform written in the 'R' language. We have completed populating the database with microarray data generated from the mouse model experiments described above. Objective completed.

Task 15: Install and update server configuration for security and accessibility (month 10). Objective Completed.

Task 16: Reconfigure the PEDB website to use PHP for faster data access and improved interactivity. (months 10-18). Objective Completed.

Task 17: Evaluate "Minimum Information about a Microarray Experiment" (MIAME) compliant database/management systems: (months 12-18). Objective Complete. All submitted mouse microarray data is now MIAME compliant.

Task 18: Implement database structure changes to make database suitable for microarray raw data, ratio data, proteomics, and image storage. (months 12-18). The database structure now houses microarray datasets. Objective completed.

Task 19: Organize and enter microarray data into chosen database and create file structure system for easy retrieval, analysis and visualization. (month 16-22). Objective completed.

Task 20: Identify mouse and human orthologs using the homologene database to determine matched pairs of genes. (months 14-22). Merge files for mouse microarray data and 2 different human array platforms: spotted cDNA and Affymetrix, have been completed that link orthologous genes. Objective completed.

Task 21: Create a Graphical User Interface for viewing and navigating between microarray overview, graphs, clustering programs, and sequence information. (months 18-26). Objective completed.

Task 22: Write scripts to automate the input of new microarrays, including a web-based entry system, and creation of new graphs on a monthly basis. (months 20-28). Note, this database system has largely been overtaken by the advent of large public database housing microarray and attendant metadata (e.g. GEO). Thus, though functional, this component of our database is redundant and no longer particularly useful. Objective completed.

Objective 4: Final Report: Complete data analyses, compile accomplishments and reportable outcomes and write final project report (Months 35-36). Objective completed.

KEY RESEARCH ACCOMPLISHMENTS

- Completed the construction and q/c of a second generation mouse prostate specific microarray that nearly doubles the gene expression representation relative to version 1.
- Completed the construction and q/c of third generation mouse prostate microarray that builds on commercially available technology (Agilent) and encompasses unique mouse prostate sequences.
- Acquired the mouse prostate cancer models with specific genetic alterations leading to PIN or invasive cancer (Nkx3.1, RXRalpha, PTEN-/-, TRAMP, AR mutation, TRAMP/TMPRSS2) and gene expression data from the mouse prostate Akt model.
- Completed the wet-lab experiments evaluating strain-specific differences in mouse prostate gene expression that could influence the development and/or progression of genetically-engineered prostate cancer.
- Completed microdissection, amplification, and microarray analysis of benign epithelium, PIN and invasive carcinoma from the anterior and ventral lobes of the PTEN-/-, TRAMP, AR mutant, TRAMP/TMPRSS2 mouse prostate cancer model systems. This analysis has identified several developmental pathways that appear to be re-activated in prostate adenocarcinoma (e.g. Wnt and Notch pathways) and determined profiles that associate with the specific initiating events in the course of cancer progression.
- Generated a molecular correlate to the human Gleason grades of prostate cancer.
- Identified congruent and discordant features between mouse models of prostate cancer with differing initiating lesions, and determined concordant and discordant features across species to human prostate cancers.

REPORTABLE OUTCOMES

Khodavirdi AC, Song S, Yang S, Wu H, Pritchard C, Nelson PS, and Roy-Burman P. (2006) Increased Expression of Osteopontin Contributes to the Progression of Prostate Cancer. *Cancer Res*. 66(2):883-8.

Chen Q, Watson JT, Marengo SR, Decker KS, Coleman I, Nelson PS, Sikes RA (2006) Gene expression in the LNCaP human prostate cancer progression model: Progression associated expression in vitro corresponds to expression changes associated with prostate cancer progression in vivo. *Cancer Lett.*

True L, Coleman I, Gifford D, Hawley, S, Huang A, Gifford D, Coleman R, Beer T, Gelmann E, Datta M, Mostaghel E, Knudsen B, Lange P, Vessella R, Lin D, Hood L, and Nelson PS. (2006) A Molecular Correlate to the Gleason Grading System for Prostate Cancer. *Proc Natl Acad Sci USA*, 103(29):10991-6.

Bianchi-Frias D, Pritchard C, Mecham BH, Coleman IM, Nelson PS. (2007) Genetic background influences murine prostate gene expression: implications for cancer phenotypes. *Genome Biology*. 8(6):R117.

He Y, Franco OE, Jiang M, Williams K, Love HD, Coleman IM, Nelson PS, Hayward SW. (2007) Tissue-Specific Consequences of Cyclin D1 Overexpression in Prostate Cancer Progression.*Cancer Res*.67(17):8188-8197.

Pritchard C, Bhattacharjee M, Hawley S, Dumpit R, Sikes R, and Nelson PS. Transcriptional Programs Reflecting Androgen-Induced Development of the Prostate Gland: Dysregulated Expression of Candidate Andromedins in Prostate Neoplasia (*submitted*).

Pritchard C, Mecham B, Dumpit R, Coleman I, Bhattacharjee M, and Nelson PS. Conserved Programs of Gene Expression Across Prostate Development and Tumorigenesis (*submitted*).

Mecham B, Heinlein C, Coleman R, Risk M, and Nelson PS. Gene expression correlates of mouse prostate carcinogenesis: alternative pathways corresponding to initiating events. (*In Preparation*)

CONCLUSIONS

The research accomplished in the context of this proposal incude: 1) assembly of the requisite mouse models to enable the generation of tumor gene expression data; 2) production of second and third-generation mouse prostate microarrays that allow for deep profiling of mouse prostate gene expression across development, cancer, and therapy; 3) identification of a specific gene (osteopontin) commonly associated with multiple mouse prostate cancer models; 4) developmnet of the methods/techniques that have enabled precise dissection of mouse prostate epithelium; 5) expansion of the Prostate Expression Database to archive microarray data; 6) determination of strain-specific gene expression differences in the mouse prostate that could contribute to phenotypic differences on prostate cancer development and progression; 7) identification of developmental pathways altered in the Pten-/- and TRAMP prostate cancer models that could contribute to the process of carcinogenesis with extrapoloation/verification of relevance in human disease; 8) Identification of specific alterations corresponding to different tumor initiating events (e.g. Pten vs p53) which may have the potential to stratify human prostate cancers according to genetic lesions; 9) identification of alterations in the tumor microenvironment that contribute to cancer progression; 10) generation of a molecular correlate to human prostate cancer grades that can be used to identify specific genes contributing to aggressive phenotypes.

REFERENCES

None

APPENDICES

Reprints of the following published manuscripts are provided as an appendix.

Khodavirdi AC, Song S, Yang S, Wu H, Pritchard C, Nelson PS, and Roy-Burman P. (2006) Increased Expression of Osteopontin Contributes to the Progression of Prostate Cancer. *Cancer Res*. 66(2):883-8.

Chen Q, Watson JT, Marengo SR, Decker KS, Coleman I, Nelson PS, Sikes RA (2006) Gene expression in the LNCaP human prostate cancer progression model: Progression associated expression in vitro corresponds to expression changes associated with prostate cancer progression in vivo. *Cancer Lett.*

True L, Coleman I, Gifford D, Hawley, S, Huang A, Gifford D, Coleman R, Beer T, Gelmann E, Datta M, Mostaghel E, Knudsen B, Lange P, Vessella R, Lin D, Hood L, and Nelson PS. (2006) A Molecular Correlate to the Gleason Grading System for Prostate Cancer. *Proc Natl Acad Sci USA*, 103(29):10991-6.

Bianchi-Frias D, Pritchard C, Mecham BH, Coleman IM, Nelson PS. (2007) Genetic background influences murine prostate gene expression: implications for cancer phenotypes. *Genome Biology*. 8(6):R117.

He Y, Franco OE, Jiang M, Williams K, Love HD, Coleman IM, Nelson PS, Hayward SW. (2007) Tissue-Specific Consequences of Cyclin D1 Overexpression in Prostate Cancer Progression.*Cancer Res*.67(17):8188-8197.

Increased Expression of Osteopontin Contributes to the Progression of Prostate Cancer

Ani C. Khodavirdi,[1] Zhigang Song,[1] Shangxin Yang,[2] Chen Zhong,[1] Shunyou Wang,[3] Hong Wu,[3] Colin Pritchard,[4] Peter S. Nelson,[4] and Pradip Roy-Burman[1,2]

Departments of [1]Pathology and [2]Biochemistry and Molecular Biology, Keck School of Medicine, University of Southern California; [3]Department of Molecular and Medical Pharmacology, University of California Los Angeles, Los Angeles, California; and [4]Division of Human Biology, Fred Hutchinson Cancer Research Center, Seattle, Washington

Abstract

Osteopontin is a secreted glycosylated phosphoprotein known to be involved in numerous physiologic functions and associated with the late stages of various cancers. We used preneoplastic and neoplastic mouse models of prostate cancer to determine the onset of elevated expression of osteopontin in the development of this disease. Osteopontin alterations occurred early in the disease with dysregulated expression observed in lesions of low-grade prostatic intraepithelial neoplasia (PIN). Over time, osteopontin expressing dysplastic cells seemed to increase in number in high-grade PIN and increased further in adenocarcinoma, and in metastasis, almost all of the cancer cells immunohistochemically stained positive for osteopontin overexpression. We examined the biological properties of human prostate cancer cell lines LNCaP and PC-3, in which osteopontin overexpression was achieved via lentiviral gene transduction. Evidence was obtained that osteopontin could contribute to a proliferative advantage in both cell types, although more significantly in LNCaP than PC-3. Osteopontin also influenced their *in vitro* invasive ability, and again, most strikingly in the weakly oncogenic LNCaP. Furthermore, excess osteopontin induced the LNCaP cells to acquire a strong intravasation potential *in vivo* in the chicken embryo chorioallantoic membrane assay for blood vessel penetration. These results establish a correlation between an increased gradient of osteopontin expression throughout the stages of murine prostate cancer, beginning from the preneoplastic lesions to distant metastases that suggests a proliferative and invasive advantages to those prostate tumor cells overexpressing osteopontin. Together, these findings support a strategy designed to target osteopontin in the context of prostate cancer therapy. (Cancer Res 2006; 66(2): 883-8)

Introduction

Osteopontin, an arginine-glycine-aspartic acid (RGD) containing glycosylated phosphoprotein that interacts with integrins and CD44 as major receptors, is a secreted protein comprising about 2% of the noncollageneous proteins of the bone (1, 2). It is described to be present in all body fluids and in the proteinaceous matrix of mineralized tissues and has multifunctional properties in cell migration, cell survival, inhibition of calcification, and cell-mediated immunity (3). In tumorigenesis, osteopontin has been implicated in tumor invasion and metastasis in prostate, colon, breast, lung, and other cancers (4–7). The finding of a strong correlation between pathologic stage and osteopontin across multiple tumor types suggests a role for osteopontin in tumor progression (6–8). In bone, this secreted adhesive protein is believed to be involved in osteoblast differentiation and bone formation and in the anchorage of osteoclasts to bone, leading to bone resorption (3, 9, 10).

Although several studies have implicated osteopontin in prostate cancer progression and metastases, the functional significance of osteopontin expression by the prostate tumor cells is only scarcely elucidated. Chemotaxis and chemoinvasion analyses with PC-3 prostate cancer cells indicated a dose-dependent increase in PC-3 cell movement induced by osteopontin, whereas cell invasion was strictly dependent on $\alpha_v\beta_3$ integrin function (11). Osteopontin is also reported to enhance cell proliferation induced by the epidermal growth factor (EGF) in prostate cancer cells (12). In this report, we describe our studies of osteopontin expression in genetically engineered mouse models for prostatic disease, which included models displaying slow, temporal development of increasingly severe preneoplastic prostatic lesions (13, 14), and a model that progresses to primary invasive adenocarcinoma of the prostate with subsequent manifestation of metastases with defined kinetics (15, 16). We present evidence that osteopontin expression, detected in preneoplastic lesions, continues to increase in adenocarcinoma, and cancer cells exhibiting high osteopontin expression seem to be enriched in the metastatic deposits. We found that all human prostate cancer cell lines tested express osteopontin. Functional studies with manipulated overexpression of osteopontin in two prostate cancer cell lines (LNCaP and PC-3) reveal that osteopontin could lead to increased proliferation, invasion, and most remarkably, to the enhanced ability to intravasate blood vessels.

Materials and Methods

Tissue collection and RNA extraction. Five mice from each of three age groups (2.5, 12, and 18 months) of the preneoplastic *ARR2PB-Fgf8b* transgenic mouse line (14) were selected for dissection and isolation of dorsolateral and ventral prostatic lobes. Similarly, ventral and lateral prostatic tissues were dissected and pooled from five 24-month-old preneoplastic model with conditional deletion of retinoid X receptor α (*RXRα*) alleles ($cRXR\alpha^{-/-}$) in the prostate (13). Littermates lacking the *Fgf8b* transgene or the *Cre* gene in the context of floxed alleles of *RXRα* served as donors of the corresponding control tissues. The source of primary prostatic adenocarcinoma was the conditional *Pten* homozygous deletion ($cPten^{-/-}$) mice (15). The whole prostates of two individual

Note: Supplementary data for this article are available at Cancer Research Online (http://cancerres.aacrjournals.org/).

A.C. Khodavirdi, Z. Song, and S. Yang contributed equally to this work.

Requests for reprints: Pradip Roy-Burman, Department of Pathology, Keck School of Medicine, University of Southern California, 2011 Zonal Avenue, Los Angeles, CA 90033. Phone: 323-442-1184; Fax: 323-442-3049; E-mail: royburma@usc.edu.

doi:10.1158/0008-5472.CAN-05-2816

experimental and age-matched control animals were used without differentiating the prostatic lobes for the comparative RNA analysis of the adenocarcinoma. RNA from *Fgf8b* and *cRXRα*$^{-/-}$ tissues were extracted using the Qiagen RNeasy Mini kit following the manufacturer's protocol, which included an on-column DNase I treatment for the removal of contaminating DNA (Qiagen, Valencia, CA). RNA from the *cPten*$^{-/-}$ tissues was extracted using TRIzol (Life Technologies, Rockville, MD).

Microarray analysis. Comparison of gene expression profiles of the preneoplastic or neoplastic mouse prostate tissues with littermate controls was carried out as previously described (15). Each experiment was done in duplicate with reversal of the fluorescent label to account for dye effects.

Reverse transcription and semiquantitative PCR for osteopontin. RNA samples from prostate tissues and prostate cancer cell lines were reverse transcribed using ThermoScript Reverse Transcription-PCR (RT-PCR) System following manufacturer's protocol (Life Technologies, Buffalo, NY) as described (14). The primer sequences (forward and reverse), annealing temperature, and product size were as follows: for mouse osteopontin, TGAAAGTGACTGATTCTGGCA and GGACGATTGGAGT-GAAAGTGT, 52°C, 375 bp; for human osteopontin, CATCTCAGAAGCA-GAATCTCCTA and GGAAAGTTCCTGACTATCAATCA, 56°C, 617 bp. To determine the linear amplification range for each primer set, 1 μL of cDNA was amplified for 40 cycles for mouse osteopontin, 35 cycles for human osteopontin, and 30 cycles for β-actin. Samples were removed every three cycles, and the optimum cycle number was determined as the approximate midpoint of the linear range of amplification. The semiquantitative PCR assays were carried out using the corresponding optimum cycle number.

Western blot analysis. The dorsolateral, ventral, and anterior prostatic lobes of *Fgf8b* or *cPten*$^{-/-}$ mice and age-matched controls were isolated and snap frozen. The tissues were ground in liquid nitrogen with previously autoclaved mortars and pestles. The pulverized tissues were dissolved in ice-cold buffer containing 10 mmol/L Tris-HCl (pH 7.4), 1 mmol/L EDTA, 1 mmol/L EGTA, 150 mmol/L NaCl, 0.5% NP40, and 1% Triton X-100. To prepare the cell culture conditioned medium, 80% to 90% confluent cells cultured in T-75 flask were washed with PBS, and 10-mL serum-free medium was added. After 24 hours, medium was collected into a 15-mL tube, centrifuged to remove the cell debris, and then concentrated by centrifuge at 7,000 rpm at 4°C for 30 minutes using a 20-mL Centrifugal Spin Concentrator (APOLLO, Continental Lab Products, San Diego, CA). Total tissue lysates or conditioned media were quantitated and fractionated by SDS-PAGE on a 10% gel and subjected to immunoblot analysis using a rabbit anti-mouse osteopontin antibody (Assay Designs, Ann Arbor, MI) in 5% bovine serum albumin. Detection for the *Fgf8b* set was achieved as described (17), whereas osteopontin expression in the *cPten*$^{-/-}$ set was detected with a fluorescein-conjugated secondary antibody and the Odyssey Infrared Imaging System (LI-COR Biotechnology, Lincoln, NE). To normalize sample loading, β-actin (Santa Cruz Biotechnology, Inc., Santa Cruz, CA) blot was done.

Immunohistochemistry. Prostate tissues were isolated and fixed in 10% buffered formalin. Following deparaffinization, the 5-μm tissue sections were rehydrated and subjected to antigen retrieval by microwaving in 0.01 mol/L sodium citrate (pH 6). Antigen unmasking was done 10 minutes for the osteopontin antibody, and 30 minutes for the androgen receptor antibody (PG-21; Upstate, Lake Placid, NY). Primary antibodies were incubated at 4°C overnight; primary antibodies were omitted on sections serving as negative control. The sections were treated with biotinylated secondary antibody and subsequent streptavidin-biotin-peroxidase. The signal was detected by 3,3′-diaminobenzidine as a chromogen substrate, and the tissues were counterstained with hematoxylin as described (13–15).

Construction of lentiviral vector. Human osteopontin cDNA was PCR amplified with primers containing *Xba*I and *Rsr*II linkers and was inserted into the polycloning site of the transducing lentivirus vector pSIN-GFP (17, 18). Lentivirus production was achieved with the three-plasmid system. Using Superfect reagent, human 293T cells at about 80% confluency were transfected with 7.5 μg of the vesicular stomatitis virus *Env*-coding plasmid, pMD.G; 15 μg of the packaging plasmid, pCMVΔ8.91; and 15 μg of either the control vector pSIN-GFP or the transgene vector pSIN-GFP-osteopontin. The media containing the pseudotyped lentiviruses were harvested daily from the 3rd to 5th day after transfection.

Infection and cell sorting. Immortalized human prostate epithelial cell lines, LNCaP and PC-3, were cultured as previously described (18). At 80% confluency, the cells were inoculated with 1 mL of the conditioned medium containing lentiviruses in the presence of 5 μg/mL polybrene for 8 hours. The cells were sorted by flow cytometry based on green fluorescent protein (GFP) fluorescence 2 days after infection.

Proliferation assay. To evaluate cellular growth, 5×10^4 GFP vector or osteopontin-GFP transfected cells were plated in 60-mm dishes in triplicates and grown with full serum medium. The cells were counted every 2 days with the Coulter Counter (Beckman Coulter, Inc., Miami, FL). The medium was changed every 2 days.

Invasion assay. Matrigel invasion assays were done with transfected prostate cancer cells. The upper chamber of the 8.0-μm inserts with polyethylene terephthalate membrane was coated with Matrigel from BD Biosciences (Bedford, MA), and the lower chamber was filled with full serum medium. Following a 24-hour pretreatment in medium containing 0.5% serum in the presence or absence of 5 μg/mL osteopontin antibody (R&D Systems, Minneapolis, MN), the cells (10^5) were added to the upper chamber, correspondingly with or without 5 μg/mL osteopontin antibody, and incubated at 37°C for 24 hours. Invasion of the cells through the membrane was detected by staining with hematoxylin and counted as previously described (18, 19).

Intravasation assay. The intravasive potential of the transfected prostate cancer cells was assessed by a PCR-based assay (20). Longitudinally incubated in a rotating incubator, chicken embryos at 9 days of gestation were selected for introducing the artificial air sac and subsequently "dropping" the chorioallantoic membrane (21). Briefly, air was suctioned through a small puncture in the side of the egg to facilitate the detachment of the chorioallantoic membrane from the shell membrane. Avoiding major blood vessels, a 1-cm^2 window was cut on the top surface, and the suspension of cancer cells was gently applied to the chorioallantoic membrane. Upon incubation at 37°C for 24, 48, and 72 hours, the lower chorioallantoic membrane was removed and snap frozen in liquid nitrogen. DNA was extracted using Puregene DNA extraction kit from Gentra Systems (Minneapolis, MN) following manufacturer's protocol. The samples were used in a subsequent nested PCR amplification for the *GFP* gene to confirm the presence of the cancer cells in the lower chorioallantoic membrane. The initial PCR products produced with GFP 1 primer set were diluted at a ratio of 1:50 and amplified with the second set (GFP 2) of primers. The experiments were repeated and confirmed with PCR amplification for *Alu* as previously described (20). The primer sequences, annealing temperatures, and product sizes were as follows: for GFP 1, CGACGTAAACGGCCACAAGT and GGTGCTCAGGTAGTGGTTGTCG, 62°C, 550 bp; for GFP 2, TACGG-CAAGCTGACCCTGAA and TGATATAGACCTTGTGGCTGTTGTAGT, 62°C, 343 bp; and for *Alu*, ACGCCTGTAATCCCAGCACTT and TCGCCCAGGCTG-GAGTGCA, 58°C, 224 bp.

Statistical analysis. All experiments were done in triplicates and repeated at least twice. Statistical comparisons were made using an unpaired, two-tailed *t* test.

Results

Analysis of osteopontin expression in prostatic lesions. Clues for consistent transcriptional alterations of osteopontin in the mouse prostatic lesions were initially obtained from the analyses of prostate gene expression profiles from three genetically engineered mouse models (Table 1). Although there was no significant increase in osteopontin gene expression in ventral or dorsolateral prostate of the *Fgf8b* mice relative to littermate controls at 2.5 months of age, the increase was clearly evident with the tissues obtained from the 12- and 18-month-old animals. This apparent 3- to 6-fold elevation of osteopontin RNA correlated with the temporal development of preneoplastic lesions in this transgenic model (14). Prostatic intraepithelial neoplasia (PIN) lesions, not seen at 2.5 months, were mostly low grade at 12 months and then turning to an abundant combination of low-grade PIN (LGPIN) and

Table 1. Mouse prostatic tissues evaluated by microarray and osteopontin expression

Mouse model	Age (mo)	Fold expression changes in lesions			
		VP	DLP	LP	Whole prostate
Fgf8b	2.5	1.7	1.8		
	12.0	3.3	5.8		
	18.0	3.9	3.0		
cRXRα$^{-/-}$	24.0	2.1		2.5	
cPten$^{-/-}$	6.0				3.2

NOTE: Anterior prostatic lobes from *Fgf8b* and *cRXRα*$^{-/-}$ mice were also tested. The results with these tissues did not exhibit a significant differential. It should be noted that the anterior prostatic lobe was found to have the lowest gene expression driven by the ARR2PB promoter (22, 27) corresponding to lowest prevalence of preneoplastic lesions in the models (13, 14).

Abbreviations: AP, anterior prostate; VP, ventral prostate; DLP, dorsolateral prostate; LP, lateral prostate.

high-grade PIN (HGPIN) with further advancing of age (14, 22). When compared with the *Fgf8b* transgenic mice, the incidence of PIN lesions, especially HGPIN, was found to be significantly less in *cRXRα*$^{-/-}$ mice (13, 22). Accordingly, prostate tissues from *cRXRα*$^{-/-}$ mice were examined at 24 months of age, after the onset of HGPIN. Although not as remarkable of an increase as seen in the *Fgf8b* mice, there was also a noticeable elevation in osteopontin mRNA levels in the *cRXRα*$^{-/-}$ ventral and lateral prostate relative to the age-matched controls. Recognizing that invasive adenocarcinoma of the prostate would have 100% penetrance in *cPten*$^{-/-}$ mice by 6 months of age, we used this age group for comparative microarray analysis (15). Compared with normal prostates, tumor-bearing prostates exhibited a 3.2-fold increase in osteopontin mRNA levels.

We used a modified semiquantitative RT-PCR method (23) to first obtain a confirmation of the microarray data (data not shown). With results supporting a correlation, tissue lysates from different prostatic lobes were subjected to Western blot analysis for osteopontin protein expression. The molecular size of osteopontin protein is known to be variable ranging between 41 and 75 kDa because of alternative RNA splicing, posttranslational modifications, and proteolytic cleavages in cell type–specific manner (7). For *Fgf8b*, four mice at 5.5 months of age were dissected to obtain pooled dorsolateral, ventral, and anterior prostatic lobes. As illustrated in Fig. 1*A*, there was ~3- to 4-fold increase in the detection of one to two osteopontin protein bands at around 65 kDa in the dorsolateral and ventral prostate compared with their age-matched controls. In contrast, but consistent with microarray and RT-PCR analyses, there was no remarkable difference in osteopontin levels between control and experimental preneoplastic tissues from the anterior prostate. Similarly, prostatic lobes from the *cPten*$^{-/-}$ mice between 1.6 and 14 months of age were analyzed. As shown in Fig. 1*B*, the development of primary prostate tumors in the cPten$^{-/-}$ mice was associated with progressively increased expression of osteopontin protein over an age range of 3.0 to 11.0 months. From a 13-month-old animal, we also examined different lobes for osteopontin expression. The content of osteopontin in all the lobes was elevated in the *cPten*$^{-/-}$ mouse compared with the corresponding lobes of its age-matched control (Fig. 1*C*). The relative increase seemed to be at least 10-fold when the intensity of the protein bands detected at 65 to 70 kDa were compared with corresponding controls.

Localization of osteopontin expression in prostatic lesions. Immunohistochemical staining for osteopontin was done on paraffin-embedded prostate tissues to determine the area of osteopontin signal localization. Each transgenic model was tested at different time points during tumorigenesis for the expression of osteopontin in LGPIN and HGPIN lesions in *Fgf8b*, cRXRα$^{-/-}$, and *cPten*$^{-/-}$ mice, and primary adenocarcinoma and metastatic lesions in *cPten*$^{-/-}$ model. It was found that the osteopontin signal was mainly localized to the cytoplasm of prostatic epithelial cells similar to such immunostaining observed in lung cancer cells (24). Some reactivity was also detected in the inflammatory cells, consistent with the known expression of osteopontin in activated immune cells (3, 25). As illustrated by the representative immunostaining photomicrographs (Fig. 2) for which the H&E staining of the corresponding sections is included in the Supplementary Fig. S1*A-D*, osteopontin signal greater than the background level was generally associated with the development of prostatic lesions in all three transgenic mouse models. Variations in signal intensity were, however, noted among cells and lesions. The increased osteopontin signal in dysplastic epithelia of LGPIN lesions (Fig. 2*A*) of *Fgf8b* line became more prominent in HPGIN lesions (Fig. 2*B*). Clearly, in contrast to the adjacent normal prostatic epithelium, most dysplastic cells in the LGPIN or HGPIN lesions exhibited considerably stronger osteopontin staining. The findings were similar with these preneoplastic lesions of *cRXRα*$^{-/-}$ mice.

The pattern of osteopontin expression was examined at various stages of prostatic tumorigenesis and metastasis in the *cPten*$^{-/-}$

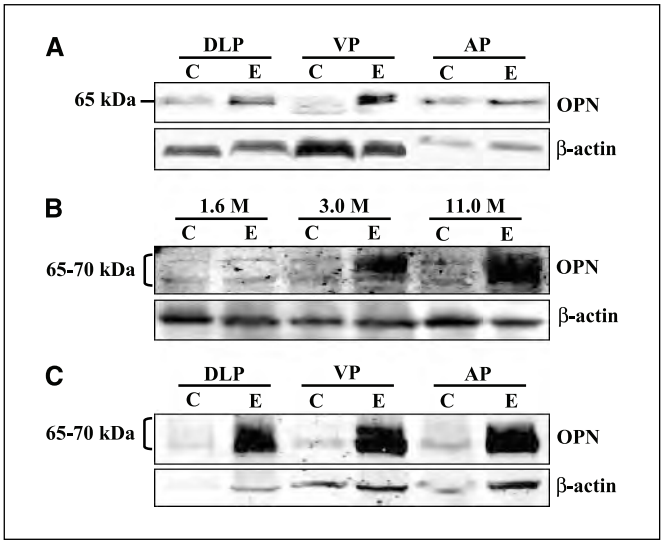

Figure 1. Western blot analysis of osteopontin (*OPN*) overexpression in preneoplastic and neoplastic prostatic tissues. *A,* osteopontin detection in 5.5-month-old *Fgf8b* transgenic and littermate control animals. Transgenics animals (*E*) and control animals (*C*). Osteopontin is detected at around 65 kDa. *Bottom,* β-actin, which served as an internal control for normalization. Overall, there was ~3- to 4-fold increase in osteopontin expression in the ventral (*VP*) as well as dorsolateral (*DLP*) lobes of the transgenic mice compared with their control counterparts. *B,* Western blot analysis of proteins extracted from the anterior prostate (*AP*) of the *cPten*$^{-/-}$ (*E*) mice and their littermate controls (*C*) at different ages as indicated in months (*M*). *C,* proteins from individual lobes (dorsolateral, ventral, and anterior) from a 13-month-old *cPten*$^{-/-}$ (*E*) mouse and its littermate control (*C*) were analyzed by Western blot.

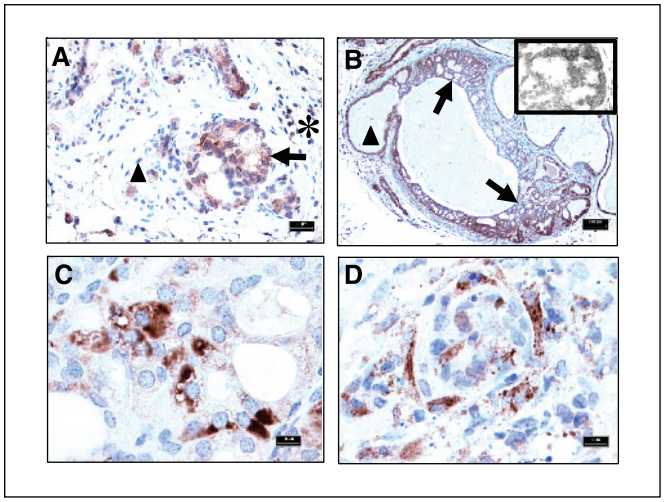

Figure 2. Immunohistochemical analysis of osteopontin in prostatic preneoplastic and neoplastic lesions. *A,* anti-osteopontin staining of a LGPIN lesion in an *Fgf8b* mouse illustrates that the increased intensity of osteopontin signal (*arrow*) is localized to the dysplastic cells compared with the minimal staining of adjacent normal epithelia (▲). Some inflammatory cells that stained positive for osteopontin were noted (*). *B,* anti-osteopontin immunostaining of a HGPIN lesion in the lateral prostatic lobe of an *Fgf8b* animal. The intensity of osteopontin signal in the dysplastic cells (*arrows*) is significantly higher than that of the normal cells (▲). *Inset,* high-power examination of osteopontin immunostaining of these dysplastic cells. *C,* anti-osteopontin immunostaining of the HGPIN lesion from the *cPten*$^{-/-}$ model. The signals are clearly shown to localize in the cytoplasm of the several atypical cells. *D,* anti-osteopontin immunostaining of an adenocarcinoma with local invasion in the lateral prostate of *cPten*$^{-/-}$ mouse. The strong signal, localized in the cytoplasm, outlined invasive cancer cells. Bar, 25 μm (*A*), 100 μm (*B*), and 10 μm (*C* and *D*).

model. LGPIN and HGPIN lesions displayed a pattern of increased osteopontin expression similar to that found in *Fgf8b* and *cRXRα*$^{-/-}$ mice. An example of HGPIN is shown in Fig. 2*C*. The trend of increase in the intensity of osteopontin staining with further progression of the disease was noted in the primary adenocarcinoma. This is illustrated with a case of tumor characterized by local microinvasion (Fig. 2*D*). In addition, examination of metastatic deposits in the lung found elevated osteopontin expression relative to the primary prostatic lesions (Fig. 3). The prostatic origin of the metastasis was verified by staining for expression of the androgen receptor. Although there were some variations in osteopontin staining intensity among individual cells, the majority of the metastasized cancer cells displayed robust immunoreactivity that set them apart from the background.

Biological effect of osteopontin overexpression in human prostate cancer cells. The expression of osteopontin was assessed in five human prostate cancer cell lines (PC-3, PC-3M, DU145, LNCaP, and CWR22R) and one nonneoplastic prostatic epithelial cell line (BPH-1) by semiquantitative RT-PCR. All of these cell lines expressed variable levels of osteopontin (Supplementary Fig. S2*A*). For the detection of secreted osteopontin protein in the cell culture medium, we used conditioned medium from some of the cell lines (BPH-1, PC-3, DU145, and LNCaP) for Western blot analyses. As shown in Fig. 4*A*, whereas all of the tested cell lines were found to produce osteopontin, the levels of mRNA and secreted protein, however, did not exhibit a strong correlation. Because it seemed that compared with the LNCaP cells, PC-3 cells expressed a higher level of protein for osteopontin, LNCaP and PC-3 were selected for studies of the biological effect of osteopontin overexpression. Each cell line was infected with lentivirions, which carried GFP or both osteopontin- and GFP-transducing genes. As previously described (17, 18), the transfected cells were sorted by fluorescence-activated cell sorting based on GFP fluorescence. The newly established cell lines were examined for osteopontin overexpression by RT-PCR (Supplementary Fig. S2*B*) with RNA prepared from cell extracts as well as by Western blot analysis of conditioned media (Fig. 4*B*).

The effect of osteopontin overexpression on cellular growth was assessed by a proliferation assay. Transfected LNCaP cells were grown in the presence of full serum over a course of 8 days. Compared with the GFP control, osteopontin-transduced LNCaP cells exhibited a strong proliferative advantage (Fig. 4*C*). The effect on proliferation was much less pronounced on the PC-3 cells (Fig. 4*D*), which already contained a higher endogenous osteopontin expression relative to the LNCaP cells. LNCaP and PC-3 cells with overexpression of osteopontin were also examined in a Matrigel invasion assay. The results showed a drastic enhancement of the invasion ability for LNCaP and a less pronounced but still significant effect on PC-3 when the cells were manipulated to express higher osteopontin levels. Furthermore, although the LNCaP and PC-3 cell lines are of different origin, it was remarkable to find that the response to osteopontin overexpression of each could be significantly suppressed by the presence of anti-osteopontin antibodies in the invasion assays (Fig. 5*A* and *B*).

To confirm the enhanced growth and invasive ability of the transfected cells *in vivo*, the intravasation assay based on the chorioallantoic membrane of the chicken egg was done. Chicken embryos at day 9 of gestation were inoculated with one million cells and incubated for 24, 48, and 72 hours. The GFP vector control LNCaP cells failed to intravasate even after 72 hours of incubation as previously reported (20). However, the presence of the osteopontin-transduced LNCaP cells in the lower chorioallantoic membrane could be readily detected by nested PCR for GFP and confirmed by PCR for *Alu* at time period of 48 or 72 but not 24 hours (Fig. 5*C*). Although both vector and osteopontin-transduced PC-3 cells were detected in the lower chorioallantoic membrane at

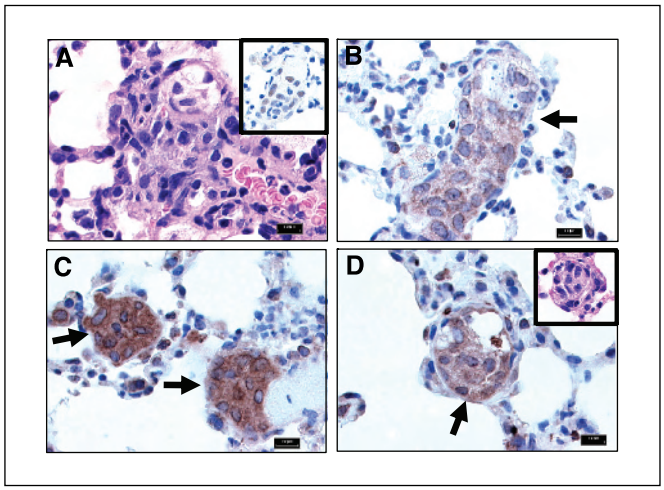

Figure 3. Osteopontin staining of lung metastases in a *cPten*$^{-/-}$ mouse. *A,* H&E staining of a metastatic lesion displaying the localization of cancer cells to the mesenchyme of the lung tissue, adjacent to a blood vessel. *Inset,* these cancer cells stained positive with anti-AR antibody, confirming their prostatic origin. *B,* anti-osteopontin staining of metastatic cancer cells in (*A*). These positively stained cancer cells (*arrow*) can be clearly differentiated from the lung tissue. *C,* two other foci of osteopontin-positive cancer cells with stronger intensity in osteopontin signal. *D,* a lymphovascular cluster of osteopontin-positive metastatic cells. *Inset,* H&E staining of the cluster. Bar, 10 μm.

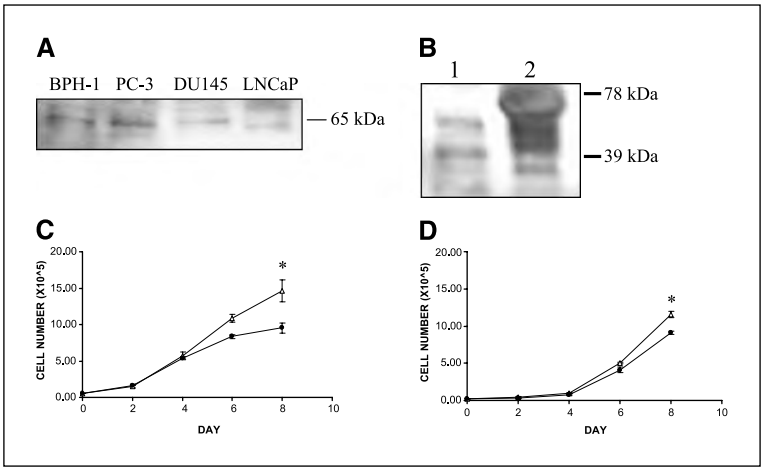

Figure 4. Detection, overexpression, and functional effects of osteopontin in prostate tumor cells. *A,* conditioned medium from some of the cell lines was examined for osteopontin protein expression by Western blots. *B,* Western blots of osteopontin with conditioned media from LNCaP/GFP (*lane 1*) and LNCaP/osteopontin (*lane 2*). *C,* proliferation of LNCaP/GFP and LNCaP/osteopontin cells in full serum medium was determined by counting the cell every 2 days using Coulter counter. Cells (10^5) were plated in each well in triplicates. *D,* analysis of growth of PC-3/GFP and PC-3/osteopontin cells as in (*C*). *, $P < 0.001$, differences in the growth between control and osteopontin-overexpressing cells were significant in both (*C*) and (*D*).

48 hours after inoculation, PC-3/osteopontin cells seemed to be more efficient in the process because their presence was detectable after 24 hours (Fig. 5*D*).

Discussion

While conducting cDNA microarray assays for differentially expressed genes in the prostatic lesions of genetically engineered mouse models, we identified osteopontin as a gene of interest. It is particularly noteworthy that in these models, whether *Fgf8b* trangenic (14) or *cRXRα*$^{-/-}$ (13) preneoplastic disease, or the *cPten*$^{-/-}$ (15) neoplastic disease system, we found significant up-regulation of osteopontin RNA and protein levels in all, relative to the corresponding littermate controls. We attempted to localize the overexpression of osteopontin in the prostatic lesions by immunohistochemistry. The increased intensity of osteopontin staining readily visible in many of the dysplastic epithelial cells of LGPIN lesions seemed to become more prominent in HGPIN. Relative to these preneoplastic lesions of all three models, significantly higher staining was observed in the primary adenocarcinoma that developed in the *cPten*$^{-/-}$ model. When the metastatic lesions in the *cPten*$^{-/-}$ mice were examined, the intensity of staining seemed to be even higher. Together, the results imply that up-regulation of osteopontin expression in prostatic lesions is consistent in all three models and independent of how the models were generated. Although osteopontin is described to be a marker for the late stages of progression of various cancers (6, 7), our results which were not conflicting, do however, point to osteopontin dysregulation beginning at a much earlier time point (e.g., at LGPINs). With advancing time, osteopontin levels seem to continue increasing with progression from LGPIN to HGPIN to adenocarcinoma, and most remarkably, the cancer cells expressing the highest levels of osteopontin seem to be selected during metastatic progression.

Our results indicate that osteopontin contributes to several steps in the process of prostate carcinogenesis and metastasis. Osteopontin seems to modulate cell proliferation and potentially the survival of the dysplastic and neoplastic prostatic cells, thus providing a selective advantage in early-stage lesions. The findings with manipulated overexpression in human prostate cancer cells as well as those of other published reports (11, 12) lend support to an autocrine effect of osteopontin overproduction on cell proliferation. This is shown with the LNCaP cells transduced with osteopontin expressing lentivirus vector. This effect was less pronounced on the PC-3 cells. PC-3 cells, however, are by nature, highly proliferative. We also used *in vitro* Matrigel invasion assay to assess the invasiveness of the cells. Although the control LNCaP cells were completely incapable of penetrating the membrane, there was a drastic enhancement in the invasive ability when osteopontin was overexpressed. A similar pattern, albeit relatively less pronounced, was produced by osteopontin overexpression in

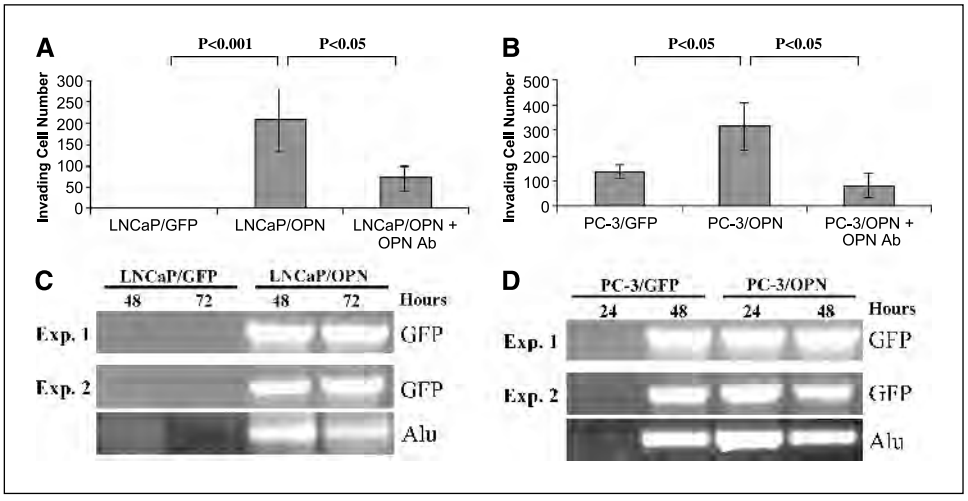

Figure 5. Matrigel and chorioallantoic membrane assays with osteopontin (*OPN*)–transduced LNCaP and PC-3 cells. *A,* in the Matrigel invasion assay, while LNCaP/GFP failed to penetrate the matrix, LNCaP/osteopontin displayed a strong invasiveness. This invasiveness could be significantly blocked by anti-osteopontin antibodies. *B,* PC-3/osteopontin demonstrated a 2-fold increase in invasive ability compared with PC-3/GFP. This bioactivity was also suppressed significantly by anti-osteopontin antibodies. *C,* nested PCR amplification for GFP using DNA extracts from the isolated lower chorioallantoic membrane. The experiment was repeated at least five times. The reproducibility of the assay is shown in a second experiment (*Exp. 2*) followed by a subsequent PCR amplification for *Alu* for confirmation of the data obtained from the GFP PCR. *D,* analysis of intravasation in transduced PC-3 cells as in (*C*).

PC-3 cells in which, besides osteopontin, multiple other factors may be contributing to its naturally highly invasive character. The fact that osteopontin could be an important player is further shown by the ability of anti-osteopontin antibodies to significantly neutralize this biological response induced by osteopontin overexpression.

Considering that intravasation is an early required event for the multistep process leading to metastasis, we also checked a potential role of osteopontin in intravasation *in vivo*. A model system, first developed by Kim et al. (20) and based on blood vessel penetration of xenotransplanted mammalian cancer cells on the chicken embryo chorioallantoic membrane assay, was used. Consistent with published work (20), PC-3 cells but not LNCaP cells were determined to be capable of intravasation in the chorioallantoic membrane model using qualitative PCR-based assays. Importantly, analysis of osteopontin-transduced LNCaP cells revealed that overexpression of osteopontin alone was sufficient to induce the ability to intravasate. The change in invasive ability *in vivo*, potentiated by the excess osteopontin production, was less pronounced in PC-3 cells compared with LNCaP. In PC-3 cells, however, higher osteopontin expression seems to affect the kinetics of intravasation apparently by accelerating the rate at which the cells access the blood vessels, as evident from the reduced time required for detectable intravasation from 48 to 24 hours of inoculation. An important question at this point is how osteopontin might be involved in facilitating tumor cell invasion. Osteopontin binds with several integrins and CD44 variants in both RGD sequence-dependent and sequence-independent manner (3). The resulting signal transduction pathways that may be activated by osteopontin are complex by nature and only poorly understood. There is, however, some relevant emerging information in this regard. For example, it has been shown that osteopontin induces activator protein (AP-1) transactivation in breast cancer cells through $\alpha_v\beta_3$ integrin–mediated c-Src kinase activity and EGF receptor (EGFR) phosphorylation, c-Src kinase being required for osteopontin-induced EGFR phosphorylation (26). AP-1 is then linked to urokinase-type plasminogen activator (uPA) production and secretion that results in stimulation of cell motility and invasion. In other work, osteopontin has been shown to stimulate LNCaP proliferation in serum-free medium but only in the presence of EGF (12). The induced proliferation is accompanied by a sustained activation of EGFR. It is also noteworthy that previous studies using the chorioallantoic membrane model showed that breaching of the vascular wall by the cancer cells is a rate-limiting step for intravasation and that cooperation between uPA/uPA receptor (uPAR) and matrix metalloproteinases (MMP) is required to complete this step (20). Thus, crucial molecules, such as uPA, uPAR, and activated MMPs, await further studies in relation to osteopontin overexpression in prostatic cancer in the context of breaching native biological barriers preventing cancer cell metastasis.

Acknowledgments

Received 8/8/2005; revised 11/7/2005; accepted 11/10/2005.

Grant support: NIH grant RO1-CA59705 (P. Roy-Burman) and NIH training grant T32-AI07078 (A.C. Khodavirdi).

The costs of publication of this article were defrayed in part by the payment of page charges. This article must therefore be hereby marked *advertisement* in accordance with 18 U.S.C. Section 1734 solely to indicate this fact.

We thank Liliana Ossowski (Mount Sinai School of Medicine, New York, NY) and James P. Quigley and Elena Deryugina (The Scripps Research Institute, La Jolla, CA) for advice and assistance with the chorioallantoic membrane assay; Cheng-Ming Chuong and Randall Widelitz (Department of Pathology) for the use of their facility for the chorioallantoic membrane work; Marian Young (NIH) for the gift of human osteopontin cDNA; Simon Hayward (Vanderbilt University, Nashville, TN) for the BPH-1 cell line; Marc Guerra (LI-COR Biotechnology) for his assistance with the osteopontin Western blot; and all the members of the Roy-Burman laboratory for their assistance in various aspects of the work.

References

1. Sodek J, Ganss B, McKee MD. Osteopontin. Crit Rev Oral Biol Med 2000;11:279–303.
2. Gerstenfeld LC. Osteopontin in skeletal tissue homeostasis: an emerging picture of the autocrine/paracrine functions of the extracellular matrix. J Bone Miner Res 1999;14:850–5.
3. Denhardt DT, Giachelli CM, Rittling SR. Role of osteopontin in cellular signaling and toxicant injury. Annu Rev Pharmacol Toxicol 2001;41:723–49.
4. Thalmann GN, Sikes RA, Devoll RE, et al. Osteopontin: possible role in prostate cancer progression. Clin Cancer Res 1999;5:2271–7.
5. Agrawal D, Chen T, Irby R, et al. Osteopontin identified as lead marker of colon cancer progression, using pooled sample expression profiling. J Natl Cancer Inst 2002; 94:513–21.
6. Rittling SR, Chambers AF. Role of osteopontin in tumour progression. Br J Cancer 2004;90:1877–81.
7. Wai PY, Kuo PC. The role of osteopontin in tumor metastasis. J Surg Res 2004;121:228–41.
8. Coppola D, Szabo M, Boulware D, et al. Correlation of osteopontin protein expression and pathological stage across a wide variety of tumor histologies. Clin Cancer Res 2004;10:184–90.
9. Reinholt FP, Hultenby K, Oldberg A, Heinegard D. Osteopontin: a possible anchor of osteoclasts to bone. Proc Natl Acad Sci U S A 1990;87:4473–5.
10. Giachelli CM, Steitz S. Osteopontin: a versatile regulator of inflammation and biomineralization. Matrix Biol 2000;19:615–22.
11. Angelucci A, Festuccia C, D'Andrea G, Teti A, Bologna M. Osteopontin modulates prostate carcinoma invasive capacity through RGD-dependent upregulation of plasminogen activators. Biol Chem 2002;383: 229–34.
12. Angelucci A, Festuccia C, Gravina GL, et al. Osteopontin enhances the cell proliferation induced by the epidermal growth factor in human prostate cancer cells. Prostate 2004;59:157–66.
13. Huang J, Powell WC, Khodavirdi AC, et al. Prostatic intraepithelial neoplasia in mice with conditional disruption of the retinoid X receptor α allele in the prostate epithelium. Cancer Res 2002;62:4812–9.
14. Song Z, Wu X, Powell WC, et al. Fibroblast growth factor 8 isoform B overexpression in prostate epithelium: a new mouse model for prostatic intraepithelial neoplasia. Cancer Res 2002;62:5096–105.
15. Wang S, Gao J, Lei Q, et al. Prostate-specific deletion of the murine Pten tumor suppressor gene leads to metastatic prostate cancer. Cancer Cell 2003;4:209–21.
16. Trotman LC, Niki M, Dotan ZA, et al. Pten dose dictates cancer progression in the prostate. PLoS Biol 2003;1:E59.
17. Zhong C, Yang S, Huang J, Cohen MB, Roy-Burman P. Aberration in the expression of the retinoid receptor, RXRα, in prostate cancer. Cancer Biol Ther 2003;2: 179–84.
18. Song Z, Powell WC, Kasahara N, van Bokhoven A, Miller GJ, Roy-Burman P. The effect of fibroblast growth factor 8, isoform b, on the biology of prostate carcinoma cells and their interaction with stromal cells. Cancer Res 2000;60:6730–6.
19. Zheng J, Rudra-Ganguly N, Powell WC, Roy-Burman P. Suppression of prostate carcinoma cell invasion by expression of antisense L-plastin gene. Am J Pathol 1999; 155:115–22.
20. Kim J, Yu W, Kovalski K, Ossowski L. Requirement for specific proteases in cancer cell intravasation as revealed by a novel semiquantitative PCR-based assay. Cell 1998;94:353–62.
21. Zijlstra A, Mellor R, Panzarella G, et al. A quantitative analysis of rate-limiting steps in the metastatic cascade using human-specific real-time polymerase chain reaction. Cancer Res 2002;62:7083–92.
22. Roy-Burman P, Wu H, Powell WC, Hagenkord J, Cohen MB. Genetically defined mouse models that mimic natural aspects of human prostate cancer development. Endocr Relat Cancer 2004;11:225–54.
23. Yang S, Zhong C, Frenkel B, Reddi AH, Roy-Burman P. Diverse biological effect and Smad signaling of bone morphogenetic protein 7 in prostate tumor cells. Cancer Res 2005;65:5769–77.
24. Hu Z, Lin D, Yuan J, et al. Overexpression of osteopontin is associated with more aggressive phenotypes in human non–small cell lung cancer. Clin Cancer Res 2005;11:4646–52.
25. O'Regan A, Berman JS. Osteopontin: a key cytokine in cell-mediated and granulomatous inflammation. Int J Exp Pathol 2000;81:373–90.
26. Das R, Mahabeleshwar GH, Kundu GC. Osteopontin induces AP-1-mediated secretion of urokinase-type plasminogen activator through c-Src-dependent epidermal growth factor receptor transactivation in breast cancer cells. J Biol Chem 2004;279:11051–64.
27. Wu X, Wu J, Huang J, et al. Generation of a prostate epithelial cell-specific Cre transgenic mouse model for tissue-specific gene ablation. Mech Dev 2001;101:61–9.

Available online at www.sciencedirect.com
SCIENCE DIRECT®
Cancer Letters xx (2006) 1–15
CANCER Letters
www.elsevier.com/locate/canlet

Gene expression in the LNCaP human prostate cancer progression model: Progression associated expression in vitro corresponds to expression changes associated with prostate cancer progression in vivo

Qian Chen [a], Jeffery T. Watson [b], Susan Ruth Marengo [c], Keith S. Decker [b], Ilsa Coleman [d], Peter S. Nelson [d], Robert A. Sikes [a,*]

[a] *Laboratory for Cancer Ontogeny and Therapeutics, Department of Biological Sciences, University of Delaware, Wolf Hall, Newark, DE 19716, USA*
[b] *Computer Information Sciences, University of Delaware, Newark, DE 19716, USA*
[c] *James and Eileen Dickee Research Laboratory, Department of Urology, Case Western Reserve University, Cleveland, OH, USA*
[d] *Division of Human Biology/Program in Genomics, Fred Hutchinson Cancer Research Center, Seattle, WA, USA*

Received 26 October 2005; received in revised form 15 December 2005; accepted 19 December 2005

Abstract

Identification of the genes involved in prostate cancer (PCa) progression to a virulent and androgen-independent (AI) form is a major focus in the field. cDNA microarray was used to compare the gene expression profile of the indolent, androgen sensitive (AS) LNCaP PCa cell line to the aggressively metastatic, AI C4-2. Thirty-eight unique sequences from a 6388 cDNA array were found differentially expressed ($\geq$2-fold, 95% CI). The expression of 14 genes was lower in C4-2 than in LNCaP cells, while the reverse was true for 24 genes. Twelve genes were validated using Q-PCR, Western blotting and immunohistochemistry (IHC) of LNCaP and C4-2 xenograft. Q-PCR showed that 10 of 12 (83.3%) genes had similar patterns of expression to the array (LNCaP > C4-2: TMEFF2, ATP1B1, IL-8, BTG1, BChE, NKX3.1; LNCaP < C4-2: BNIP3, TM4SF1, AMACR, UCH-L1). By Western blot, 4/5 genes examined: TMEFF2, NKX3.1, AMACR, and UCH-L1, not IL-8, were consistent with RNA profiling. Protein expression levels were confirmed in human tumor xenografts using IHC. A large proportion of the markers found in this expression profile is consistent with those recently identified in human PCa tissues along with several novel genes that remain to be examined. These data further demonstrate the utility of the LNCaP human PCa progression model as a tool to investigate the phenotypic changes required for the progression to AI and metastasis.

Keywords: cDNA microarray; Prostate; Neoplasm; Cell lines; Androgen insensitive; Progression

1. Introduction

Prostate cancer (PCa) is the most commonly diagnosed cancer and the second leading cause of cancer-related death in North American men [1]. PCa is a heterogeneous disease that arises from multiple independent foci and has a stochastic pattern of

* Corresponding author. Tel.: +1 302 831 6050; fax: +1 302 831 2281.
E-mail address: rasikes@udel.edu (R.A. Sikes).

0304-3835/$ - see front matter © 2006 Published by Elsevier Ireland Ltd.
doi:10.1016/j.canlet.2005.12.027

progression. The exact role of androgen in the development and progression of PCa is a subject of intense study [2]. The matter is complicated further because even in the healthy prostate, some functions are androgen dependent while others are merely sensitive to androgens. These complications are compounded by the fact that functions which are androgen dependent or sensitive varies with the age and maturity of the male as well as with the stage of PCa. In this paper, we will use the term androgen sensitive (AS) to include both androgen dependent and androgen sensitive functions.

Prostate specific antigen (PSA) allows the diagnosis of low grade, localized PCa, that allows the physician to offer the patient several efficacious treatment options. In contrast, metastatic PCa remains essentially incurable. Androgen ablation therapy, either by chemical or by surgical castration, is the last line of defense and has been gold standard for the treatment of advanced PCa since Charles Huggins first pioneered this approach in 1941 [3,4]. Although the initial response is a dramatic reduction and palliation of symptoms, PCa eventually progresses to a lethal, hormone-refractory stage, for which no curative therapies currently exist. It has become clear that the progression from the AS stage to the androgen-independent (AI) or hormone-refractory stage is the critical step that determines whether an individual's disease can be cured.

The LNCaP cell line was isolated by Horoszewicz et al. [5] from a subclavian lymph node metastasis of PCa. The cell line retains several key markers including: PSA, prostate specific membrane antigen (PSMA) and the androgen receptor (AR). Through passage and hormonal manipulation in vivo, the lineage-related LNCaP sublines have resulted in a series of cells that mimic the progression of PCa from the original AS LNCaP cell line to the AI C4-2 and C4-2B cell lines, whose xenografts are able to sustain robust growth in castrate hosts. The AI C4-2 and C4-2B cell lines are highly tumorigenic and metastatic, including spontaneous metastasis to bone, whereas the AS LNCaP cell line is only weakly tumorigenic and is nonmetastatic [6,7].

It was long assumed that differential gene expression occurred during the malignant progression of cancer but until the development of the differential display [8], the techniques required to isolate the genes with differential expression profiles were so laborious that such studies were impractical. Microarray technology has further simplified the simultaneous comparison of thousands of gene transcripts thereby allowing for comparisons to be made between multiple stages of cell growth, growth factor treatment or tissue development. In the current study, we took advantage of microarray technology and two cell lines from the LNCaP human prostate cancer progression model (AS, LNCaP and AI, C4-2) to identify genes potentially involved in the progression of AS PCa to the lethal AI phenotype. After eliminating duplicates on the list, 38 genes were found differentially expressed between the two cell lines ($\geq$2-fold change, 95% CI). Quantitative-PCR (Q-PCR), Western blot and immunohistochemistry (IHC) were used to corroborate the results obtained by the microarray analysis and also to compare gene expression between the cell lines cultured in vitro versus culturing in situ as xenografts. There was strong agreement between the results obtained by microarray and those obtained by the analysis of mRNA and protein by traditional methods. Importantly, there was an excellent correlation between the results obtained in tissue culture and those obtained from the xenografts, once again demonstrating the robustness of the LNCaP progression model as a tool for the investigation of the progression of PCa from its AS to its AI phenotypes.

2. Materials and methods

2.1. Cell lines and culture

The LNCaP cell line is essentially as described by Horoszewicz et al. [5] and the C4-2 subline was derived from LNCaP as described by Thalmann et al. [6,7,9]. The usage of both cell lines was restricted to passages 25–35 for microarray and PCR, and passages 12–25 for Western blot where a passage is defined as a 1:8 split of approximately confluent cultures. PC-3 and DU145 cells, as described by Kaighn et al. [10] and Stone et al. [11], respectively, were used with LNCaP as sources of driver RNA for microarray hybridizations. Cell lines were maintained in T-medium (GIBCO Cell Culture, Invitrogen, Inc., Carlsbad, CA [12]) supplemented with 5% FBS and 1% penicillin/streptomycin (P/S) (GIBCO, 10,000 units/ml penicillin and 10,000 μg/ml streptomycin). For microarray analysis, LNCaP or C4-2 cells were plated at high density ($\geq 2.5 \times 10^6$ cells/60 mm dish) in 5% FBS and allowed to recover overnight. High density cultures were chosen to minimize the return of growth associated genes that may be differentially expressed during log phase and to mimic the high contact density of cells found in tissues. The next day, the media was changed to phenol-free, high-glucose RPMI 1640 (GIBCO) supplemented with 1% P/S. RNA was isolated 24 h later. For PCR and Western blot analyses, LNCaP and C4-2 cells were allowed to grow to confluence in a 100 mm dish in T-medium/5% FBS. Cells were harvested from both the confluent cultures directly or after 24 h of serum starvation in RPMI 1640. A rat neuronal cell line, PC12, was a gift from Dr Jeffery Twiss (Department of Research, A.I. DuPont Hospital for Children, Wilmington, DE) was maintained in Ham's F12K and 10% FBS. PC12 cell

lysate was used as the positive control for UCH-L1 protein in Western blot.

2.2. RNA extraction

Total RNA was extracted using the QIAGEN RNeasy Mini Kit (QIAGEN, Inc., Valencia, CA) or Trizol (Invitrogen) according to the manufacturer's instructions. RNA was quantified by A260 nm using a BioRad SmartSpec 3000 spectrophotometer (BioRad Lab, Hercules, CA). RNA integrity and loading were assessed visually by running a 2 μg aliquot of total RNA through denaturing gel electrophoresis, staining with ethidium bromide (EtBr) and examining the relative intensities of the ribosomal bands.

2.3. Microarray analysis

cDNA microarrays were constructed by Fred Hutchinson Cancer Research Center as described previously [13–15]. Briefly, a nonredundant set of 6388 prostate-derived cDNA clones and expressed sequence tags (ESTs) was identified from the Prostate Expression Database (http://www.pedb.org/), which is a public sequence repository of ESTs derived from human prostate cDNA libraries. Individual clone inserts were amplified by PCR, purified, and spotted in duplicate onto Type IV glass microscope slides (Amersham, Inc., Piscataway, NJ) using a GenII robotic spotting tool (Molecular Dynamics, Sunnyvale, CA).

Four independent RNA samples from each cell line were prepared for microarray hybridization. The RNAs were reverse transcribed to cDNAs, labeled with Cy3 or Cy5 dyes, and combined with a reference standard comprised of equal mixtures of RNA from LNCaP, DU145, and PC-3 cell lines.

For each experiment, each cDNA was represented twice on each slide and the experiments were performed on duplicate chips with dye swap and there were four independent RNA samples per cell line. Therefore, in these data, there are 16 independent hybridization events or data points per gene per cell line. Intensity ratios for each cDNA clone hybridized with probes derived from the respective cell lines were calculated as log(2) (gene of interest intensity/control intensity).

2.4. Statistical methods

Statistical analysis of the microarray data was performed using BRB (http://linus.nci.nih.gov/BRB-ArrayTools.html) microarray tools, which was developed by the Biometric Research Branch of the Division of Cancer Treatment & Diagnosis of the National Cancer Institute under the direction of Dr Richard Simon, and verified by Significance Analysis of Microarrays (SAM, http://www-stat-class.stanford.edu/SAM/servlet/SAMServlet). The analysis was done using a 'combine and conquer' strategy, comparing trials and then combining those trials that proved highly similar in order to reduce the complexity of the problem. Once all the highly similar trials were combined, the remaining trials were compared and the most differentially expressed genes were identified.

2.5. Reverse-transcript PCR (RT-PCR) and quantitative/real-time PCR (Q-PCR)

RNAs were extracted from the LNCaP and C4-2 cell lines as described above resulting in two groups of serum-free samples and three groups of 5% FBS samples for each cell line. cDNA reactions were performed as described previously [7,16] using 0.5 μg of total RNA (SuperScript III First-Strand Synthesis System for RT-PCR, Invitrogen). For the 12 differentially expressed genes that were selected for additional study, intron spanning primers were designed with the aid of the following programs: (1) primer 3 (http://frodo.wi.mit.edu/cgi-bin/primer3/primer3_www.cgi); (2) QIAGEN oligo tool kit (http://oligos.qiagen.com/oligos/toolkit.php); (3) Vector NTI 9.0 (InforMax, Frederick, MD, USA). For each reaction, 50 pmol of each primer was used. PCR primer sequences are shown below (Sigma-Genosys, Woodlands, TX). The full names of these genes are listed in Table 2.

TMEFF2-f-869: 5′-GTGTGATGCTGGTTATACTGG-3′, *r-1041*: 5′-TCTGGGGCATTTCCTTGTGAT-3′;
ATP1B1-f-215: 5′-GCAGTTGGTTTAAGATCCTTC-3′, *r-367*: 5′-GAATCTGTGTTAATCCTGGCG-3′;
IL-8-f-114: 5′-GACATACTCCAAACCTTTCCAC-3′, *r-293*: 5′-TTCTCAGCCCTCTTCAAAAAC-3′;
BTG1-f-442: 5′-AGGAGCTGCTGGCAGAACATT-3′, *r-579*: 5′-TGCTCAGTCCAATCCGCTGTG-3′;
BchEG1-f-1529: 5′-AGACTCAGAACAATAGCACAAG-3′, *r-1690*: 5′-TATTTCCTGTCATTTCCAAGA-3′;
NKX3.1-f-74: 5′-CGCTCACGTCCTTCCTCATC-3′, *r-291*: 5′-CCTTTCTGGCTCGGTCTCTGC-3′;
HSP90K-f-462: 5′-GTATGCTTGGGAGTCTTCTGCT-3′, *r-605*: 5′-ACTACTTCTTTGACCCGCCTCT-3′;
HSPA8-f-1024: 5′-GGTATTGAAACTGCTGGTGGAG-3′, *r-1358*: 5′-TTATCCTTTGTCATGGCACGCT-3′;
E1B-f-94: 5′-GTTCCAGCCTCGGTTTCTATT-3′, *r-234*: 5′-CCTGTTGGTATCTTGTGGTGTC-3′;
TM4SF1-f-400: 5′-AGCACCGAGGGCCAGTACCTT-3′, *r-512*: 5′-CCACCAAGAGCCAAGAGGATAG-3′;
AMACR-f-471: 5′-CTTTGTCAGGTGTTCTCTCAA-3′, *r-652*: 5′-TGTTCCTTCCACCATATTTGC-3′;
UCHL*1-f-523*: 5′-GCCAATGTCGGGTAGATGAC-3′ *r-665*: 5′-AGCGTCCTTCAGCAGGGTGT-3′.

Optimal annealing temperatures (T_A) and cycle parameters were determined using a 12-step gradient starting at 10 °C below the calculated melting temperature (T_m) to the T_m (QIAGEN Taq PCR kit; *Eppendorf* MasterTaq Kit, Hamburg, Germany) using an Eppendorf Mastercycler Gradient Thermal cycler. PCR products were resolved in 2.0% agarose

(GIBCO)/0.5×TAE (2.42 g/l Tris base, 0.57 ml/l (v/v) acetic acid, 186 mg/l EDTA) gels stained with EtBr. β2-Microglobulin was used as a positive control. The primer sequence used was: *β2-f*, 5′-GCAAGGACTGGTCTTTCTATCTCTTG-3′; *β2-r*, 5′-TCAACCTCCATGATGCTGCTTAC-3′. PCR products were purified by QIAquick PCR Purification Kit (Qiagen) and sequenced in the University of Delaware Sequencing Core (http://bluehen.ags.udel.edu/) to confirm the identity of amplicon sequences. Q-PCRs were then run using the optimal T_A to compare and estimate the fold change in gene expression between the LNCaP and C4-2 cell lines for each gene target. The QIAGEN Quanti-Tect SYBR-Green PCR Kit (Qiagen) and the real-time information BioRad iCycler iQ Real-time detection system (BioRad labs) were used as described by the manufacturer.

2.6. Calculation of cycle number differences in Q-PCR

In Q-PCR, the number of cycles (CN) is related directly to the number of amplified copies of the mRNA from a given gene (AC) and the efficiency of the PCR reaction (EFF) as described by the following formula: $AC = OC \times (1 + EFF)^{CN}$, where OC is the original gene or mRNA copy number. This formula can also be used to compare the original level of mRNA copy number of a specific gene in different reactions if one assumes the EFFs of the same gene in the same experiment (paralleled reactions) are the same. For example, we had two different samples used in one PCR experiment. When we determine the threshold we will have two CNs: CN_1 and CN_2, for those samples crossing the threshold. At these points, the two reactions have exactly the same AC. Using the above formula:

$$AC = OC_1 \times (1 + EFF)^{CN_1} \quad \text{and}$$

$$AC = OC_2 \times (1 + EFF)^{CN_2}$$

$$\text{So } OC_1 \times (1 + EFF)^{CN_1} = OC_2 \times (1 + EFF)^{CN_2}$$

Now we can calculate the ratio between their OCs:

$$OC_1/OC_2 = (1 + EFF)^{CN_2}/(1 + EFF)^{CN_1}$$

$$= (1 + EFF)^{(CN_2 - CN_1)}$$

Thus, if $CN_2 > CN_1$ then $OC_2 < OC_1$, e.g. the reaction passing the threshold earlier has a higher mRNA copies in the original sample. If one assumes the reaction efficiency is 100%, 3.32 cycle number difference ($\Delta CN = CN2 - CN1$) indicates 10 times difference in original copy (OC) numbers. Since the exact OC does not need to be calculated, the PCR EFF in each reaction was not determined. The final results showed in both Table 3 and Fig. 3 are all cycle number differences (ΔCN) but not original mRNA copy differences (ΔOC).

2.7. Antibodies

Two antigenic peptides were designed based on the TMEFF2 predicted gene product sequence and structure using the online software http://us.expasy.org/ and http://workbench.sdsc.edu/. The first peptide was within the putative extracellular domain (TMEFF2-EC) and consisted of amino acids 148–162, N-HEGSGETSQKETSTC-C. The second peptide was within the putative cytoplasmic domain (TMEFF2-CP) and consisted of amino acids 345–359, N-CPRSNRIHRQKQNTG-C. Polyclonal antiserum was prepared by conjugation of the peptides to keyhole limpet hemocynanin (KLH) and injection into rabbits (Sigma-Genosys). The titer for immunoreactivity was performed by ELISA using peptide-coated plates as described by Mahana et al. [17].

The goat anti-IL-8 antibody, an affinity purified IgG, was purchased from R&D systems (R&D no. AF-208-NA, Minneapolis, MN). The Nkx3.1 monoclonal antibody (Invitrogen-ZYMED) was used for Western blot. A polyclonal rabbit serum was used for UCH-L1 (Chemicon no. AB1761, Temecula, CA; gift of Dr J. Twiss), NKX3.1 (gift from Dr E. Gelmann, Georgetown University), AMACR (gift from Dr R.J. Wanders, Academic Medical Center, Amsterdam, Netherlands), mouse anti-α tubulin (Zymed Laboratories, Inc.) and mouse anti-histone H1 (Upstate). The secondary antibodies used were: horseradish peroxidase (HRP) conjugated donkey anti-rabbit IgG (Amersham Bioscience), HRP conjugated donkey anti-mouse IgG (Jackson ImmunoResearch Laboratory, West Grove, PA, USA) and biotin-SP-conjugated affinity pure donkey anti-goat IgG (H+L; Jackson Labs.). The biotin-SP-conjugated secondary antibody was detected using the streptavidin–peroxidase kit (Biogenex, San Ramon, CA).

2.8. Western blot analysis

Five milliliters of fresh medium (T-medium/5%FBS or serum free RPMI 1640) was added and the cultures were incubated an additional 48 h before harvest. The experiment was repeated twice with different passages of cells. The conditioned medium was collected from all cultures after 48 h and centrifuged 1000×*g*, for 5 min to remove cellular debris. Proteins in the conditioned medium were concentrated using the Amicon Ultra-4 Centrifuge Filter Devices (Millipore, Billerica, MA).

Whole cell lysates were extracted in radioimmunoprecipitation (RIPA) buffer containing 50 mM Tris–HCl pH 7.4, 150 mM NaCl, 1 mM EDTA, 1% Triton X-100, 1% sodium deoxycholate, 0.1% SDS and 10% protease inhibitor cocktail (Roche, Indianapolis, IN). Protein concentration was determined by the method of Lowry et al. [18] using the BCA protein assay (Pierce, Rockford, IL). Nuclear proteins were prepared for NKX3.1 detection using the NE-PER Nuclear and Cytoplasmic Extraction kit (Pierce). Cytoplasmic protein expression was normalized to α-tubulin, while nuclear

proteins were normalized to histone H1 expression using blots from four separate experiments as described below.

Proteins were resolved using 4–12% SDS-PAGE gradient gels (NuPAGE Bis–Tris Gel, Invitrogen-Novex). For the whole cell lysates, 30 μg/well was loaded and for nuclear proteins, 20 μg/well was loaded. For the secreted proteins in the conditioned media, loading was normalized to the cell number and the protein content of the whole cell lysates. Proteins were transferred electrophoretically to Immun-Blot PVDF Membrane (BioRad) at 25 V for 3 h. Immunodetection was accomplished using ECL reagents and manufacturer's protocols (Amersham Biosciences). The membrane was blocked overnight at 4 °C in PBS containing 5% nonfat dry milk (NFDM; Nestle, Solon, OH). Antibodies were diluted in PBS-T (0.1% Tween-20, Fisher) and incubated for 1 h. Following this and all other incubations, membranes were washed in PBS-T 3×5 min. The working concentrations of the primary antibodies were: AMACR: 1:5000 [19]; NKX3.1: 1:2500; UCH-L1: 1:2000; IL-8: 0.1 μg/ml; TMEFF2-CP: 1:1000; α-tubulin 1:1500 and histone H1 1:500. All antibody incubations were for 1 h unless otherwise indicated. The primary antibody was diluted in PBS-T. For all antibodies except IL-8, the second antibody was HRP-conjugated anti-rabbit, at 1:5000 in PBS-T. For IL-8, the membrane was incubated with biotin-conjugated donkey anti-goat (1:5000 in PBS-T) dilution) followed by an incubation in streptavidin conjugated horseradish peroxidase (HRP) for 30 min (1:5000 in PBS-T). HRP activity was detected using ECL Western blotting detection reagents and exposure to KODAK BioMax MR Film (KODAK, Herts, UK). The relative amounts of target protein/lane was determined using the AlphaEase FC Software Version 3.1.2 (Alpha Innotech Corporation, San Leandro, CA)

2.9. Immunohistochemistry (IHC)

LNCaP and C4-2 tumor xenografts were grown subcutaneously, phosphate or zinc-buffered formalin fixed and embedded in paraffin as described previously [7,20,21]. Tumor sections (5–6 μm) were deparaffinized in two changes of Xylene (Fisher) followed by rehydration in a graded series of ethanols. Antigen retrieval was performed by microwaving the slides in 10 mM citrate acid, pH 6, for 20 min at 40% power. Endogenous peroxidase was quenched by a 30 min incubation in 3% hydrogen peroxide. Tissue sections were blocked with 4% bovine serum albumin (BSA) in PBS for 30 min at room temperature (RT). Sections were exposed to primary antibodies (AMACR: 1:12,000; UCH-L1: 1:5000; IL-8: 5 μg/ml; TMEFF2-CP: 1:2000), for 1 h at RT or overnight at 4 °C. Sections were washed 3×5 min with PBS and then incubated with HRP conjugated secondary antibody in blocking buffer (1:200, 30 min, RT). Diaminobenzidine (Sigma) was used as the chromagen for peroxidase activity (5–10 min, depending on the antibody). For biotin conjugated secondary antibodies, streptavidin-HRP was used at a 1:200 dilution at RT for 30 min, prior to exposure to the chromagen. Sections stained for cytoplasmic or secretory proteins were counterstained with hematoxylin, and those stained for nuclear proteins were counter stained with methyl green. Sections were then dehydrated in a graded series of ethanols, incubated 2×5 min in xylenes and mounted with permount. Sections were evaluated and photographed using a Zeiss Axioskop 2 microscope (Solent Scientific, Segensworth, UK) and a SPOT digital camera (Diagnostic Instruments, Sterling Heights, MI, USA).

3. Results

3.1. Identification of genes differentially expressed in the LNCaP and C4-2 prostate cancer progression model

Gene expression measurements from the microarray platforms were analyzed using BRB microarray tools and SAM. Fig. 1 shows the relative expression of genes expressed by LNCaP vs. C4-2 cells. For analysis, values were converted to Log(2) ratios and differences in signal intensity ≧2-fold were considered to be significantly different. Fifty-one genes were identified as being expressed differentially between the two cell lines by BRB analysis. After evaluation of the array and elimination of duplicates, 38 unique gene sequences were identified (Table 1). Fourteen of these genes were

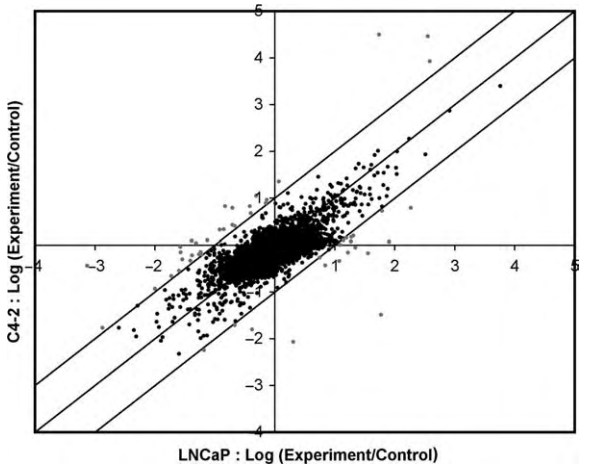

Fig. 1. Scatter plot for BRB microarray analysis result. Differentially expressed genes between LNCaP and C4-2 cell lines are shown at the 95% confidence interval as indicated by parallel lines. A 2-fold or greater change in signal intensity as defined by Log (2) ratio change equals 2, was assigned as significant. Using these criteria, the dots below the parallel lines represent genes expressed higher in LNCaP than in C4-2; those dots above the parallel lines represent genes expressed higher in C4-2 than in LNCaP. There are 51 spots shown as the redundant clones and false positive clones were not removed from this analysis. All redundant clones expression ratios were consistently in the same direction.

Table 1
List of differentially expressed genes based on microarray analysis

Hugo	Description	Fold change expression LNCaP/C4-2
Receptor signaling/cell adhesion		
TMEFF2	Transmembrane protein with EGF-like and two follistatin-like domains 2	9.556
PCDHGA12	Protocadherin gamma subfamily A, 12	2.157
TM4SF1	Transmembrane 4 L six family member 1	1/3.762
Cell cycle		
CP110	CP110 protein	2.042
Inflammatory/immune response		
IL-8	Interleukin 8	3.563
AZGP1	Alpha-2-glycoprotein 1, zinc	1/2.135
Metabolism		
BCHE	Butyrylcholinesterase	2.627
SAT	Spermidine/spermine N1-acetyltransferase	2.603
DKFZP566E144	Small fragment nuclease	1/2.051
PKM2	Pyruvate kinase, muscle	1/2.070
GLYATL1	Glycine-*N*-acyltransferase-like 1	1/2.075
MEST	Mesoderm specific transcript homolog	1/2.106
GPI	Glucose phosphate isomerase	1/2.368
PGK1	Phosphoglycerate kinase 1	1/2.380
PFKFB3	6-Phosphofructo-2-kinase/fructose-2,6-biphosphatase 3	1/2.450
HMGCS2	3-Hydroxy-3-methylglutaryl-coenzyme A synthase 2	1/2.902
LDHA	Lactate dehydrogenase A	1/3.155
AMACR	Alpha-methylacyl-CoA racemase	1/6.489
UCH-L1	Ubiquitin carboxyl-terminal esterase L1	1/6.798
Stress response		
SOD2	Superoxide dismutase 2, mitochondrial	3.302
MT2A	Metallothionein 2A	2.778
SSR4	Signal sequence receptor, delta	1/2.106
HSPA8	Heat shock 70 kDa protein 8	1/2.120
DDIT4	DNA-damage-inducible transcript 4	1/2.198
HSPCA	Heat shock 90 kDa protein 1, alpha	1/2.369
BNIP3	BCL2/adenovirus E1B 19kDa interacting protein 3	1/2.787
Regulation of transcription		
BTG1	B-cell translocation gene 1 anti-proliferative	2.674
NKX3-1	NK3 transcription factor related, locus 1	2.048
HMGB1	High-mobility group box 1	1/2.095
SAP18	sin3-Associated polypeptide, 18 kDa	1/2.105
NSEP1	Nuclease sensitive element binding protein 1	1/2.114
Transport/ion binding		
ATP1B1	ATPase, Na+/K+ transporting, beta 1 polypeptide	5.155
VPS25	Vacuolar protein sorting 25	2.083
SLC16A3	Solute carrier family 16, member 3	1/2.145
SLC22A3	Solute carrier family 22, member 3	1/2.570
Unknown		
TncRNA	Trophoblast-derived noncoding RNA	2.656
FLJ22386	Leucine zipper domain protein	1/2.161
C13orf12	Chromosome 13 open reading frame 12	1/2.681

The 38 unique genes listed, from 51 hits, were confirmed by both BRB and SAM programs and were common to both methods. The genes have been sorted by function or cellular organelle as indicated. HUGO designations are provided for unique identification of the sequence. These can be used to find the genes on the PEDB web site or through the NCBI website. These data represent the relative fold expression difference of mRNA level of LNCaP/C4-2.

expressed at higher levels in LNCaP than in C4-2 cells, while the remaining 24 were expressed at lower levels in LNCaP than in C4-2 cells. SAM analysis identified 215 genes (33 positive, 182 negative), including the 51 genes (38 unique) identified by BRB, as being expressed differentially (DELTA 1.0393), where the delta represents the fold change in $\log_2$ fluorescence intensity. The identity and fold differences for these

genes are shown in Table 1. Dye swap had no influence on gene expression profiles. Furthermore, within a chip, the gene expression profiles between replicate had ≧94% identity.

3.2. Q-PCR validation of microarray results

Twelve genes were selected for additional analysis based on their magnitude of change or their putative role in PCa progression (LNCaP > C4-2: TMEFF2, ATP1B1, IL-8, BChEG1, BTG1, NKX3.1; LNCaP < C4-2: HSP90K, HSPA8, E1B, TM4SF1, AMACR, UCH-L1; Table 2). The properties of the Q-PCR primers and average cycle number difference for each Q-PCR reaction are shown in Table 3. PCR products were sequenced to confirm that they corresponded to the gene of interest prior to the performance of Q-PCR (data not shown). β2-Microglobulin was used to normalize the Q-PCR data across samples. Fig. 2 illustrates typical Q-PCR results. At least four independent RNA samples, two from serum containing and two from serum-free cultures were analyzed. Statistical analysis revealed only nominal differences between the serum containing and serum-free cultures and data from these replicates were pooled (Table 3). Statistical analyses were done separately for each group by calculating the average of cycle number differences of multiple Q-PCR results between LNCaP and C4-2 cell lines (Table 3, Fig. 3). Fig. 3 shows the final results and demonstrates that for 83.3% of the candidate genes (10/12) the reported changes in mRNA expression were qualitatively similar for microarray analysis and Q-PCR.

3.3. Western blot results corroborate protein levels for differentially expressed genes

To confirm that the changes in message were reflected in changes in protein expression, Western blot was performed on four candidates (TMEFF2, UCH-L1, NKX3.1, AMACR, and IL-8). TMEFF2 and UCH-L1 were selected because of their high changes in gene expression and NKX3.1, AMACR, and IL-8 were selected because of their putative roles in hPCa progression [22–28]. For each protein, Western blots were repeated at least four times with four independently isolated protein samples (two serum containing, two serum-free; Fig. 4). Consistent with the reported

Table 2
List of the 12 genes validated by PCR

Genes	Full name	Function
TMEFF2	Tomoregulin 2	Transmembrane protein with both epidermal growth factor and follistatin domains; frequently hypermethylated in human tumors
ATP1B1	Na+/K ATPase beta subunit 1	Maintains sodium and potassium homeostasis in animal cells. Beta-subunit functions as a suppressor to cancer cell invasions
IL-8	Interleukin 8	Cytokine that plays a role in chemoattraction and activation of neutrophils; has similarity to several platelet-derived factors
BTG1	B-cell translocation gene 1	BTG/Tob family proteins control cell growth negatively. Induces a novel apoptosis pathway
BChE	Butyrylcholinesterase gene 1	Implicated in developmental processes as a stimulator of cellular proliferation
NKX3.1	NKX3.1	A homeo box-containing gene, prostate/testis specific. A putative prostate tumor suppressor
BNIP3	E1B 19k/Bcl2 binding protein	E1B 19 kDa protein is required for adenovirus induced cellular transformation and oncogenicity; inhibits apoptosis
HSPA8	Heat shock protein 70k	Heat shock proteins that interact with AR as molecular chaperones
HSPCA	Heat shock protein 90k	
TM4SF1	Transmembrane 4 superfamily member 1	Appears to be involved in cancer invasion and metastasis
AMACR	alpha-Methylacyl-CoA racemase	Plays an important role in peroxisomal beta-oxidation of branched-chain fatty acids. It is highly expressed in prostate cancer
UCH-L1	Ubiquitin carboxyl-terminal hydrolase 1	Neuron-specific protein involved in the ubiquitin-mediated proteolytic pathway

Differentially expressed genes chosen for further examination. The first six genes, italized, were expressed at higher levels in LNCaP than in C4-2 (positive fold change in Table 1); the last six genes were expressed at higher levels in C4-2 than in LNCaP (negative fold change in Table 1).

Table 3
Critical aspects of Q-PCR analysis for differentially expressed genes

Gene	Tm of primers	Product size (bp)	Ta	Average ΔCN ($CN_{LNCaP} - CN_{C4-2}$)		
				+serum	−serum	Total
TMEFF2	63.0–67.6	172	62	−7.8	−11.3	−9.5
ATP1B1	59.2–63.5	153	60	*0.2*	−1.4	−0.7
IL-8	61.2–62.2	179	56	−4.4	−0.2	−1.9
BTG1	67.6–70.9	138	61	−1.2	−1.3	−1.3
BchE	57.7–58.6	161	55	−3.7	−5.9	−5.0
NKX3.1	70.3–69.5	217	65	−0.6	−1.6	−1.0
BNIP3	63.1–63.1	140	56	*−0.1*	0.5	0.2
HSPA8	64.5–67.4	154	60	*−0.8*	*−1.2*	*−1.0*
HSPCA	63.5–64.1	143	60	0.5	*−0.7*	*−0.2*
TM4SF1	70.0–65.9	113	56–57	1.8	1.2	1.5
AMACR	59.5–63.5	182	56	2.4	2.2	2.3
UCH-L1	64.2–68.4	143	63–64	10.4	8.3	9.2

The Q-PCR was run under 'optimal Ta', which was derived by gradient PCR. 'Average of ($CN_{LNCaP} - CN_{C4-2}$)' lists the statistical result of the Q-PCR by displaying the calculated cycle number (CN) differences (ΔCN) between cell lines. If the CN_{LNCaP} is greater than the CN_{C4-2}, the number in the table is negative thereby indicating that the gene is expressed higher in LNCaP than in C4-2. If reverse, the number in the table is positive. The Q-PCR results are shown in separate columns for (+) serum and (−) serum. The average value from both conditions is also given. Italicized values are discordant to the overall expression pattern from the microarray.

changes in message by microarray and Q-PCR, the levels of protein encoding TMEFF2, NKX3.1 and IL-8 were greater in LNCaP than in C4-2 while the opposite was true for AMACR and UCH-L1. The expression of NKX3.1 is regulated by androgen [29], and this may explain why the protein is only barely detectable in serum-free media.

3.4. Immunohistochemistry of LNCaP and C4-2 Xenografts

For many applications such as studies focusing on progression to androgen independence and the development of metastatic capabilities, it is highly desirable to utilize actual tumors instead of cell lines cultured in vitro, thereby avoiding potential culture artifact. To confirm that the observed changes in TMEFF-2, UCH-L1, and IL-8 were present in tumor xenografts IHC was performed (Fig. 5). Consistent with the reports for AMACR expression in specimens of human PCa tissue [30–34], cytoplasmic AMACR staining was intense and localized to the cytoplasm, presumably peroxisomal vesicles in C4-2 tumor xenografts but virtually undetectable in LNCaP tumor xenografts (Fig. 5A–C).

TMEFF-2 showed very strong immunoreactivity in the cytoplasm and cell membrane of LNCaP xenografts; in contrast there was a marked reduction in expression of TMEFF-2 in the C4-2 xenografts (Fig. 5D–F).

UCH-L1 protein expression in xenografted tumor specimens accurately reflected the pattern of expression observed in cultures of LNCaP and C4-2 cells (Fig. 5G–I). LNCaP tumor sections stained lightly, while the C4-2 tumor sections were slightly more intense (Fig. 5G–I). In both tumor xenografts, staining was localized to the cytoplasm, which is consistent with UCH-L1's role as a ubiquitin carboxyl terminal esterase [35–37].

In LNCaP tumor xenografts, IL-8 staining was generally weak with scattered areas of intense staining; in contrast, staining in C4-2 tumor xenografts was essentially negative (Fig. 5J–L). Again, this expression profile is consistent with that expressed by the cell lines in culture and predictive of the marker as seen in our tumor xenografts.

4. Discussion

Although PCa has been studied for more than half a century, the mechanism underlying PCa metastasis and the development of androgen-independence remains both an intensive and elusive area of investigation. For the past two decades, the LNCaP cell line [5], and more recently its staged variants [38,39], have been extremely productive models for the study of PCa and its progression to AI and the development of metastatic capabilities. The staged variants are composed of a lineage-related series of cell sublines, LNCaP, C4, C4-2, C4-2-B series, which reflects in a heritable manner the key steps of PCa progression to an increasingly malignant phenotype, spontaneous metastasis to bone with paraplegia in vivo and the development of AI [6,7].

cDNA microarrays are efficient tools to screen for global changes in mRNA levels. In order to identify

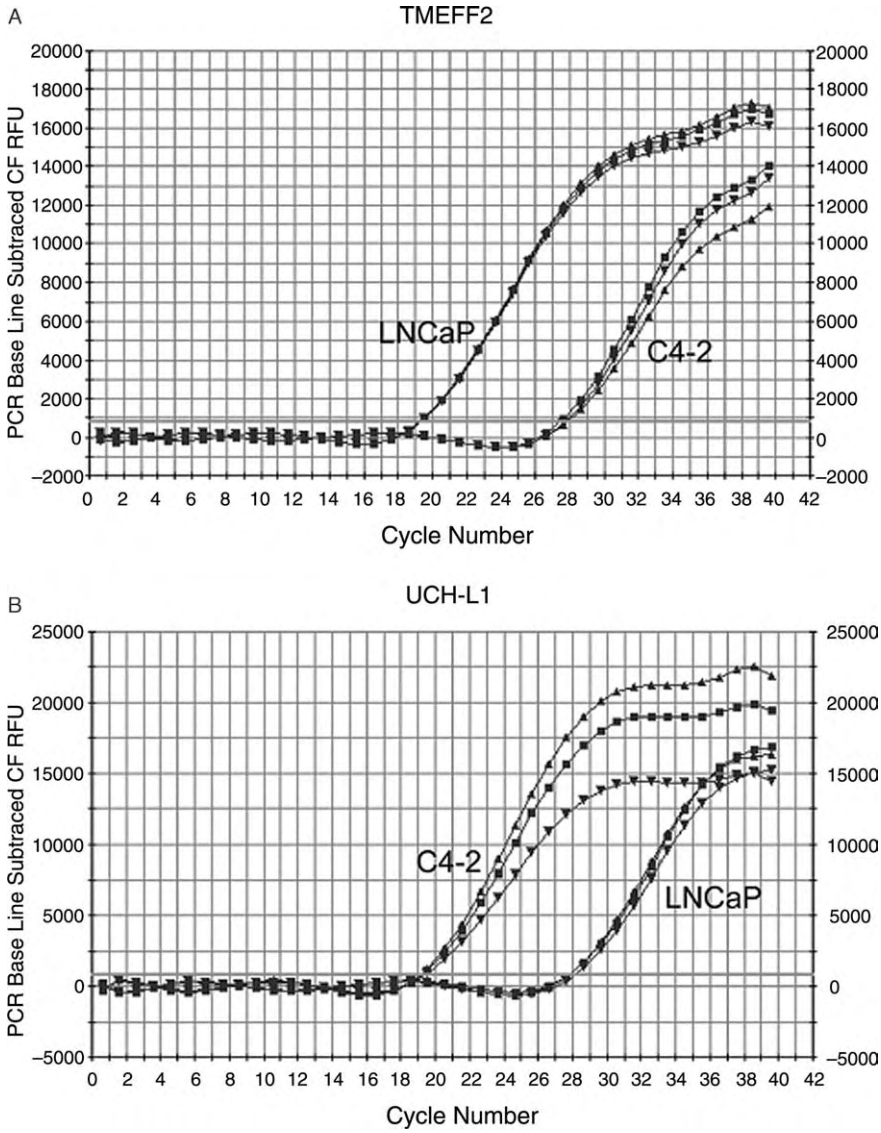

Fig. 2. Examples of Q-PCR results. TMEFF2 (A) and UCH-L1 (B) Q-PCR 'Amplify/Cycle Graphs' are shown here as examples. These two genes showed the largest change in mRNA level by cDNA microarray as listed at either end of Table 1. They also have the greatest cycle number difference in Q-PCR (see Table 3).

genes associated with androgen independence and a more malignant phenotype, we compared LNCaP and C4-2 cell lines using gene profiling. Herein we have reported the identification of 38 unique genes whose expression pattern changes between AS LNCaP and AI C4-2 cells when plated at high density in vitro. Two different analysis tools (BRB and SAM) were used to analyze the data. Twelve of the 38 genes were validated by Q-PCR based on their level of expression and prominence in PCa biomarker studies. HSPA8 was the only gene that showed an expression profile that differed between the microarray data set and that obtained by Q-PCR, indicating a high degree of reliability in this dataset. The lack of correlation between HSPA8 and the microarray may be due to the fact that there are several closely related heat shock proteins and near redundant entries in GenBank. As a result, we may have designed primers to, and queried a different sequence than that printed on the microarray. Most importantly, with the exception of IL-8, we have demonstrated clearly that the level of several of these transcripts and the corresponding proteins changed in a manner consistent with observations reported in human prostate cancer in situ thereby firmly establishing the

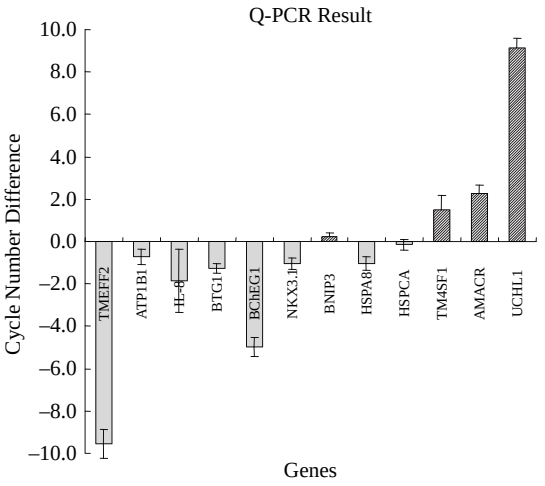

Fig. 3. Q-PCR summary. Combined results of Q-PCR reactions of (−) serum and (+) serum are shown in this figure. The *X*-axis indicates the genes examined. The six genes on the left were expressed higher in LNCaP while the six genes on the right were expressed higher in C4-2 cells by microarray analysis. The *Y*-axis demonstrates the cycle number difference (ΔCN) between two cell lines in Q-PCR analysis. Negative numbers (shaded bars) mean the mRNA levels are higher in LNCaP; positive numbers (hatched bars) mean the mRNA levels are higher in C4-2. Using this method, 10/12 (83.3%) genes pulled from the microarray analysis were expressed differentially in the same manner as predicted by the microarray using fresh RNA isolates and confirmation by Q-PCR.

importance of this model system in the search for genes associated with the malignant progression of PCa. This study represents the third known study of molecular profiling between LNCaP and C4-2 cells but the only one using high-density cultures. In the study by Bisoffi et al. [40], 1176 genes from an Atlas cDNA array were screened yielding 12.7% down regulated and 15.3% up regulated. The differentially expressed genes varied dramatically from ours by finding a number of growth regulatory genes, including EGFR, IGF1R, SAPK4 and K-ras among others that we attribute to log-phase growth conditions. Similarly, Trojan et al. [41], using the HG-U133A Affymetrix chip covering about 22,000 genes, found only 42 differentially expressed probe sets that reduced to 14 candidates for association with progression or metastatic progression. They also used log-phase cells of later passage numbers and LNCaP cells of a different origin than ours. These authors, similar to Bisoffi et al., found several growth factors, growth factor receptor signaling molecules and cell cycle regulated genes despite the fact that 33/38 of our differentially expressed cDNAs are represented on the HG-U133A array. Not found on this affymetrix chip are TMEFF2, SAT, GLYATL1, AMACR and VPS25. This supports the contention that the high-density growth conditions of the cells for our experiments were key to the acquisition of the gene sequences pulled in our analysis. The final comparison of LNCaP and C4-2 cells, performed by Liu et al. [42], examined the expression of cluster of differentiation (CD) antigens to determine the lineage relatedness and possible origin of LNCaP sublines. These authors conclude that C4-2 is derived from a pre-existing subpopulation of LNCaP cells selected by passage in vivo while the CL1 cell line, selected by androgen deprivation in vitro, probably arose as a unique event due to the culture conditions. Therefore, we have provided a novel context, essentially high-density serum-free cultures, that can be used to induce the expression of prostate cancer tissue biomarkers in prostate cancer cell lines in vitro. Below we analyze the significance of each gene tested to confirm our microarray and their possible role in PCa progression.

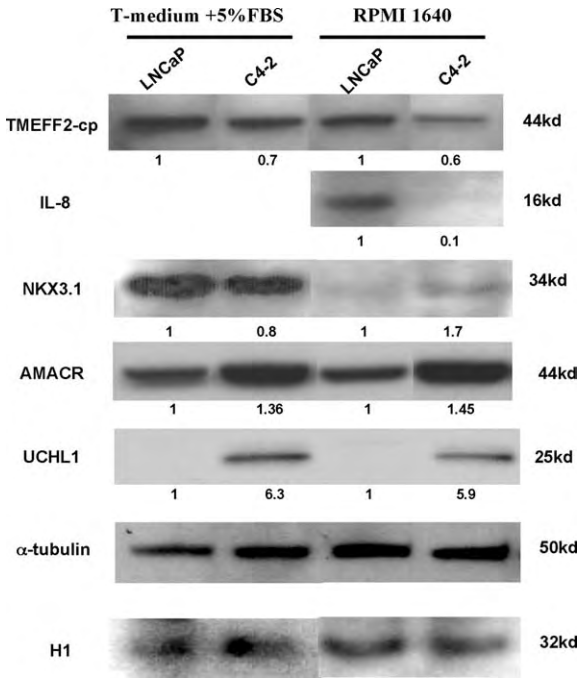

Fig. 4. Protein expression from selected differentially expressed mRNAs. Western blot analysis was used to detect the protein level of TMEFF2, IL-8, NKX3.1, AMACR and UCH-L1 genes products. The apparent molecular weight of each protein is labeled on the right. L+, LNCaP with serum; C+, C4-2 with serum; L−, LNCaP serum free; C−, C4-2 serum free. The numbers below each band indicate the average relative density from four separate blots normalized to LNCaP cells (see methods for details). IL-8 was not blotted for cell conditioned medium in serum due to the presence of serum Il-8. A single blot for each gene representing the best reflection of the expression ratios of four experiments is shown as an example. Cytoplasmic proteins were normalized to α-tubulin, while nuclear proteins were normalized to histone H1.

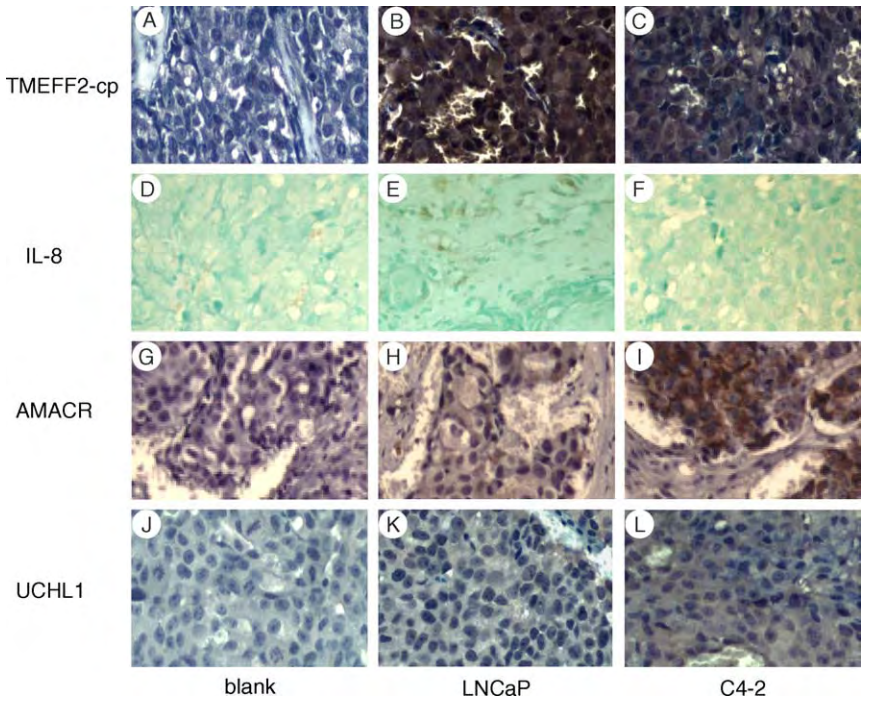

Fig. 5. Immunohistochemistry of LNCaP and C4-2 in vivo tumors. Figures B, E, H, and K are representative subcutaneous LNCaP tumor xenografts; similarly, C, F, I and L are representative subcutaneous C4-2 tumor xenografts. Negative controls are shown for LNCaP tumor xenografts, A, D, G, and J, where primary antibody was omitted. Similar background levels were obtained for C4-2 tumors (data not shown). TMEFF2 is higher in LNCaP than in C4-2 (C≫B); IL-8 is higher in LNCaP (E≫F); AMACR expression is higher in C4-2 than in LNCaP (I≫H); and, UCH-L1 is higher in C4-2 (L>K). Final magnification is 100×.

In order to discriminate between possible tissue culture artifact and gene expression in a tumor context in vivo, we examined the expression of TMEFF2, IL-8, NKX3.1, AMACR and UCH-L1 in both cultured cells and tumor xenografts of LNCaP and C4-2. TMEFF2 is a tomoregulin family member. These are two pass transmembrane proteins having a single EGF-like domain that has high homology to both the EGF/Neuregulin family of growth factors and two follistatin modules [43] that may bind TGF-β related growth factors, the activins [44]. Activins inhibit prostate glandular branching by activating the TGF-β receptor, a function opposed by follistatin in organ culture [45,46]. Therefore, follistatins actually increase prostate branching and ductal morphogenesis. Release of the follistatin domain from TMEFF1 or 2, therefore, would likely result in increased prostate cancer growth, in part, by antagonizing TGF-β growth inhibition. Since the loss of TGF-β action and related molecules, e.g. inhibin-α [47], have been implicated in the loss of growth control in prostate cancer [48–50], the role of TMEFF and its follistatin domain are of intense interest. TMEFF2 is expressed at high levels in the normal brain and prostate as well as in primary PCa with high levels of mRNA expression in LNCaP and LAPC-AD cells as compared to PC-3 and DU145 [51,52]. Its expression is regulated by androgen and it has been demonstrated to suppress growth of PCa cell lines [51]. IHC analysis in human tissue showed significant protein expression in 74% of primary PCa and 42% of metastatic lesions [52]. In the data set presented here, microarray analysis detected a dramatic decrease in expression in C4-2 as compared to LNCaP cells. This was confirmed by Q-PCR, Western blot, and most importantly in IHC of tumor xenografts. These observations support the hypothesis that TMEFF2 is a tumor/growth suppressor whose expression decreases as PCa progresses to the metastatic phenotype or AI. Therefore, TMEFF2 expression is lost with progression to the AI and represents another candidate gene involved in PCa tumor suppression. On a final note, it is interesting that TMEFF1 and TMEFF2 may play the opposite role in different tissues. TMEFF1 appears to be up regulated in AI-PCa [51] and uterine leiomyoma [53], while TMEFF2 is down regulated in AI-PCa. In brain, TMEFF1 is associated with increased malignant

potential and not tumor suppression [54]. Clearly, more work needs to be done to determine the signaling responsible for these differences in different tissues.

Ferrer et al. [24] reported the presence of IL-8 in tissue sections from patients with PCa, but not in patients with benign prostatic hyperplasia. Similarly, Lehrer et al. demonstrated elevated serum levels IL-8 in patients with PCa and those with bone metastases [28]. Kim et al. [23] and Inoue et al. [26] showed that the expression of IL-8 in human PCa cells is associated with angiogenesis, tumorigenicity, and metastasis in vitro and in vivo. IL-8 has also been shown to be up regulated in stroma of strongly invasive melanoma [55]. Lee et al. [25] have shown that over expression of IL-8 in LNCaP cells results in AI growth. In contrast, IL-8 expression in the C4-2 cell line was decreased compared to LNCaP. There are several potential explanations for this discrepancy. First, this may correlate with C4-2's tendency to form osteoblastic rather than osteoclastic-resorptive bone metastasis [7,20] since IL-8 may mediate the effects of PTHrP and stimulate the osteoclastic phenotype [56]. In support of this premise, constitutively elevated levels of IL-8 have been found almost exclusively in osteoclastic PCa, such as PC-3 and DU145 [20,26,28] and have been implicated in a more aggressive phenotype and the formation of osteoclastic bone metastases [56]. This is supported by reports of increased IL-8 in serums of PCa patients with cancer [27] and bone metastases in particular [28] and probably reflects the increased bone turnover associated with both osteoblastic and sclerotic lesions. Second, we have examined only subcutaneous xenografts of LNCaP and C4-2 and this may have dramatically decreased overall IL-8 production by the xenograft. Greene et al. [57] have shown that orthotopic xenograft tumor cells produce more IL-8 than subcutaneous xenografts.

NKX3.1 is a homeo-box containing gene whose protein product functions as a transcription factor. The expression of the NKX3.1 gene is androgen regulated [29] and highly restricted to the prostate and testis [58,59]. Loss of Nkx3.1 protein is common in hPCa as well as in prostatic intraepithelial neoplasia and its loss may be a very early marker of cellular transformation [59,60]. On this basis, it has been classified as a putative prostate tumor suppressor gene [59]. The data presented here supports this hypothesis in that there was a dramatic decrease in the expression of NKX3.1 at both the mRNA and, more conclusively, at the protein level in the C4-2 cell line. We tried numerous protocols, including those with antigen retrieval, to immunostain Nkx3.1 in our tissue xenografts but were not successful. This may be due to overfixation resulting in poor access to the protein or issues of antibody avidity and specificity. Nonetheless, the decrease is well established in our cell lines and numerous human tissue samples as described above.

α-Methylacyl CoA racemase (AMACR), also known as P504S, is an enzyme that plays an important role in peroxisomal beta-oxidation of branched-chain fatty acids [61,62]. The neuropathies Refsum disease and X-linked adrenoleukodystrophy, are thought to result from the accumulation of specific fatty acids, due to mutations in AMACR [19]. Over expression of wild type AMACR was detected in both PCa clinical tissues and PCa cell lines but not in normal prostate tissues. Once over expressed, the AMACR protein level remains elevated as PCa progresses to higher stage and grade [30,31,63,64]. AMACR expression appears to be androgen-independent [31,33], nonetheless, the expression is low in metastatic or hormone-refractory PCa but elevated in neoadjuvant hormone therapy patient samples. It has been proposed that AMACR has the potential to complement PSA as a new and perhaps better diagnostic marker for PCa [30,31]. Decreased expression of AMACR has been demonstrated to be associated with decreased proliferation of PCa cell lines by an androgen-independent mechanism [33]. Herein we report the up regulation of AMACR levels in the LNCaP progression model. The protein was expressed at low levels in LNCaP cells and tumor sections while the level was up regulated substantially in the AI and metastatic C4-2 cell line and tumor xenografts. Therefore, AMACR may well have a role in the development of metastatic and AI PCa as described above.

Ubiquitin carboxyl-terminal esterase L1 (UCH-L1) is a member of the UCH family. This enzyme catalyzes the hydrolysis of C-terminal ubiquityl esters and generates ubiquitin monomers [65,66]. Early studies indicated that UCH-L1 is expressed at high levels in neuroendocrine and neuronal tissues and comprises 1–2% of total brain protein [35,67,68]. Mutation of this gene is related to Parkinson's disease by inducing abnormal protein accumulation due to lack of ubiquitin [36,69,70]. UCH-L1 is expressed in the developing Wölffian duct and prostate of humans during early glandular development as well as in PCa [37] although double labeling implies sparse co-localization with chromogranin A. Immunostaining of the developing rat prostate for UCH-L1 and other NE markers indicates that rat NE cells do not express UCH-L1 [71]. Nonetheless, UCH-L1 appears to be up regulated in tumors containing neuroendocrine cells [72]. No

evidence has been found to show a relationship between UCH-L1 and PCa progression, however several publications demonstrated this gene's expression is related to the presence of a neural or neuroendocrine component in several different cancers [72–76] where it is being evaluated as a tumor marker. The presence of neuroendocrine cells in PCa has been correlated to a poor prognosis independent of tumor stage and grade [77–79]. We found higher expression of UCH-L1 in the more aggressive AI C4-2 than in the AS LNCaP cell line in vitro. Further, IHC showed increased UCH-L1 levels in C4-2 tumor xenografts as compared to LNCaP tumors. As LNCaP cells can be induced to neuroendocrine differentiate in vitro and constitutively express some neuroendocrine markers, the expression of UCH-L1 by this cell line is not surprising. However, the utility of UCH-L1 as a rapid marker for neuroendocrine differentiation and its role as a prognostic indicator remain to be validated. It should be noted that the role of this protein in neoplastic transformation or neuroendocrine differentiation has not been evaluated.

In summary, using high density plating of PCa cells of a lineage related, androgen sensitive to androgen-independent human prostate cancer progression model, we have identified 51 candidate genes whose expression is dramatically different in cell lines from opposite ends of the spectrum in LNCaP human prostate cancer progression series. As such, they represent potential candidates regulating the progression to the more malignant and AI PCa phenotype. Importantly, validation of several of our candidate genes corresponded dramatically to changes observed for these markers in human PCa tissues. Future studies will be needed to explore the potential roles of the remaining candidates detected in this extremely versatile model of human PCa progression.

Acknowledgments

This work was supported by a grant from the NIH, R01 DK63919 (RAS), the University of Delaware Start-up funds (RAS), R21 DK62073 (SRM) and CA85859 (PSN) and PC041158 (PSN). Special thanks are given to Dr Ed Gelmann and Dr R.J. Wanders for the donation of their antibodies for these studies.

References

[1] A. Jemal, T. Murray, E. Ward, A. Samuels, R.C. Tiwari, A. Ghafoor, et al., Cancer statistics, 2005, CA Cancer J. Clin. 55 (2005) 10–30.

[2] E. Deutsch, L. Maggiorella, P. Eschwege, J. Bourhis, J.C. Soria, B. Abdulkarim, Environmental, genetic, and molecular features of prostate cancer, Lancet Oncol. 5 (2004) 303–313.

[3] C. Huggins, C.V. Hodges, Studies on prostate cancer: I. The effect of castration, of estrogen and of androgen injection on serum phosphatases in metastatic carcinoma of the prostate, Cancer Res. 1 (1941) 293–297.

[4] C. Huggins, R.E. Stevens, C.V. Hodges, Studies on prostate cancer: Ii. The effects of castration on advanced carcinoma of the prostate gland, Arch. Surg. 43 (1941) 209–223.

[5] J.S. Horoszewicz, S.S. Leong, T.M. Chu, Z.L. Wajsman, M. Friedman, L. Papsidero, et al., The lncap cell line—a new model for studies on human prostatic carcinoma, Prog. Clin. Biol. Res. 37 (1980) 115–132.

[6] G.N. Thalmann, P.E. Anezinis, S.M. Chang, H.E. Zhau, E.E. Kim, V.L. Hopwood, et al., Androgen-independent cancer progression and bone metastasis in the lncap model of human prostate cancer, Cancer Res. 54 (1994) 2577–2581.

[7] G.N. Thalmann, R.A. Sikes, T.T. Wu, A. Degeorges, S.M. Chang, M. Ozen, et al., Lncap progression model of human prostate cancer: androgen-independence and osseous metastasis, Prostate 44 (2000) 91–103 (101; 144(102)).

[8] P. Liang, A.B. Pardee, Differential display of eukaryotic messenger RNA by means of the polymerase chain reaction, Science 257 (1992) 967–971.

[9] H.C. Wu, J.T. Hsieh, M.E. Gleave, N.M. Brown, S. Pathak, L.W. Chung, Derivation of androgen-independent human lncap prostatic cancer cell sublines: role of bone stromal cells, Int. J. Cancer 57 (1994) 406–412.

[10] M.E. Kaighn, K.S. Narayan, Y. Ohnuki, J.F. Lechner, L.W. Jones, Establishment and characterization of a human prostatic carcinoma cell line (pc-3), Invest. Urol. 17 (1979) 16–23.

[11] K.R. Stone, D.D. Mickey, H. Wunderli, G.H. Mickey, D.F. Paulson, Isolation of a human prostate carcinoma cell line (du 145), Int. J. Cancer 21 (1978) 274–281.

[12] S.M. Chang, L.W. Chung, Interaction between prostatic fibroblast and epithelial cells in culture: role of androgen, Endocrinology 125 (1989) 2719–2727.

[13] K. Wang, L. Gan, E. Jeffery, M. Gayle, A.M. Gown, M. Skelly, et al., Monitoring gene expression profile changes in ovarian carcinomas using cdna microarray, Gene 229 (1999) 101–108.

[14] M. Bonham, H. Arnold, B. Montgomery, P.S. Nelson, Molecular effects of the herbal compound pc-spes: identification of activity pathways in prostate carcinoma, Cancer Res. 62 (2002) 3920–3924.

[15] P.S. Nelson, N. Clegg, H. Arnold, C. Ferguson, M. Bonham, J. White, et al., The program of androgen-responsive genes in neoplastic prostate epithelium, Proc. Natl Acad. Sci. USA 99 (2002) 11890–11895.

[16] D. Theodorescu, H.F. Frierson Jr., R.A. Sikes, Molecular determination of surgical margins using fossa biopsies at radical prostatectomy, J. Urol. 161 (1999) 1442–1448.

[17] W. Mahana, A. Paraf, Mice ascites as a source of polyclonal and monoclonal antibodies, J. Immunol. Methods 161 (1993) 187–192.

[18] O.H. Lowry, N.J. Rosebrough, A.L. Farr, R.J. Randall, Protein measurement with the folin phenol reagent, J. Biol. Chem. 193 (1951) 265–275.

[19] S. Ferdinandusse, S. Denis, P.T. Clayton, A. Graham, J.E. Rees, J.T. Allen, et al., Mutations in the gene encoding peroxisomal

alpha-methylacyl-coa racemase cause adult-onset sensory motor neuropathy, Nat. Genet. 24 (2000) 188–191.

[20] T.T. Wu, R.A. Sikes, Q. Cui, G.N. Thalmann, C. Kao, C.F. Murphy, et al., Establishing human prostate cancer cell xenografts in bone: induction of osteoblastic reaction by prostate-specific antigen-producing tumors in athymic and scid/bg mice using lncap and lineage-derived metastatic sublines, Int. J. Cancer 77 (1998) 887–894.

[21] A. Degeorges, F. Wang, H.F. Frierson Jr., A. Seth, L.W. Chung, R.A. Sikes, Human prostate cancer expresses the low affinity insulin-like growth factor binding protein igfbp-rp1, Cancer Res. 59 (1999) 2787–2790.

[22] R. Aalinkeel, M.P. Nair, G. Sufrin, S.D. Mahajan, K.C. Chadha, R.P. Chawda, et al., Gene expression of angiogenic factors correlates with metastatic potential of prostate cancer cells, Cancer Res. 64 (2004) 5311–5321.

[23] S.J. Kim, H. Uehara, T. Karashima, M. McCarty, N. Shih, I.J. Fidler, Expression of interleukin-8 correlates with angiogenesis, tumorigenicity, and metastasis of human prostate cancer cells implanted orthotopically in nude mice, Neoplasia 3 (2001) 33–42.

[24] F.A. Ferrer, L.J. Miller, R.I. Andrawis, S.H. Kurtzman, P.C. Albertsen, V.P. Laudone, et al., Angiogenesis and prostate cancer: in vivo and in vitro expression of angiogenesis factors by prostate cancer cells, Urology 51 (1998) 161–167.

[25] L.F. Lee, M.C. Louie, S.J. Desai, J. Yang, H.W. Chen, C.P. Evans, et al., Interleukin-8 confers androgen-independent growth and migration of lncap: differential effects of tyrosine kinases src and fak, Oncogene 23 (2004) 2197–2205.

[26] K. Inoue, J.W. Slaton, B.Y. Eve, S.J. Kim, P. Perrotte, M.D. Balbay, et al., Interleukin 8 expression regulates tumorigenicity and metastases in androgen-independent prostate cancer, Clin. Cancer Res. 6 (2000) 2104–2119.

[27] R.W. Veltri, M.C. Miller, G. Zhao, A. Ng, G.M. Marley, G.L. Wright Jr., et al., Interleukin-8 serum levels in patients with benign prostatic hyperplasia and prostate cancer, Urology 53 (1999) 139–147.

[28] S. Lehrer, E.J. Diamond, B. Mamkine, N.N. Stone, R.G. Stock, Serum interleukin-8 is elevated in men with prostate cancer and bone metastases, Technol. Cancer Res. Treat. 3 (2004) 411.

[29] K.S. Korkmaz, C.G. Korkmaz, E. Ragnhildstveit, S. Kizildag, T.G. Pretlow, F. Saatcioglu, Full-length cdna sequence and genomic organization of human nkx3a—alternative forms and regulation by both androgens and estrogens, Gene 260 (2000) 25–36.

[30] R. Kuefer, S. Varambally, M. Zhou, P.C. Lucas, M. Loeffler, H. Wolter, et al., Alpha-methylacyl-coa racemase: expression levels of this novel cancer biomarker depend on tumor differentiation, Am. J. Pathol. 161 (2002) 841–848.

[31] J. Luo, S. Zha, W.R. Gage, T.A. Dunn, J.L. Hicks, C.J. Bennett, et al., Alpha-methylacyl-coa racemase: a new molecular marker for prostate cancer, Cancer Res. 62 (2002) 2220–2226.

[32] M.A. Rubin, M. Zhou, S.M. Dhanasekaran, S. Varambally, T.R. Barrette, M.G. Sanda, et al., Alpha-methylacyl coenzyme a racemase as a tissue biomarker for prostate cancer, J. Am. Med. Assoc. 287 (2002) 1662–1670.

[33] S. Zha, S. Ferdinandusse, S. Denis, R.J. Wanders, C.M. Ewing, J. Luo, et al., Alpha-methylacyl-coa racemase as an androgen-independent growth modifier in prostate cancer, Cancer Res. 63 (2003) 7365–7376.

[34] M. Zhou, A.M. Chinnaiyan, C.G. Kleer, P.C. Lucas, M.A. Rubin, Alpha-methylacyl-coa racemase: a novel tumor marker over-expressed in several human cancers and their precursor lesions, Am. J. Surg. Pathol. 26 (2002) 926–931.

[35] K.D. Wilkinson, K.M. Lee, S. Deshpande, P. Duerksen-Hughes, J.M. Boss, J. Pohl, The neuron-specific protein pgp 9.5 is a ubiquitin carboxyl-terminal hydrolase, Science 246 (1989) 670–673.

[36] Y. Liu, L. Fallon, H.A. Lashuel, Z. Liu, P.T. Lansbury Jr., The uch-l1 gene encodes two opposing enzymatic activities that affect alpha-synuclein degradation and parkinson's disease susceptibility, Cell 111 (2002) 209–218.

[37] G. Aumuller, H. Renneberg, M. Leonhardt, H. Lilja, P.A. Abrahamsson, Localization of protein gene product 9.5 immunoreactivity in derivatives of the human wolffian duct and in prostate cancer, Prostate 38 (1999) 261–267.

[38] R.E. Sobel, M.D. Sadar, Cell lines used in prostate cancer research: a compendium of old and new lines—part 1, J. Urol. 173 (2005) 342–359.

[39] R.E. Sobel, M.D. Sadar, Cell lines used in prostate cancer research: a compendium of old and new lines—part 2, J. Urol. 173 (2005) 360–372.

[40] M. Bisoffi, I. Klima, E. Gresko, P.N. Durfee, W.C. Hines, J.K. Griffith, et al., Expression profiles of androgen independent bone metastatic prostate cancer cells indicate up-regulation of the putative serine–threonine kinase gs3955, J. Urol. 172 (2004) 1145–1150.

[41] L. Trojan, A. Schaaf, A. Steidler, M. Haak, G. Thalmann, T. Knoll, et al., Identification of metastasis-associated genes in prostate cancer by genetic profiling of human prostate cancer cell lines, Anticancer Res. 25 (2005) 183–191.

[42] A.Y. Liu, K.D. Brubaker, Y.A. Goo, J.E. Quinn, S. Kral, C.M. Sorensen, et al., Lineage relationship between lncap and lncap-derived prostate cancer cell lines, Prostate 60 (2004) 98–108.

[43] D.W. Eib, T.M. Holling, A. Zwijsen, N. Dewulf, E. de Groot, E. van den Eijnden-van Raaij, et al., Expression of the follistatin/egf-containing transmembrane protein m7365 (tomoregulin-1) during mouse development, Mech. Dev. 97 (2000) 167–171.

[44] D. Zipori, M. Barda-Saad, Role of activin a in negative regulation of normal and tumor b lymphocytes, J. Leukoc. Biol. 69 (2001) 867–873.

[45] B. Cancilla, R.A. Jarred, H. Wang, S.L. Mellor, G.R. Cunha, G.P. Risbridger, Regulation of prostate branching morphogenesis by activin a and follistatin, Dev. Biol. 237 (2001) 145–158.

[46] C.R. Dowling, G.P. Risbridger, The role of inhibins and activins in prostate cancer pathogenesis, Endocr. Relat. Cancer 7 (2000) 243–256.

[47] G.P. Risbridger, S.L. Mellor, S.J. McPherson, J.F. Schmitt, The contribution of inhibins and activins to malignant prostate disease, Mol. Cell. Endocrinol. 180 (2001) 149–153.

[48] C. Lee, S.M. Sintich, E.P. Mathews, A.H. Shah, S.D. Kundu, K.T. Perry, et al., Transforming growth factor-beta in benign and malignant prostate, Prostate 39 (1999) 285–290.

[49] I.Y. Kim, H.J. Ahn, D.J. Zelner, J.W. Shaw, S. Lang, M. Kato, et al., Loss of expression of transforming growth factor beta type i and type ii receptors correlates with tumor grade in human prostate cancer tissues, Clin. Cancer Res. 2 (1996) 1255–1261.

[50] I.Y. Kim, H.J. Ahn, S. Lang, M.G. Oefelein, R. Oyasu, J.M. Kozlowski, et al., Loss of expression of transforming growth factor-beta receptors is associated with poor prognosis in prostate cancer patients, Clin. Cancer Res. 4 (1998) 1625–1630.

[51] S. Gery, C.L. Sawyers, D.B. Agus, J.W. Said, H.P. Koeffler, Tmeff2 is an androgen-regulated gene exhibiting antiproliferative effects in prostate cancer cells, Oncogene 21 (2002) 4739–4746.

[52] D.E. Afar, V. Bhaskar, E. Ibsen, D. Breinberg, S.M. Henshall, J.G. Kench, et al., Preclinical validation of anti-tmeff2-auristatin e-conjugated antibodies in the treatment of prostate cancer, Mol. Cancer Ther. 3 (2004) 921–932.

[53] X. Wu, A. Blanck, G. Norstedt, L. Sahlin, A. Flores-Morales, Identification of genes with higher expression in human uterine leiomyomas than in the corresponding myometrium, Mol. Hum. Reprod. 8 (2002) 246–254.

[54] S. Gery, D. Yin, D. Xie, K.L. Black, H.P. Koeffler, Tmeff1 and brain tumors, Oncogene 22 (2003) 2723–2727.

[55] P.G. Gallagher, Y. Bao, A. Prorock, P. Zigrino, R. Nischt, V. Politi, et al., Gene expression profiling reveals cross-talk between melanoma and fibroblasts: implications for host-tumor interactions in metastasis, Cancer Res. 65 (2005) 4134–4146.

[56] M.S. Bendre, D.C. Montague, T. Peery, N.S. Akel, D. Gaddy, L.J. Suva, Interleukin-8 stimulation of osteoclastogenesis and bone resorption is a mechanism for the increased osteolysis of metastatic bone disease, Bone 33 (2003) 28–37.

[57] G.F. Greene, Y. Kitadai, C.A. Pettaway, A.C. von Eschenbach, C.D. Bucana, I.J. Fidler, Correlation of metastasis-related gene expression with metastatic potential in human prostate carcinoma cells implanted in nude mice using an in situ messenger rna hybridization technique, Am. J. Pathol. 150 (1997) 1571–1582.

[58] C.J. Bieberich, K. Fujita, W.W. He, G. Jay, Prostate-specific and androgen-dependent expression of a novel homeobox gene, J. Biol. Chem. 271 (1996) 31779–31782.

[59] W.W. He, P.J. Sciavolino, J. Wing, M. Augustus, P. Hudson, P.S. Meissner, et al., A novel human prostate-specific, androgen-regulated homeobox gene (nkx3.1) that maps to 8p21, a region frequently deleted in prostate cancer, Genomics 43 (1997) 69–77.

[60] S.A. Abdulkadir, J.A. Magee, T.J. Peters, Z. Kaleem, C.K. Naughton, P.A. Humphrey, et al., Conditional loss of nkx3.1 in adult mice induces prostatic intraepithelial neoplasia, Mol. Cell. Biol. 22 (2002) 1495–1503.

[61] S. Ferdinandusse, H. Rusch, A.E. van Lint, G. Dacremont, R.J. Wanders, P. Vreken, Stereochemistry of the peroxisomal branched-chain fatty acid alpha- and beta-oxidation systems in patients suffering from different peroxisomal disorders, J. Lipid Res. 43 (2002) 438–444.

[62] S. Ferdinandusse, S. Denis, L. IJlst, G. Dacremont, H.R. Waterham, R.J. Wanders, Subcellular localization and physiological role of alpha-methylacyl-coa racemase, J. Lipid Res. 41 (2000) 1890–1896.

[63] A. Sreekumar, B. Laxman, D.R. Rhodes, S. Bhagavathula, J. Harwood, D. Giacherio, et al., Humoral immune response to alpha-methylacyl-coa racemase and prostate cancer, J. Natl Cancer Inst. 96 (2004) 834–843.

[64] C.G. Rogers, G. Yan, S. Zha, M.L. Gonzalgo, W.B. Isaacs, J. Luo, et al., Prostate cancer detection on urinalysis for alpha methylacyl coenzyme a racemase protein, J. Urol. 172 (2004) 1501–1503.

[65] C.N. Larsen, B.A. Krantz, K.D. Wilkinson, Substrate specificity of deubiquitinating enzymes: ubiquitin c-terminal hydrolases, Biochemistry 37 (1998) 3358–3368.

[66] C.N. Larsen, J.S. Price, K.D. Wilkinson, Substrate binding and catalysis by ubiquitin c-terminal hydrolases: identification of two active site residues, Biochemistry 35 (1996) 6735–6744.

[67] J.F. Doran, P. Jackson, P.A. Kynoch, R.J. Thompson, Isolation of pgp 9.5, a new human neurone-specific protein detected by high-resolution two-dimensional electrophoresis, J. Neurochem. 40 (1983) 1542–1547.

[68] I.N. Day, R.J. Thompson, Molecular cloning of cdna coding for human pgp 9.5 protein. A novel cytoplasmic marker for neurones and neuroendocrine cells, Fed. Eur. Biochem. Soc. Lett. 210 (1987) 157–160.

[69] H.C. Ardley, G.B. Scott, S.A. Rose, N.G. Tan, P.A. Robinson, Uch-l1 aggresome formation in response to proteasome impairment indicates a role in inclusion formation in parkinson's disease, J. Neurochem. 90 (2004) 379–391.

[70] Y.L. Wang, A. Takeda, H. Osaka, Y. Hara, A. Furuta, R. Setsuie, et al., Accumulation of beta- and gamma-synucleins in the ubiquitin carboxyl-terminal hydrolase l1-deficient gad mouse, Brain Res. 1019 (2004) 1–9.

[71] R. Rodriguez, J.M. Pozuelo, R. Martin, N. Henriques-Gil, M. Haro, R. Arriazu, et al., Presence of neuroendocrine cells during postnatal development in rat prostate: immunohistochemical, molecular, and quantitative study, Prostate 57 (2003) 176–185.

[72] B. Ermisch, K. Schwechheimer, Protein gene product (pgp) 9.5 in diagnostic (neuro-) oncology. An immunomorphological study, Clin. Neuropathol. 14 (1995) 130–136.

[73] T. Takano, A. Miyauchi, F. Matsuzuka, H. Yoshida, Y. Nakata, K. Kuma, et al., Pgp9.5 mrna could contribute to the molecular-based diagnosis of medullary thyroid carcinoma, Eur. J. Cancer 40 (2004) 614–618.

[74] T. Takase, K. Hibi, T. Yamazaki, H. Nakayama, M. Taguchi, Y. Kasai, et al., Pgp9.5 overexpression in esophageal squamous cell carcinoma, Hepatogastroenterology 50 (2003) 1278–1280.

[75] J. Rode, A.P. Dhillon, J.F. Doran, P. Jackson, R.J. Thompson, Pgp 9.5, a new marker for human neuroendocrine tumours, Histopathology 9 (1985) 147–158.

[76] T. Otsuki, K. Yata, A. Takata-Tomokuni, F. Hyodoh, Y. Miura, H. Sakaguchi, et al., Expression of protein gene product 9.5 (pgp9.5)/ubiquitin-c-terminal hydrolase 1 (uchl-1) in human myeloma cells, Br. J. Haematol. 127 (2004) 292–298.

[77] E. Bollito, A. Berruti, M. Bellina, A. Mosca, E. Leonardo, R. Tarabuzzi, et al., Relationship between neuroendocrine features and prognostic parameters in human prostate adenocarcinoma, Ann. Oncol. 12 (Suppl. 2) (2001) S159–S164.

[78] P.A. di Sant'Agnese, K.L. de Mesy Jensen, Neuroendocrine differentiation in prostatic carcinoma, Hum. Pathol. 18 (1987) 849–856.

[79] T. Krupski, G.R. Petroni, H.F. Frierson Jr., J.U. Theodorescu, Microvessel density, p53, retinoblastoma, and chromogranin a immunohistochemistry as predictors of disease-specific survival following radical prostatectomy for carcinoma of the prostate, Urology 55 (2000) 743–749.

A molecular correlate to the Gleason grading system for prostate adenocarcinoma

Lawrence True*†, Ilsa Coleman‡, Sarah Hawley§, Ching-Ying Huang‡, David Gifford‡, Roger Coleman‡, Tomasz M. Beer¶, Edward Gelmann‖, Milton Datta**, Elahe Mostaghel‡††, Beatrice Knudsen§, Paul Lange†, Robert Vessella†, Daniel Lin†, Leroy Hood‡‡§§, and Peter S. Nelson*†‡‡††¶¶

Departments of *Pathology and †Urology, University of Washington, Seattle, WA 98195; Divisions of ‡Human Biology, §Public Health Sciences, and ††Clinical Research, Fred Hutchinson Cancer Research Center, Seattle, WA 98109; ¶Department of Medicine and Cancer Institute, Oregon Health & Science University, Portland, OR 97239; ‖Lombardi Comprehensive Cancer Center, Georgtown University, Washington, DC 20007; **Department of Pathology, Emory University, Atlanta, GA 30322; and ‡‡Institute for Systems Biology, Seattle, WA 98103

Contributed by Leroy Hood, May 11, 2006

Adenocarcinomas of the prostate can be categorized into tumor grades based on the extent to which the cancers histologically resemble normal prostate glands. Because grades are surrogates of intrinsic tumor behavior, characterizing the molecular phenotype of grade is of potential clinical importance. To identify molecular alterations underlying prostate cancer grades, we used microdissection to obtain specific cohorts of cancer cells corresponding to the most common Gleason patterns (patterns 3, 4, and 5) from 29 radical prostatectomy samples. We paired each cancer sample with matched benign lumenal prostate epithelial cells and profiled transcript abundance levels by microarray analysis. We identified an 86-gene model capable of distinguishing low-grade (pattern 3) from high-grade (patterns 4 and 5) cancers. This model performed with 76% accuracy when applied to an independent set of 30 primary prostate carcinomas. Using tissue microarrays comprising >800 prostate samples, we confirmed a significant association between high levels of monoamine oxidase A expression and poorly differentiated cancers by immunohistochemistry. We also confirmed grade-associated levels of defender against death (DAD1) protein and HSD17β4 transcripts by immunohistochemistry and quantitative RT-PCR, respectively. The altered expression of these genes provides functional insights into grade-associated features of therapy resistance and tissue invasion. Furthermore, in identifying a profile of 86 genes that distinguish high- from low-grade carcinomas, we have generated a set of potential targets for modulating the development and progression of the lethal prostate cancer phenotype.

carcinoma | monoamine oxidase A | microarray | expression profile

The prognosis and choice of therapy for prostate cancer is based primarily on three parameters obtained at the time of diagnosis: clinical stage, serum prostate-specific antigen (PSA), and the Gleason score of the cancer (1). The Gleason grading system, which is based on microscopic tumor architecture, consists of five histological patterns that annotate cancers into categories exhibiting well differentiated (pattern 1) to poorly differentiated (pattern 5) features (2, 3). A number from 1 to 5 is assigned to the most prevalent pattern. A second number, also from 1 to 5, is assigned to the second most prevalent pattern. The Gleason grade, which is the sum of these two numbers, has a value between 2 and 10. In current practice, the vast majority of prostate cancers have a Gleason score of ≥6 (4, 5). Hence, tumors composed of patterns 3, 4, and/or 5 are considered clinically significant. The reporting of individual Gleason patterns is not a trivial distinction, because the amount of pattern 4 and the presence of any pattern 5 has been highly correlated with probability of cancer dissemination, response to therapy, disease outcome, patient-management decisions, and clinical-trial enrollment (6, 7). Numerous studies have demonstrated a direct correlation between Gleason score and clinical measurements of disease outcome, including death due to tumor within 15 years and likelihood of remaining free of biochemical evidence of disease recurrence after either definitive, potentially curative radical prostatectomy or radiation therapy (8). Although different Gleason patterns are histologically distinctive, the molecular features underlying these tumor phenotypes are not precisely defined. In this study, we sought to characterize the molecular profile of prostate carcinomas of specific Gleason patterns. Tumor cell transcript levels were used to develop a model capable of distinguishing the low-grade (pattern 3) from high-grade (patterns 4 and 5) tumors. We validated the predictive power of the model by using an independent set of primary prostate cancers and confirmed grade-associated differences in protein-expression levels using a third sample cohort. Together, these results identify both consistent and divergent features of the molecular framework that underlies the histological classification of cancer grade.

Results and Discussion

Gene-Expression Profiles Associated with Prostate Cancer Grades. To identify molecular alterations correlating with histological tumor grade, we used laser-capture microdissection to exclusively acquire the epithelial cell component of prostate carcinoma foci corresponding to individual Gleason pattern 3, 4, or 5 cancers. After linear amplification, gene-expression alterations in tumor cells were measured by cDNA microarray hybridizations in a head-to-head fashion against patient-matched microdissected benign secretory epithelial cells. A total of 121 benign and neoplastic samples from 59 radical prostatectomies and 30 prostate needle core biopsies contributed to the analysis.

To assess the generalized applicability and consistency of the methods, we first sought to identify consistent prostate cancer-associated transcript alterations irrespective of grade. Using microdissected epithelium from radical prostatectomy samples, we identified 736 genes with altered expression levels between benign and neoplastic epithelium (false discovery rate <0.01%). This cohort included several genes previously reported to be differentially expressed in prostate cancers, such as *hepsin*, *AMACR*, and *CAMKK2* (Fig. 1*A*) (9–12). These findings provided validation that our methods replicated results of earlier expression-profiling studies, despite using the very small sample quantities obtained by laser microdissection and subjecting the

Conflict of interest statement: No conflicts declared.

Abbreviations: IHC, immunohistochemical; MAOA, monoamine oxidase A; PAM, prediction analysis for microarrays; TMA, tissue microarray.

Data deposition: The microarray data sets reported in this paper have been deposited in the Gene Expression Omnibus (GEO) database (accession no. GSE5132).

§§To whom correspondence may be addressed. E-mail: lhood@systemsbiology.org.

¶¶To whom correspondence may be addressed at: Division of Human Biology, Fred Hutchinson Cancer Research Center, Mailstop D4-100, 100 Fairview Avenue, Seattle, WA 98109-1024. E-mail: pnelson@fhcrc.org.

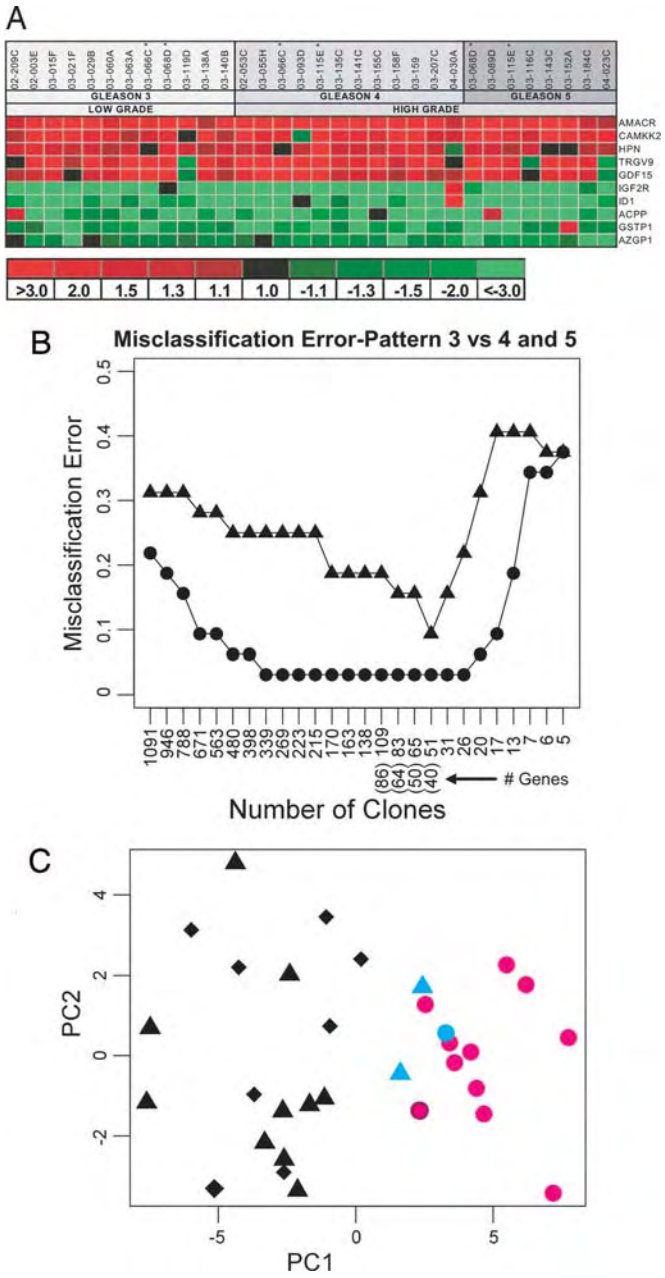

Fig. 1. Gene-expression changes associated with prostate cancer grade. (*A*) Genes differentially expressed between microdissected benign and neoplastic prostate epithelium were identified in a supervised analysis of transcript profiles of 32 matched samples from 29 individuals. A Statistical Analysis Of Microarrays (SAM) one-sample *t* test comparing cancerous epithelium to matched benign epithelium across all Gleason patterns identified 736 differentially expressed genes (false discovery rate ≤0.05%). Cancer-associated transcript alterations for several genes with previously described alterations in prostate carcinoma are shown. (*B*) Identification of gene-expression alterations predictive of Gleason pattern. PAM analysis of gene-expression profiles generated from microdissected Gleason pattern 3, 4, and 5 cancers. Circles represent the training error. Triangles represent the leave-one-out cross-validation error. The *x* axis shows the number of array clones (and corresponding unique genes) used for classification. (*C*) Principal-components analysis of grade-specific prostate cancers using the 40-gene (51-clone) Gleason pattern classifier. For each sample, the score on the first (*x* axis) and second (*y* axis) principal component is plotted. Gleason pattern 3 (circle) samples are generally distinct from Gleason pattern 4 and 5 sample space (triangle and diamond, respectively). Pattern 4 and 5 samples were intermixed, indicating a high degree of molecular similarity. Three misclassified samples (under cross-validation of the 40-gene model) between pattern 3 and pattern 4/5 cancers are denoted in blue.

RNA from these samples to amplification and transcript quantitation by microarray analysis.

To identify gene-expression alterations that associated with specific Gleason patterns, we used a supervised-learning approach, Prediction Analysis for Microarrays (PAM) that represents a modification of standard nearest-neighbor classification (13). Models comprising 40, 64, and 86 genes were able to partition Gleason 3 vs. Gleason 4 and 5 cancers with 90%, 84%, and 81% accuracy (under leave-one-out cross-validation) (Fig. 1*B*). We were unable to identify a cohort of genes that could distinguish between pattern 4 and 5 cancers with sufficiently high accuracy to be useful, suggesting a high degree of similarity between these cancer histologies or substantial molecular heterogeneity in one or both of these groups. Therefore, we grouped pattern 4 and 5 cancers together for subsequent comparisons. Principal-components analysis of the 40-gene model demonstrated segregation of cancers according to histological grade, with only one pattern 4/5 cancer misclassified as a pattern 3, and two pattern 3 cancers misclassified as pattern 4/5 (Figs. 1*C* and 2*A*). Rereview of the histology and the specific composition of cells acquired by laser-capture microdissection did not alter the histological classification of these samples. Although Gleason patterns can be reproducibly categorized (14), there are clear examples of heterogeneity in clinical behavior within each histological category (15). Further studies are required to determine whether molecular signatures within a specific cancer pattern exhibit prognostic power.

Performance Characteristics of the Gleason Grade Classifier. To determine the general applicability of the Gleason pattern classifier, we generated and analyzed an independent prostate cancer gene-expression data set derived from microdissected matched benign and neoplastic epithelium from 30 prostate needle biopsies. We measured expression alterations by microarray hybridization and assessed the models that provided the greatest discriminatory power in the original prostatectomy samples. The classifier comprised 86 genes (109 clones), including the 40 genes with 90% discriminatory power in the original radical prostatectomy cases performed with highest accuracy, producing a 76% overall correct classification rate ($P = 0.056$, Fisher's exact test) (Fig. 2*B*) on this independent sample set. Of the 12 cancers histologically called Gleason pattern 3, all but one was correctly classified. Of the cancers with a histological classification of 4 or 4 + 5, 6 of 11 were correctly identified (Fig. 2*B*). As expected, microdissected samples recognized to contain mixed grades of 3 + 4 or 4 + 3 cancer cells were divided between pattern 3 or pattern 4 molecular categories. These results suggest that pattern 3 cancers exhibit relatively consistent molecular alterations, whereas cancers with histological features of patterns 4 and 5 are more diverse and, in some cases, exhibit molecular features common to pattern 3 cancers.

We next attempted to compare our results with other reports correlating prostate tumor gene expression with grade. These comparisons were problematic, because all publicly available prostate cancer data sets generated expression profiles and classifiers based on Gleason-sum scores rather than individual patterns. For example, a given Gleason-sum score 8 cancer could be composed of patterns 5 + 3 or 4 + 4. Reports by Singh *et al.* (11) and LaPointe *et al.* (12) identified 29 and 42 genes, respectively, that statistically associated with Gleason-sum score. However, only three genes, *SPARC*, *BGN*, and *COL1A2*, were in common between these analyses. None of the genes comprising our classifier were present in the published grade-associated gene sets. An additional contributor to these discrepancies concerns the use of samples that, although enriched for tumor, also contain variable amounts of tumor-adjacent stroma, benign glands, and inflammatory cells. Alterations in the expression of genes in tumor-adjacent stroma is well recognized (16). In the

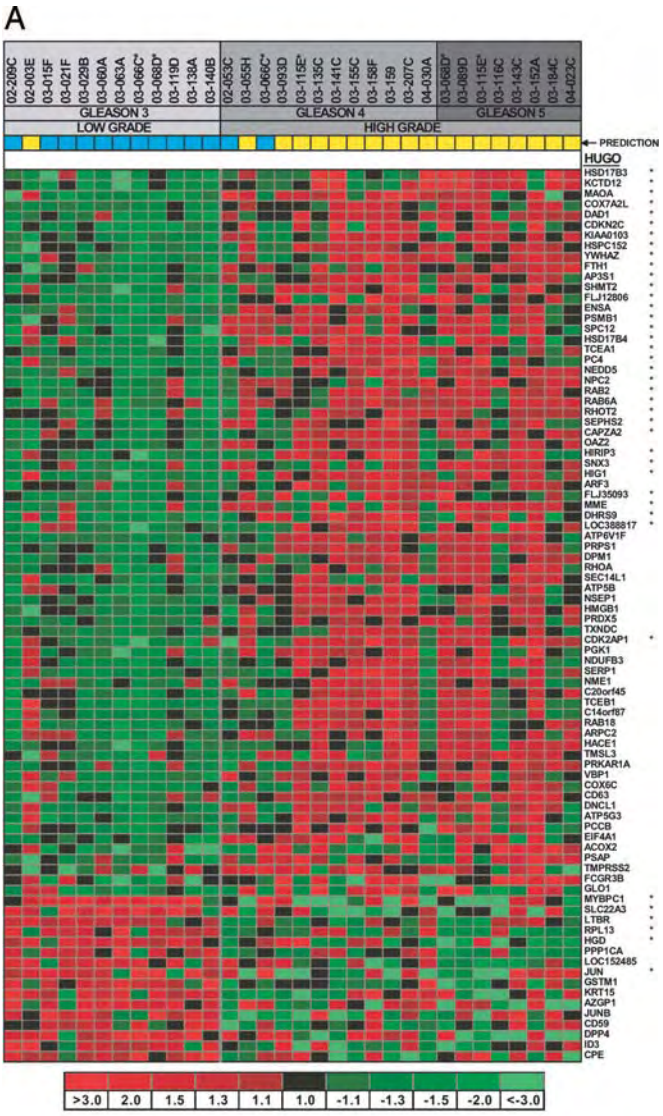

B

		Predicted	
		Gleason 3	Gleason 4 or 5
Observed	Gleason 3	11	1
	Gleason 3+4	3	2
	Gleason 4	5	5
	Gleason 4+3	1	1
	Gleason 5	0	1

Fig. 2. Genes associated with specific Gleason pattern prostate cancers. (*A*) Shown are the 86 genes exhibiting the greatest discriminatory power to partition cancer grades using an independent set of prostate cancer tissues. Genes are ordered according to *t* test score. The 40 genes used in the original PAM model are denoted by asterisks. (*B*) Application of the 86-gene Gleason classification model to an independent test set of 23 prostate cancers of singular pattern (e.g., 3 + 3) or exclusively high grade (4 + 4 or 4 + 5) resulted in an overall classification accuracy of 74%. The predicted pattern of 7 additional cancers of mixed low grade and high grade (3 + 4 and 4 + 3) varied between pattern 3 and pattern 4/5. The functional properties of grade-classifying genes are annotated in Table 1, which is published as supporting information on the PNAS web site.

context of these studies, the expression of *SPARC* has been shown to be up-regulated in the stroma adjacent to non-small-cell lung cancers (17) and pancreatic carcinomas (18) and may be similarly overexpressed in prostate cancer-adjacent stroma. A final source of discrepancies between studies involves technical variables, attributable, for example, to the use of different platforms (cDNA arrays vs. Affymetrix chips) and the necessity of amplifying RNA before hybridization.

Although the grade-discriminatory gene sets derived from our analyses and those of prior studies exhibited no concordance, we explored the ability of the Gleason grade classifier to partition prostate cancers in available data sets that were composed of singular grade combinations such as 3 + 3 and 4 + 4. Of 86 genes used in our classifier, 77 were present in the study by LaPointe *et al.*, with sufficient data to allow for grade-associated analyses. Unsupervised hierarchical clustering of samples using these 77 genes produced two major clusters generally partitioned according to grade. Of 26 tumors with Gleason 3 + 3 histology, 19 (73%) were correctly classified, as were 11 of 15 tumors (73%) with 4 + 4 or 4 + 5 Gleason patterns.

Characteristics and Confirmation of Gleason Grade-Associated Molecular Alterations. Several genes that we found to be associated with prostate cancer cell differentiation patterns have been linked to cancer grade or stage classifications. A study of breast carcinomas found a statistical relationship between increased expression of the antioxidant enzyme peroxiredoxin 5 (PRDX5) and larger tumor size, positive lymph node status, and shorter survival (19). Elevated levels of the transcription elongation factor TCEB1/Elongin C are associated with advanced androgen-independent prostate cancers (20), and changes in the subcellular localization of the membrane metalloendopeptidase MME/CD10 expression are linked to prostate cancer grade (21). Immunohistochemical analysis of the Akt-regulated transcriptional repressor NSEP/YB-1 demonstrates a strong positive correlation with Gleason grade (22). NSEP/YB-1 may influence cancer progression through multiple mechanisms that include enhancement of anchorage-independent cell growth and up-regulation of the *p*-glycoprotein multidrug-resistance protein (22, 23).

Many genes exhibiting altered expression in high- relative to low-grade prostate cancers possess characteristics supporting potential roles in cancer cell survival, invasion, or metastasis. Of the 86 genes we used for grade classification, 6 are located on chromosome 8. Of these, 4 map to 8q21–23, a region shown to be amplified in >40% of primary prostate cancers in association with higher cancer grades (24). The expression of 4 genes involved in aspects of sex hormone metabolism or regulation were increased in higher-grade cancers, including two members of the 17β-hydroxysteroid dehydrogenase (HSD) family, HSD17β3 and HSD17β4. The 3-α-hydroxysteroid dehydrogenase DHRS9 is capable of catalyzing the conversion of 3-α-androstanediol to dihydrotestosterone (25) and also contributes to the β-oxidation of fatty acids. The expression of HSD17β4, also known as D-bifunctional protein, was recently shown to be up-regulated in neoplastic prostate epithelium (26). We confirmed this result using quantitative RT-PCR analysis of microdissected prostate epithelium and further confirmed the grade-associated elevation of HSD17β4 transcripts found in the microarray-based analyses (see *Supporting Materials and Methods* and Fig. 4, which are published as supporting information on the PNAS web site). Together, these results suggest the emergence of mechanisms that favor intracrine utilization of alternative androgen precursors by tumor cells. Five members of the *ras* homologue gene family *RHOT2*, *RHOA*, *RAB2*, *RAB6A*, and *RAB18* were up-regulated in high-grade cancers. The *RAB18*-related gene, *RAB25*, was recently shown to influence the malignant potential of breast and ovarian cancers, suggesting that members of this gene family may be general mediators of epithelial cancer progression (27). The products of *RHOA*, *CAPZA2*, *HMGB1*, *NM23H1*, *CD63*, and Saposin C have all been

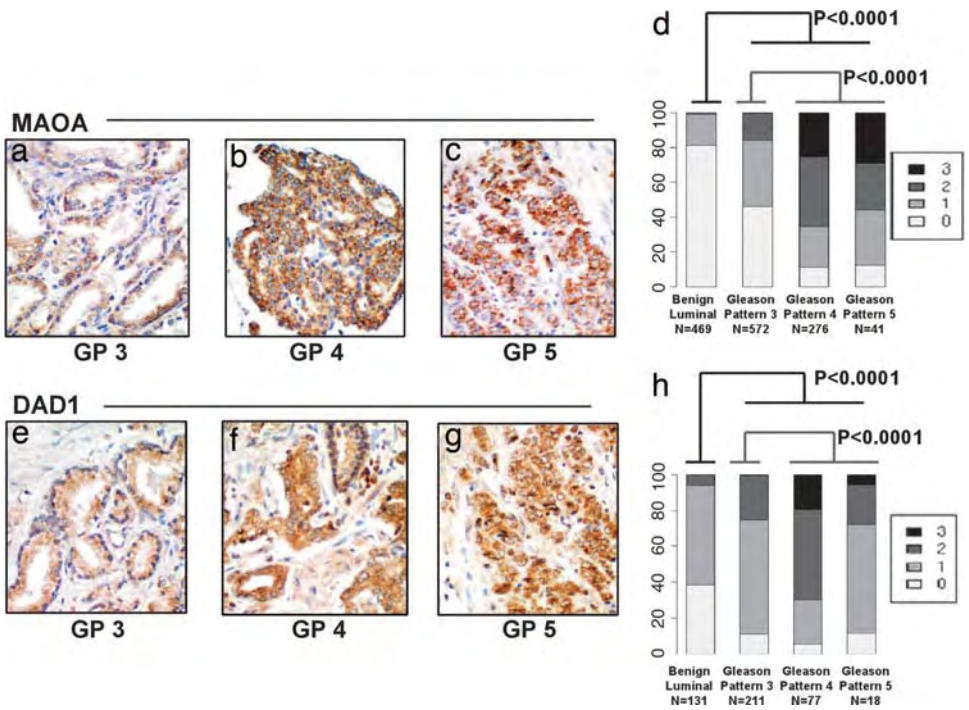

Fig. 3. IHC analysis of Gleason grade-associated gene expression. Representative immunohistochemical staining of Gleason pattern 3 (*a* and *e*), 4 (*b* and *f*), and 5 (*c* and *g*) prostate adenocarcinoma for MAOA (*a–c*) and DAD1 (*e–g*) expression. Magnifications are ×400. Summary of MAOA (1,358 scoreable samples) (*d*) and DAD1 (437 scoreable samples) (*d* and *h*) expression quantitation in tissue cores comprised of benign secretory epithelium and specific Gleason pattern adenocarcinomas.

shown to directly modulate tumor progression through enhanced cell motility, invasion, or metastasis.

Immunohistochemical (IHC) Analysis of Gleason Grade-Associated Protein Expression. In current clinical practice, diagnostic and prognostic cancer markers are most commonly assessed by using IHC quantitation. We sought to determine whether grade-associated alterations identified through transcript profiling would have corresponding changes in protein levels discernable by IHC. Although immunoperoxidase histochemistry is an imprecise method of protein quantification, it is the only technique currently available for assessing protein levels in small tissue samples and localizing expression to specific cell types. We focused on two pathways known to be associated with prostate cancer behavior: neuroendocrine effectors and apoptosis (28, 29–31). Of the 80 genes in the grade classifier with known biological functions, 5 are reported to modulate neuropeptide or amine metabolism: monoamine oxidase A (*MAOA*), *YWHAZ/14–3-3-ζ*, *OAZ2*, *CPE*, and *SLC22A3*. MAOA is encoded by a polymorphic gene located on the X chromosome that catalyzes the oxidative deamination of biogenic amines, such as catecholamines and indolamine transmitters, throughout the body. Gene variants conferring up to 50-fold differences in MAOA activity have been associated with a variety of neurological and psychosocial disorders, but few studies of MAOA in the context of cancer biology have been reported. The physiological functions of amine oxidases remain to be completely established, but amine metabolism is linked to essential cellular processes such as cell growth and differentiation (32). The byproducts of amine metabolism include H_20_2 and hydroxyl radicals that may contribute to aspects of tumorigenesis, including redox-sensitive pathways such as MAP-kinase signaling (33).

To further characterize the association between *MAOA* expression and the differentiation state of prostate cancers, we measured MAOA protein levels by IHC on panels of tissue microarrays (TMAs) representing independent patient cohorts not evaluated in the initial analyses of transcript levels. A comparison of 469 benign and 889 cancerous samples demonstrated that MAOA protein expression was elevated in cancerous epithelium relative to benign secretory epithelium ($P < 0.0001$, proportional odds-regression analysis) (34) (Fig. 3 *a–d*), and MAOA expression was significantly elevated in Gleason 4 or 5 samples relative to Gleason 3 samples ($P < 0.0001$, proportional odds-regression analysis). The finding that high levels of expression of MAOA protein characterizes high-grade prostate carcinoma raises the possibility that patients on long-term MAOA inhibitors might have lower frequencies of high-grade prostate cancer if MAOA plays a mechanistic role in the development of high-grade prostate cancer.

Six genes functionally linked to the regulation of apoptosis were present in the cohort of grade-classifying genes. Of these, the gene encoding defender against death (DAD1) provides an intriguing link between apoptosis and the influence of tumor survival factors associated with perineural invasion (PNI). DAD1 is a downstream target of the NFkB survival pathway and exhibits an antiapoptotic function (35). *In vitro* studies modeling PNI-associated prostate cancer growth measured increased proliferation, reduced apoptosis, and elevated expression of NFkB and DAD1 in tumor cells located in proximity to ganglia and nerve tissue (36). We evaluated the expression of DAD1 protein by IHC in TMAs of formalin-fixed radical prostatectomy cores that, together, comprised 131 benign and 306 cancerous samples. High DAD1 expression was significantly associated with cancerous epithelium relative to benign secretory epithelium ($P < 0.0001$). In agreement with the transcript analyses, DAD1 protein levels also exhibited a strong association with Gleason pattern. Cancers of patterns 4 and 5 were more likely to stain intensely than low-grade cancer of pattern 3 ($P < 0.0001$) (Fig. 3 *e–h*).

Conclusions

In this study, we have identified a panel of molecular alterations that associate with the histological interpretation of prostate cancer grades. The panel performed with high accuracy across three independent panels of prostate adenocarcinomas processed and analyzed by using divergent techniques. Gleason patterns 4 and 5 cancers were virtually indistinguishable at the molecular level with our model. This finding is in accord with the clinical observation that Gleason patterns 4 and 5 tumors are associated with similar prognoses and, thus, are managed identically (37). If demonstrated to be mechanistically involved in cancer progression, the proteins encoded by grade-discriminating genes could serve as targets for pharmaceutical inhibition. Grade-discriminatory proteins may also have utility as serum markers for identifying high-grade prostate cancer. In this context, the association of MAOA expression with prostate cancer and grade is a finding that further implicates neuroendocrine features as mediators of prostate carcinogenesis. This finding has clinical importance, because the presence and extent of a neuroendocrine component in a prostate carcinoma correlates with tumor aggressiveness (37). The ready availability of monamine oxidase inhibitors offers an immediate opportunity to determine the clinical relevance of this finding.

Materials and Methods

Tissue Acquisition. All materials were acquired and used in conformity with Institutional Review Board-approved protocols at the University of Washington and Oregon Health & Science University. Two types of tissue were used for this study: fresh, nonfixed tissue as a source of RNA for laser microdissection and formalin-fixed, paraffin-embedded tissue for IHC studies. The nonfixed tissue consisted of frozen tissue blocks from radical prostatectomies and an independent sample set of frozen tissue blocks containing prostate needle core biopsies. Details of tissue handling are provided in *Supporting Materials and Methods*. Fixed tissue samples consisted of two types: blocks corresponding to the fresh tissue samples that were used for the laser microdissection preparations and TMAs.

Laser-Capture Microdissection (LCM) and RNA Preparation. Frozen sections (8 μm) were cut from optimal cutting temperature medium (OCT) blocks and immediately fixed in cold 95% ethanol. After brief (5–10 seconds) staining with hematoxylin using the HistoGene staining solution (Arcturus Engineering Mountain View, CA), the sections were dehydrated in 100% ethanol, followed by xylenes (per the manufacturer's protocol). Epithelial cells (≈5,000) from both histologically benign glands and cancer glands were separately laser-capture microdissected by using the Arcturus PixCell II instrument. Only one Gleason pattern was included in each laser-captured cancer sample. A total of 32 different Gleason patterns were captured from the 29 radical prostatectomy samples: 12 Gleason pattern 3, 12 Gleason pattern 4, and 8 Gleason pattern 5 samples. A total of 30 Gleason patterns were captured from the 30 needle core biopsy samples, with some samples comprising combinations of Gleason patterns. Matched benign epithelium was captured for each cancer sample, for a total of 121 samples. Digital photographs were taken of tissue sections before, during, and after LCM and assessed independently by two investigators to confirm the Gleason patterns of the laser-captured cells. RNA extraction and amplification were performed by using standard procedures described in *Supporting Materials and Methods*.

Microarray Hybridization, Data Acquisition, and Analysis. Prostate Expression Database cDNA microarrays were prepared on polyL-lysine-coated glass microscope slides by using a robotic spotting tool as described in ref. 38. cDNA probes were made from 2 μg of amplified RNA and randomly labeled with either Cy3 or Cy5 dye to account for dye bias. Patient-matched normal and cancer probes were combined, filtered, and competitively hybridized to microarrays under a coverslip for 14 h at 63°C. Further details are provided in *Supporting Materials and Methods*.

Fluorescent array images were collected for both Cy3 and Cy5 emissions by using a GenePix 4000B fluorescent scanner (Axon Instruments, Foster City, CA). The image-intensity data were gridded and extracted by using GENEPIX PRO 4.1 software. The specifics of microarray data processing are provided in *Supporting Materials and Methods*. Microarray data sets from this study are deposited in the GEO respository under accession no. GSE5132.

To compare the overall expression patterns of all radical prostatectomy cancer samples to their patient-matched normal samples, the filtered log-ratio measurements were analyzed by using the Significance Analysis of Microarrays (SAM) procedure (39) (www-stat.stanford.edu/~tibs/SAM). In this analysis, a one-sample *t* test was used to determine which genes were significantly differentially expressed between cancer samples and their patient-matched normal samples. We call the set of significant genes the expression profile associated with prostate cancer.

To identify gene-expression alterations associated with specific Gleason patterns, we used Prediction Analysis for Microarrays (PAM) (13), a supervised classification method. Full technical details are provided on the PAM web site (www-stat.stanford.edu/~tibs/PAM). We divided the radical prostatectomy samples into two classes (Gleason pattern 3 and Gleason pattern 4 or 5) and applied PAM to identify several small gene cohorts that classified the samples with low error rates under leave-out-one cross-validation. To evaluate the predictive properties of these gene sets, we classified an independent sample set of Gleason pattern cancers composed of prostate needle core biopsy samples. An additional visual assessment of the degree to which our gene model partitioned the radical prostatectomy samples by Gleason pattern was undertaken by using principal-components analysis of the samples (40).

Quantitative (q)RT-PCR. cDNA was generated from 1 μg of aRNA by using 2 μg of random hexamers for priming reverse transcription by SuperScript II (200 units per reaction; Invitrogen). qRT-PCRs were done in triplicate, by using ≈5 ng of cDNA, 0.2 mM each primer, and SYBR green PCR master mix (Applied Biosystems) in a 20-μl reaction volume. Reactions were carried out and analyzed by using an Applied Biosystems 7900 sequence detector. Samples were normalized to the cycle threshold value obtained during the exponential amplification of RPL13A. The expression level of HSD17B4 was calculated. Values were reported as the ratio of gene expression in neoplastic to normal epithelium. Additional details and primer sequences are provided in *Supporting Materials and Methods*.

TMAs. Eight TMAs were used for these studies. All samples in all arrays were provided in duplicate. Two arrays of predominantly primary prostate cancers (of 159 and 234 samples, respectively) have been described (41). Six arrays represented a range of Gleason grades, a mix of prostate cancer tissue of different biologic states [normal, atrophy, benign prostatic hyperplasia (BPH), prostatic intraepithelial neoplasia (PIN), primary prostate carcinoma, and metastatic prostate carcinoma], and a mix of different normal and neoplastic tissues. Altogether, 469 unique samples of benign prostate glands and 889 unique samples of primary prostate carcinoma (572 Gleason pattern 3, 276 Gleason pattern 4, and 41 Gleason pattern 5) were used for MAOA immunostaining. And 131 unique samples of benign prostate glands and 306 unique samples of primary prostate carcinoma (211 Gleason pattern 3, 77 Gleason pattern 4, and 18 Gleason pattern 5) were used for DAD1 immunostaining.

IHC. Antibodies recognizing MAOA (sc-20156; Santa Cruz Biotechnology) and DAD1 (sc-25557; Santa Cruz Biotechnology) were used to stain TMAs composed of benign and neoplastic prostate tissues. Specificity of labeling was confirmed by both omission of the primary antibody and immunostaining the sections with a primary antibody against an irrelevant antigen. Immunolocalization was done by using a three-step avidin–biotin–peroxidase method. The sections were counterstained with hematoxylin. Further details are provided in *Supporting Materials and Methods*.

IHC stains were evaluated by using the following categorical compositional scale: 0, no expression; 1, ≤5% of the cells express the antigen; 2, 5–20% of the cells express the antigen; and 3, 20–100% of cells express the antigen. The following cell types were evaluated: secretory and basal epithelial, high-grade PIN, and Gleason pattern 3, pattern 4, and pattern 5 tumor cells. When a section had several Gleason patterns, each pattern was scored.

To test for differences in the staining intensity of different cell types, we used a proportional-odds model and included the covariates Gleason grade and tissue source. The model was fit in SAS (SAS Institute, Cary, NC), implementing a generalized estimating-equations approach to account for multiple sections from the same patient. Further details of the analytical methods are provided in *Supporting Materials and Methods*.

We thank Mahul Amin for helpful suggestions and assistance with study design; Devon Felise and Julie Hahn for tissue collection; members of the immunohistochemistry laboratories at the University of Washington (supervisor, Farinaz Shokri) and Fred Hutchinson Cancer Research Center (Kimberly Adolphson and Linda Cherepow); Ruth Dumpit for assistance with microarray hybridizations; members of the Nelson laboratory for helpful discussions; Andrew Glass and Lukas Bubendorf for TMA construction; and Ying Zhang of the Biostatistics and Bioinformatics Shared Resource of the Lombardi Comprehensive Cancer Center for statistical support. This work was supported by Department of Defense Grants DAMD17-03-2-033 and PC041158 and National Institutes of Health Grants P01CA85859, DK65204, and the Pacific Northwest Prostate Cancer SPORE Grant P50CA97186.

1. Partin, A. W., Kattan, M. W., Subong, E. N., Walsh, P. C., Wojno, K. J., Oesterling, J. E., Scardino, P. T. & Pearson, J. D. (1997) *J. Am. Med. Assoc.* **277,** 1445–1451.
2. Gleason, D. F. & Mellinger, G. T. (1974) *J. Urol.* **111,** 58–64.
3. Epstein, J. I., Allsbrook, W. C., Jr., Amin, M. B. & Egevad, L. L. (2005) *Am. J. Surg. Pathol.* **29,** 1228–1242.
4. Epstein, J. I. (2000) *Am. J. Surg. Pathol.* **24,** 477–478.
5. Albertsen, P. C., Hanley, J. A., Barrows, G. H., Penson, D. F., Kowalczyk, P. D., Sanders, M. M. & Fine, J. (2005) *J. Natl. Cancer Inst.* **97,** 1248–1253.
6. Chan, T. Y., Partin, A. W., Walsh, P. C. & Epstein, J. I. (2000) *Urology* **56,** 823–827.
7. Rasiah, K. K., Stricker, P. D., Haynes, A. M., Delprado, W., Turner, J. J., Golovsky, D., Brenner, P. C., Kooner, R., O'Neill, G. F., Grygiel, J. J., *et al.* (2003) *Cancer* **98,** 2560–2565.
8. Albertsen, P. C., Fryback, D. G., Storer, B. E., Kolon, T. F. & Fine, J. (1995) *J. Am. Med. Assoc.* **274,** 626–631.
9. Magee, J. A., Araki, T., Patil, S., Ehrig, T., True, L., Humphrey, P. A., Catalona, W. J., Watson, M. A. & Milbrandt, J. (2001) *Cancer Res.* **61,** 5692–5696.
10. Dhanasekaran, S. M., Barrette, T. R., Ghosh, D., Shah, R., Varambally, S., Kurachi, K., Pienta, K. J., Rubin, M. A. & Chinnaiyan, A. M. (2001) *Nature* **412,** 822–826.
11. Singh, D., Febbo, P. G., Ross, K., Jackson, D. G., Manola, J., Ladd, C., Tamayo, P., Renshaw, A. A., D'Amico, A. V., Richie, J. P., *et al.* (2002) *Cancer Cell* **1,** 203–209.
12. Lapointe, J., Li, C., Higgins, J. P., van de Rijn, M., Bair, E., Montgomery, K., Ferrari, M., Egevad, L., Rayford, W., Bergerheim, U., *et al.* (2004) *Proc. Natl. Acad. Sci. USA* **101,** 811–816.
13. Tibshirani, R., Hastie, T., Narasimhan, B. & Chu, G. (2002) *Proc. Natl. Acad. Sci. USA* **99,** 6567–6572.
14. Allsbrook, W. C., Jr., Mangold, K. A., Johnson, M. H., Lane, R. B., Lane, C. G., Amin, M. B., Bostwick, D. G., Humphrey, P. A., Jones, E. C., Reuter, V. E., *et al.* (2001) *Hum. Pathol.* **32,** 74–80.
15. Graefen, M., Karakiewicz, P. I., Cagiannos, I., Quinn, D. I., Henshall, S. M., Grygiel, J. J., Sutherland, R. L., Stricker, P. D., Klein, E., Kupelian, P., *et al.* (2002) *J. Clin. Oncol.* **20,** 3206–3212.
16. Cunha, G. R., Hayward, S. W. & Wang, Y. Z. (2002) *Differentiation* **70,** 473–485.
17. Koukourakis, M. I., Giatromanolaki, A., Brekken, R. A., Sivridis, E., Gatter, K. C., Harris, A. L. & Sage, E. H. (2003) *Cancer Res.* **63,** 5376–5380.
18. Sato, N., Fukushima, N., Maehara, N., Matsubayashi, H., Koopmann, J., Su, G. H., Hruban, R. H. & Goggins, M. (2003) *Oncogene* **22,** 5021–5030.
19. Karihtala, P., Mantyniemi, A., Kang, S. W., Kinnula, V. L. & Soini, Y. (2003) *Clin. Cancer Res.* **9,** 3418–3424.
20. Porkka, K., Saramaki, O., Tanner, M. & Visakorpi, T. (2002) *Lab. Invest.* **82,** 629–637.
21. Albrecht, M., Mittler, A., Wilhelm, B., Lundwall, A., Lilja, H., Aumuller, G. & Bjartell, A. (2003) *Eur. Urol.* **44,** 415–422.
22. Gimenez-Bonafe, P., Fedoruk, M. N., Whitmore, T. G., Akbari, M., Ralph, J. L., Ettinger, S., Gleave, M. E. & Nelson, C. C. (2004) *Prostate* **59,** 337–349.
23. Sutherland, B. W., Kucab, J., Wu, J., Lee, C., Cheang, M. C., Yorida, E., Turbin, D., Dedhar, S., Nelson, C., Pollak, M., *et al.* (2005) *Oncogene* **24,** 4281–4292.
24. Tsuchiya, N., Slezak, J. M., Lieber, M. M., Bergstralh, E. J. & Jenkins, R. B. (2002) *Genes Chromosomes Cancer* **34,** 363–371.
25. Chetyrkin, S. V., Belyaeva, O. V., Gough, W. H. & Kedishvili, N. Y. (2001) *J. Biol. Chem.* **276,** 22278–22286.
26. Zha, S., Ferdinandusse, S., Hicks, J. L., Denis, S., Dunn, T. A., Wanders, R. J., Luo, J., De Marzo, A. M. & Isaacs, W. B. (2005) *Prostate* **63,** 316–323.
27. Cheng, K. W., Lahad, J. P., Kuo, W. L., Lapuk, A., Yamada, K., Auersperg, N., Liu, J., Smith-McCune, K., Lu, K. H., Fishman, D., *et al.* (2004) *Nat. Med.* **10,** 1251–1256.
28. Puccetti, L., Supuran, C. T., Fasolo, P. P., Conti, E., Sebastiani, G., Lacquaniti, S., Mandras, R., Milazzo, M. G., Dogliani, N., De Giuli, P. & Fasolis, G. (2005) *Eur. Urol.* **48,** 215–221 and Discussion, pp. 221–223.
29. Weinstein, M. H., Partin, A. W., Veltri, R. W. & Epstein, J. I. (1996) *Hum. Pathol.* **27,** 683–687.
30. Stapleton, A. M., Zbell, P., Kattan, M. W., Yang, G., Wheeler, T. M., Scardino, P. T. & Thompson, T. C. (1998) *Cancer* **82,** 168–175.
31. Krajewska, M., Krajewski, S., Banares, S., Huang, X., Turner, B., Bubendorf, L., Kallioniemi, O. P., Shabaik, A., Vitiello, A., Peehl, D., *et al.* (2003) *Clin. Cancer Res.* **9,** 4914–4925.
32. Pietrangeli, P. & Mondovi, B. (2004) *Neurotoxicology* **25,** 317–324.
33. Tonks, N. K. (2005) *Cell* **121,** 667–670.
34. McCullagh, P. & Nelder, J. (1989) *Generalized Linear Models* (Chapman and Hall, London).
35. Patel, N. M., Nozaki, S., Shortle, N. H., Bhat-Nakshatri, P., Newton, T. R., Rice, S., Gelfanov, V., Boswell, S. H., Goulet, R. J., Jr., Sledge, G. W., Jr. & Nakshatri, H. (2000) *Oncogene* **19,** 4159–4169.
36. Ayala, G. E., Dai, H., Ittmann, M., Li, R., Powell, M., Frolov, A., Wheeler, T. M., Thompson, T. C. & Rowley, D. (2004) *Cancer Res.* **64,** 6082–6090.
37. Abrahamsson, P. A. (1999) *Prostate* **39,** 135–148.
38. Clegg, N., Eroglu, B., Ferguson, C., Arnold, H., Moorman, A. & Nelson, P. S. (2002) *J. Steroid Biochem. Mol. Biol.* **80,** 13–23.
39. Tusher, V. G., Tibshirani, R. & Chu, G. (2001) *Proc. Natl. Acad. Sci. USA* **98,** 5116–5121.
40. Raychaudhuri, S., Stuart, J. M. & Altman, R. B. (2000) *Pac. Symp. Biocomput.* 455–66.
41. Zellweger, T., Ninck, C., Mirlacher, M., Annefeld, M., Glass, A. G., Gasser, T. C., Mihatsch, M. J., Gelmann, E. P. & Bubendorf, L. (2003) *Prostate* **55,** 20–29.

Research

Genetic background influences murine prostate gene expression: implications for cancer phenotypes

Daniella Bianchi-Frias, Colin Pritchard, Brigham H Mecham, Ilsa M Coleman and Peter S Nelson

Address: Divisions of Human Biology and Clinical Research, Fred Hutchinson Cancer Research Center, Fairview Avenue, Seattle, WA 98109-1024, USA.

Correspondence: Peter S Nelson. Email: pnelson@fhcrc.org

Published: 18 June 2007

Genome ***Biology*** 2007, **8:**R117 (doi:10.1186/gb-2007-8-6-r117)

The electronic version of this article is the complete one and can be found online at http://genomebiology.com/2007/8/6/R117

Received: 5 October 2006
Revised: 30 April 2007
Accepted: 18 June 2007

Abstract

Background: Cancer of the prostate is influenced by both genetic predisposition and environmental factors. The identification of genes capable of modulating cancer development has the potential to unravel disease heterogeneity and aid diagnostic and prevention strategies. To this end, mouse models have been developed to isolate the influences of individual genetic lesions in the context of consistent genotypes and environmental exposures. However, the normal prostatic phenotypic variability dictated by a genetic background that is potentially capable of influencing the process of carcinogenesis has not been established.

Results: In this study we used microarray analysis to quantify transcript levels in the prostates of five commonly studied inbred mouse strains. We applied a multiclass response *t*-test and determined that approximately 13% (932 genes) exhibited differential expression (range 1.3-190-fold) in any one strain relative to other strains (false discovery rate ≤10%). Expression differences were confirmed by quantitative RT-PCR, or immunohistochemistry for several genes previously shown to influence cancer progression, such as *Psca*, *Mmp7*, and *Clusterin*. Analyses of human prostate transcripts orthologous to variable murine prostate genes identified differences in gene expression in benign epithelium that correlated with the differentiation state of adjacent tumors. For example, the gene encoding apolipoprotein D, which is known to enhance resistance to cell stress, was expressed at significantly greater levels in benign epithelium associated with high-grade versus low-grade cancers.

Conclusion: These studies support the concept that the cellular, tissue, and organismal context contribute to oncogenesis and suggest that a predisposition to a sequence of events leading to pathology may exist prior to cancer initiation.

Background

Family history and race represent two of the greatest contributors to the probability of developing cancer of the prostate. Recent estimates suggest that 42% of prostate cancer risk may be attributed to heritable factors that include the influence of rare alleles capable of exerting substantial effects,

common alleles with weak effects, and gene interactions that act to amplify or buffer phenotypes [1]. Racial background accounts for disparities of more than 40-fold in the incidence of prostate cancer between Western and Asian men, and also associates with cancer progression and lethality [2]. Importantly, risks attributed to racial categories may reflect not only genetic variables, but also a myriad of shared environmental exposures that include diet, infectious disease, and medication use.

Cancer susceptibility represents a continuum of interactions between the host and environment. At the extremes, each can exert dominant effects on the neoplastic process. For example, inherited differences in specific gene products, such as p53, Rb, and APC, lead to the near-universal development of cancers, regardless of differences in the host environment [3]. Similarly, exposures to ionizing radiation or chemical mutagens can produce high rates of neoplasia regardless of the host genetic background. However, most human malignancies cannot be attributed to specific genes or extrinsic agents that exert dominant effects, but rather arise in the setting of complex multi-factorial gene-environment relationships. In this context, studies of twins have found that genetic background is associated with a large proportion of supposedly nonhereditary cancers, a finding supported by the familial clustering of specific malignancies [1].

The identification of low-penetrance genetic modifiers that influence cancer phenotypes has been challenging in humans due to substantial genetic heterogeneity and the inability to identify, quantify and control for a wide-range of environmental variables. Furthermore, tumors arising in specific organ sites may exhibit multiple different histologies that include differentiation state and the propensity to progress at variable rates [4,5]. To overcome these hurdles, inbred strains of model organisms such as the mouse have been used to control environmental influences, homogenize tumor histologies, and reduce the complexity of genetic backgrounds [6]. Manipulating these variables has facilitated studies that link genomic loci with the propensity to develop neoplasia and the identification of genes that modulate tumor behavior. Despite highly similar genomes, striking differences in tumorigenesis and metastasis have been observed in different rodent strains induced to develop cancers of the lung, breast, intestine, skin, and prostate [7-11]. Breeding strategies designed to isolate the genes responsible for cancer susceptibility have successfully identified modifying loci [12]. The characterization of specific genes modulating cancer phenotypes indicates that carcinogenesis is influenced by tumor-intrinsic features as well as variables in the host macro- and microenvironments [13]. Intrinsic cellular properties include proliferation rates, genome stability, differentiation potential and the ability to senesce or undergo apoptosis. Tumor-'extrinsic' factors that influence the process of carcinogenesis include hormone concentrations, immune response, drug metabolism, and features of the local stroma involving matrix and neovascularization. Importantly, many cancer-modifying loci exhibit multiple genetic interactions that suggest the existence of molecular networks that underlie cancer predisposition [6,7].

Studies of prostate carcinogenesis in rodent models developed using chemical mutagens or gene-targeting strategies have clearly demonstrated modifications of cancer incidence and progression rates dependent on the host genotype. The substantial tumor-promoting or tumor-suppressing effects exerted by innate host factors suggests that features of benign tissues could allow the behavior of tumor growth to be predicted. To support this hypothesis, influential biochemical or tissue variations must occur and must exhibit measurable characteristics. While variations in immune effectors and hormone levels represent likely influences on prostate carcinogenesis in these model systems, differences intrinsic to the prostate gland could also account for tumor incidence rates between strains. One measurement of phenotypic potential involves the identification and quantification of cellular gene transcription.

To date, global analyses of gene expression in the normal prostate gland of mouse strains have not been reported. In this study, we used microarray analysis to profile prostate gene expression across five inbred mouse strains commonly used for modeling prostate development and carcinogenesis. We found substantial strain-dependent differences in prostate transcript expression patterns, including several genes implicated in prostate cancer development and progression. Analyses of these strain-variable genes in the human prostate enabled the determination of associations between transcript expression levels and phenotypes of prostate cancer, such as tumor grade. The results indicate that variables in prostate gene expression present prior to cancer initiation could modify tumorigenesis.

Results and discussion

Determination of strain-specific differences in mouse prostate gene expression

Several studies have demonstrated the influence of genetic background on the development and progression of prostate cancer in rodents. Using a genetically engineered mouse model driving SV40T antigen expression in the prostate gland, designated TRAMP, Gingrich *et al.* [14] determined that prostate tumors arising in a mixed C57BL/6 × FVB background display reduced latency, increased primary tumor growth and enhanced metastatic progression when compared to tumor development in a pure C57BL/6 background. A recent study of *Pten* deficient mice reported a critical role for genetic background that influenced the onset, tumor spectrum, and progression rates for cancers that included prostate carcinoma [15]. Strain-specific effects have also been observed in mice with inactivation of the prostate-specific *Nkx3.1* homeobox gene: the occurrence of intraepithelial

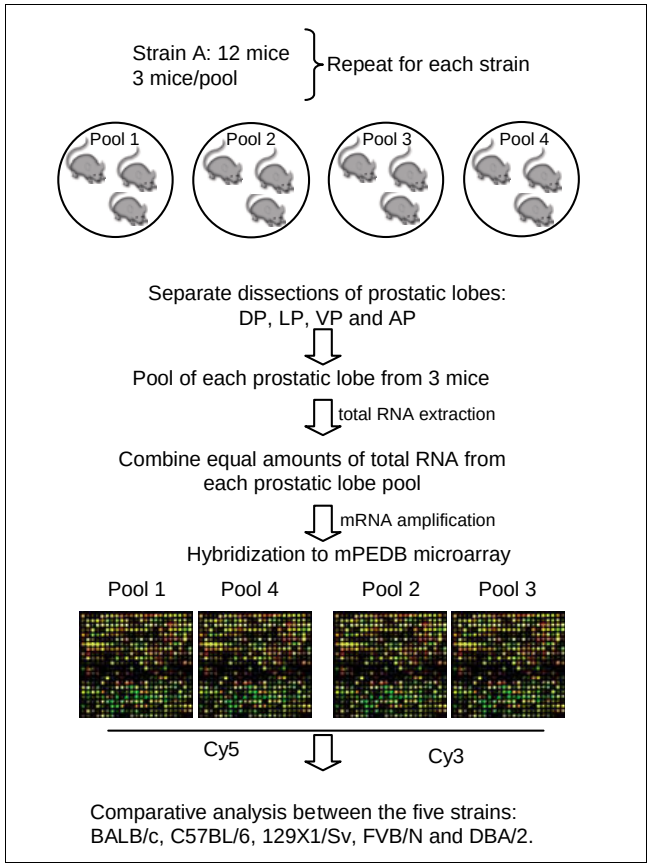

Figure 1
Experimental design. Prostates from 12 mice from each of 5 strains of *Mus musculus* (C57BL/6, 129X1/Sv, BALB/c, FVB/N and DBA/2) were resected and individual lobes were dissected: DP, dorsal prostate; LP, lateral prostate; VP, ventral prostate; AP, anterior prostate. Each experimental sample represents a pool of equal amounts of RNA for each prostatic lobe from three animals. Four independent experimental samples were created per strain: 12 mice divided into 4 pools of 3 mice each for a total of 4 microarray experiments per strain. Amplified RNA from each experimental sample was hybridized against a reference pool onto custom mouse prostate cDNA microarrays using alternate dye-labeling to account for dye-specific effects.

neoplasia was more frequent in C57BL/6 and FVB/N strains than in the 129/SvImJ background (Cory Abate-Shen, personal communication). Genetic background has also been reported to influence transgenic models of rat prostate carcinogenesis, with cancer incidence rates ranging from 0% to 83%, depending on strain background [11].

To ascertain the extent of gene expression variability in the normal prostate arising in the context of different genetic backgrounds, we used cDNA microarray analysis to measure transcript abundance levels for approximately 8,300 genes in the prostate glands of five frequently studied strains of *Mus musculus*; C57BL/6, 129X1/Sv, BALB/c, FVB/N and DBA/2. Four biological replicates consisting of tissues pooled from groups of three individuals were generated to facilitate statistical analyses and control for individual variability (Figure 1). We employed a common reference pool design to control for technical differences in array construction and hybridization. The transcript level of each gene was measured as the ratio of the intensity of hybridization signal for a strain-specific experiment relative to that for the reference pool.

To determine the extent and magnitude of prostate gene expression variation between strains, we generated a one-way ANOVA table for each gene and compared the within-strain mean square (intra-strain replicates) to the between-strain mean square. As expected, the vast majority of genes exhibited low variance across the 20 array experiments. Furthermore, few differences were observed in the intra-strain comparisons, a result likely influenced by the pooling of samples to minimize the contribution of any individual mouse. However, comparisons of gene expression between strains identified substantial reproducible differences in the expression of many genes (range from 1.3 to 190-fold; Figure 2a). We used significance analysis of microarrays (SAM) procedures and applied a multiclass response *t*-test to identify genes whose expression in one strain significantly differed from the other four strains. Approximately 13% of the genes (932 genes) exhibited significant differential expression given a moderate estimate of false positive differences of 10%. The heat map revealed that the pattern of variability in transcript levels did not result from variations unique to a particular strain, but rather represents genetic variability across all five strains assessed (Figure 2b).

To explore the relationships between strains, we performed average linkage hierarchical clustering using all the genes (data not shown) and then using only the 932 genes that were differentially expressed between strains as determined by the SAM analysis (Figure 2b). The resulting dendrograms are identical, indicating that strain specific variation is not entirely explained by a small number of genes exhibiting large changes in gene expression. The expression patterns derived from prostates of the same strain are highly concordant and produce a consistent grouping of samples according to their strain of origin (Figure 2b). Overall, the samples are divided into three major branches: branch I is represented by BALB/c; branch II is represented by C57BL/6 and DBA/2; and branch III is represented by 129X1/Sv and FVB/N. Furthermore, within each branch, sub-branches clearly grouped pools according to strain.

In order to further characterize the relationship between strains, we performed principal components analysis (PCA) using the 932 differentially expressed genes (Figure 2c). The first four components explained 70% of the total variance. As expected, each of these informative components identified a subset of genes that discriminated between at least two of the strains. Taken together, these results show that strain-specific variation results from the differential expression of large numbers of genes and that this signal is stronger than the within-strain variability when using sample pools.

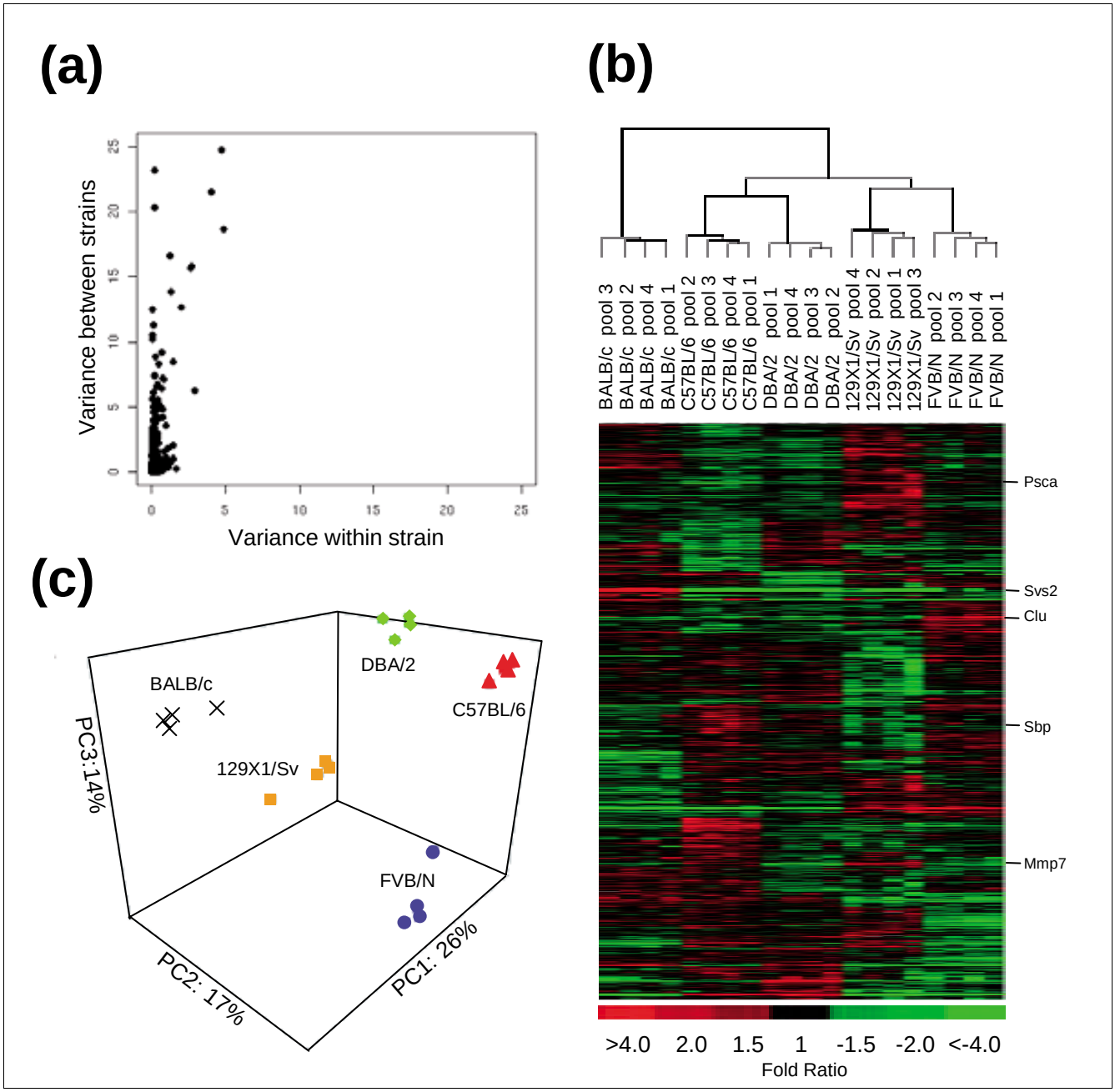

Figure 2
Prostate gene expression differences among strains. **(a)** Scatter plot of variance in gene expression levels between strains and within strains. **(b)** Average-linkage hierarchical clustering for the 932 differentially expressed genes among the five mouse strains (FDR <10%). Heat map colors reflect fold ratio values between sample and reference pool and mean-centered across samples. Columns represent biological replicates for each strain. Rows represent individual genes. Values shown in red are relatively larger than the overall mean; values shown in green are relatively smaller than the overall mean (see scale). Genes whose expression changes were confirmed by qRT-PCR, western blot or immunohistochemistry are listed. **(c)** Separation of the five strains in three-dimensional principal component space by applying PCA to the 932 genes with strain variance.

Among the expressed genes, those encoding pituitary tumor-transforming 1 (*Pttg1)* and adenylate cyclase-associated protein 1 (*Cap1)* were found to be differentially expressed between prostates of C57BL/6 and 129X1/Sv strains. Previous studies have found concordant strain-dependent differences in the expression of these genes in other mouse tissues [16]. Transcripts encoding several members of the histocompatibility complex also exhibited strain-dependent differences. Relative to other strains, H2-Ea is expressed highly in prostates of DBA/2 and BALB/c mice; H2-k is expressed highly in 129X1/Sv and C57BL/6; H2-Q1 is expressed highly in 129X1/Sv, FVB/N and C57BL/6; and transcripts encoding

Table 1

Pairwise comparisons of mouse prostate gene expression between strains of *Mus musculus*

Strain	C57BL/6	129X1/Sv	FVB/N	BALB/c	DBA/2
129X1/Sv	124*	-	88	102	116
FVB/N	237	88	-	172	226
BALB/c	173	102	172	-	196
DBA/2	198	116	226	196	-

*Values represent the number of genes with significant differences in transcript abundance measurements between strains. Significance was defined as a SAM gene-specific q-value less than 0.05.

H2-D1 were least abundant in the C57BL/6 strain. Interestingly, the pattern of expression of this gene family did not correlate with the known H2 haplotypes of the strains, a finding also reported in a study evaluating strain-specific gene expression variation in the mouse hippocampus [17].

To identify differentially expressed genes unique to individual strains, we performed a pair-wise comparison of transcript abundance levels between each strain for a total of 10 pair-wise comparisons. The number of genes found to be differentially expressed between any two strains varied depending on the strains compared (Table 1). Strains 129X1/Sv and FVB/N exhibit the fewest differences in prostate gene expression (88 genes) whereas strains FVB/N and C57BL/6 exhibit the greatest number of transcript abundance differences (237 genes). Analyses of the promoter regions of these strain-variable genes did not identify sequence motifs that would suggest common regulatory mechanisms.

Confirmation of strain-dependent differences in prostate gene expression

Several genes exhibiting strain-dependent differences in prostate expression have been studied in the context of prostate development (for example, *Sbp*), androgen regulation (*Fabp5*, *Odc*), tumorigenesis (for example, *Psca*, *Azgp1*, *Apod*, *Mmp7*, *Egf*, *Mgst1*, *Clusterin*), and the progression of metastatic cancer (*Cxcl12*, *B2m*, H2 family members) [8]. To confirm the microarray results, we selected several of these genes for analysis by quantitative real-time reverse-transcription PCR (qRT-PCR). Primer pairs specific to *Svs2*, *Psca*, *Mmp7*, *Spb* and *Clusterin* were used to quantify transcripts in the same RNA samples used in the microarray experiments (Figure 3a; Figure 4a for clusterin). We measured transcripts encoding the housekeeping gene encoding ribosomal protein S16 to normalize the qRT-PCR data. From the microarray results, S16 expression did not vary significantly between strains.

Overall, the qRT-PCR transcript measurements for the five genes tested were in good agreement with the microarray data, though the magnitude of relative fold differences in the qRT-PCR assay was greater compared to the microarray results. This observation is partly due to intrinsic limitations in the microarray experimental design, where transcript levels were measured as the ratio between an experimental sample (strain sample) relative to that for the reference sample (pool of all strains). The expression of *Mmp7* varied between 5- and 15-fold between strains with the greatest difference observed in a comparison of 129X1/Sv and DBA/2 mice (Figure 3a). The expression of *Psca* varied up to 40-fold between strains and the expression of *Clusterin* was at least 70-fold greater in the FVB/N mice relative to any other strain.

Assessments of strain-associated variation in prostate cellular composition and cell type-specific gene expression

We hypothesized that strain-specific disparities in the ratios of cell types within the prostate gland could be reflected as measurable differences in transcript levels. The rodent prostate is composed principally of luminal secretory epithelium, basal epithelium, and a stroma consisting primarily of fibroblasts and smooth muscle, with a smaller component of endothelium, nerve cells, neuroendocrine cells, and inflammatory infiltrates. Since our transcript profiling studies were performed using whole prostates containing mixtures of the various cell types, we could not exclude the possibility that differences in gene expression between strains were a result of differences in cell type ratios between strains. To address this, we performed an *ad hoc* analysis using two prostates per strain, and calculated the percentage of prostate area occupied by stroma and epithelium for each lobe. Based on the estimated effect sizes and the corresponding *p* values, we did not identify significant strain-associated differences in the ratios of cell types between strains (data not shown).

To further confirm that prostate gene expression differences arise from intrinsic genetic variation and not cell ratio effects, we microdissected secretory epithelium from two strains: C57BL/6 and 129X1/Sv. We measured the transcript levels for two genes, *Sbp* and *Mmp7*, that exhibited strain-associated differences in the microarray studies. As shown in Figure 3b, transcript levels of *Mmp7 and Sbp* were four-fold higher and four-fold lower, respectively, in microdissected epithelium from 129X1/Sv relative to C57BL/6. These findings are in agreement with the differences in transcript levels observed for these genes in the analyses of whole prostates from these strains (compare Figures 3a and 3b). Together, these results support the conclusion that differences in

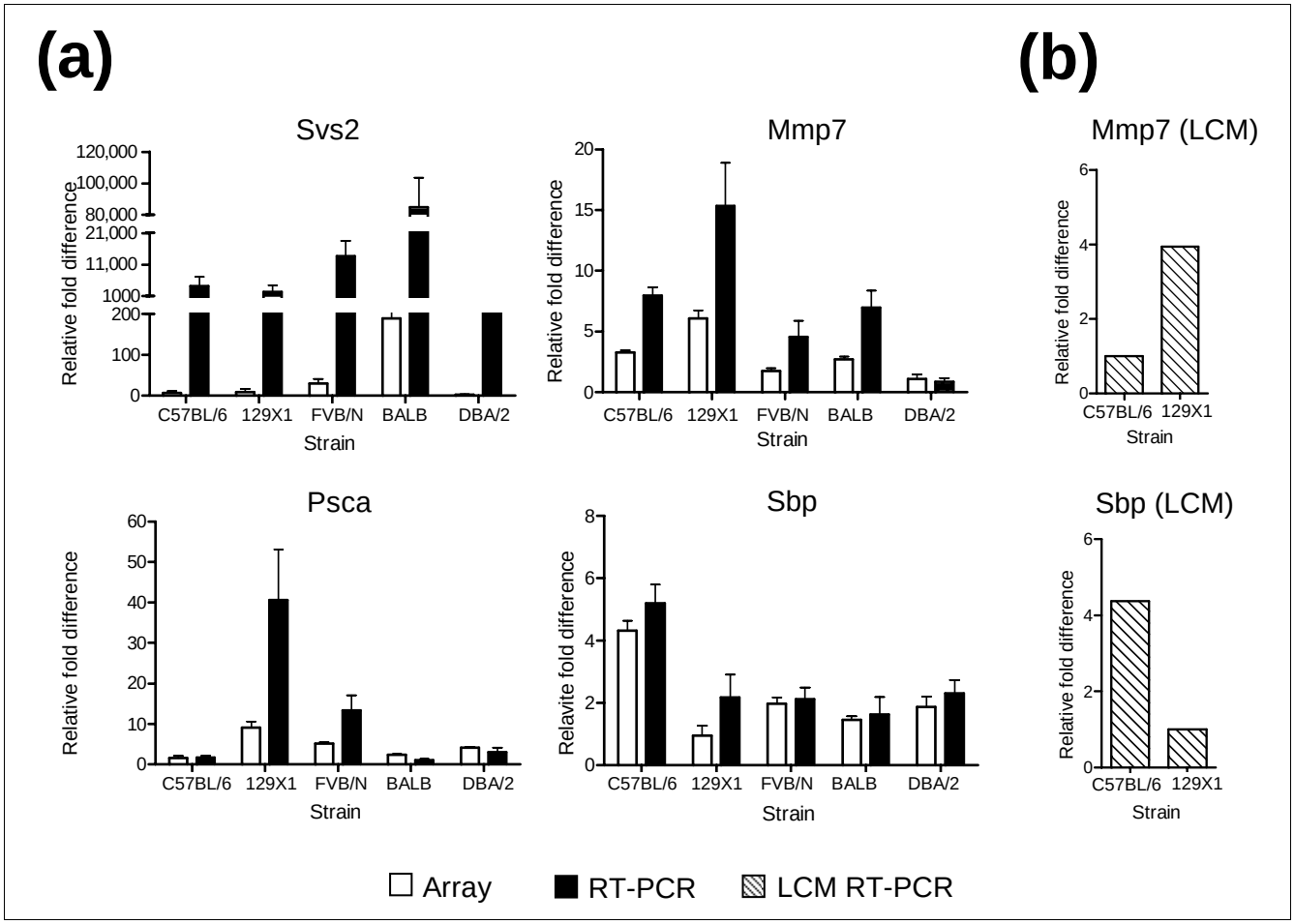

Figure 3

Analysis of strain-dependent differences in prostate gene expression by qRT-PCR. RNAs from preparations used in the **(a)** microarray analysis or **(b)** microdissected epithelium were reverse transcribed and amplified using qRT-PCR with primers specific for *seminal vesicle secretion 2* (*Svs2*), *matrix metallopeptidase 7* (*Mmp7*), *prostate stem cell antigen* (*Psca*) and *spermine binding protein* (*Sbp*). Ribosomal protein S16 expression levels were used to normalize qRT-PCR data. Normalized results are expressed relative to the lowest expressing value. Error bars indicate the standard deviation of four biological independent replicates. qRT-PCR for microdissected epithelium is represented by one sample per strain for each gene. White bars denote measurements from the microarray analysis. Black bars denote measurements generated by qRT-PCR from whole prostate. Diagonal lines denote measurements generated by qRT-PCR from microdissected prostate epithelium.

prostate gene expression between strains, at least for the genes independently assessed in microdissected epithelium, represent an intrinsic cellular property rather than possible differences in prostatic cell type ratios between strains. Furthermore, the experimental design and microarray methods are capable of identifying transcript abundance differences between strains for genes expressed in a cell type- and lobe-specific manner (for example, *Sbp* [18,19]), even when diluted by mRNAs from all lobes and multiple cell types. However, it is likely that subtle, yet biologically relevant alterations in constituents of the stroma and glandular microenvironment also exist between strains. Identifying these differences will likely require detailed cell type-specific assays.

Strain-associated differences in prostate protein expression

We next sought to determine if strain-associated differences in prostate transcript levels were reflected by concordant differences in protein expression. We chose to evaluate protein levels of clusterin, which is encoded by a gene studied extensively in the context of prostate carcinogenesis and therapy resistance [20-22]. Clusterin, also known as testosterone-repressed prostate message 2 (*TRPM-2*), is of particular interest in view of active efforts to target its expression as a treatment for human prostate cancer [20]. Although the function(s) of clusterin remains somewhat enigmatic, recent studies indicate that antiapoptotic effects are mediated in part through direct interactions with activated Bax [22]. We have previously shown that clusterin expression is increased in

tumors developing in mice with a prostate specific deletion of the *Pten* tumor suppressor gene [23]. Microarray hybridization and qRT-PCR quantified clusterin transcripts at levels ten-fold or greater in prostates of FVB/N mice relative to all other strains (Figure 4a). A western blot analysis using ventral prostate protein extracts detected higher clusterin levels in prostates of the FVB/N strain when compared with DBA/2 and C57BL/6 strains (Figure 4b). We next performed immunohistochemistry to determine the cellular localization of clusterin expression. With the exception of the ventral lobe, we did not detect major differences in clusterin expression between mouse strains. However, substantially greater clusterin immunoreactivity was observed in the secretory epithelium of the ventral lobe of the FVB/N strain, relative to any other lobe and all other strains. Staining was particularly intense in the apical region of the epithelium, suggesting that the secretory form of clusterin is the predominant differentially expressed isoform in FVB/N ventral prostate epithelium (Figure 4c,d). Based on these results, we speculate that elevated clusterin levels may contribute to the enhanced rate of prostate tumor development and progression observed in the TRAMP FVB/N genotype.

Biological pathway analysis of mouse prostate gene expression profiles

The substantial number of genes found to be differentially expressed in the prostates of different mouse strains suggested that specific groups of genes could share common regulatory mechanisms or participate in particular functional pathways. To address this possibility, we focused on differences between the C57BL/6 strain relative to other strains due to the reduced tumorigenicity observed in transgenic mouse prostate cancer models arising in the C57BL/6 background [14,15,24]. We used a method termed 'gene set test' (GST) in BioConductor that is analogous to the recently described gene set enrichment analysis (GSEA) algorithm [25] to determine if genes displaying relative differences in prostates of C57BL/6 mice were enriched in a database of biologically defined gene sets assembled by the Gene Ontology (GO) consortium. Only three of 258 gene sets, NADH dehydrogenase activity, NADH dehydrogenase (ubiquinone) activity, and phosphoinositide binding were statistically enriched in the C57BL/6 prostates (false discovery rate (FDR) ≤25%). While specific components of these pathways or networks could represent modifiers of the cancer phenotype, the results also suggest that influential genetic variation is broadly dispersed across functional biological pathways. This conclusion is tempered by acknowledged limitations to these studies that include the imperfect nature of algorithms used to determine gene enrichment and the fact that transcript measurements do not reflect the complete picture of biological pathways and networks.

Gene expression variability in the human prostate: correlations with cancer phenotype

Having established that consistent measurable differences in murine prostate gene expression occur in the context of genetic background, we next sought to determine if the orthologous genes were also variable in the human prostate, and whether the underlying normal gene expression levels, potentially representing quantitative traits, associate with aspects of human prostate carcinogenesis. We focused on transcript alterations between the C57BL/6 and FVB/N strains due to experimental evidence demonstrating that for the TRAMP model system of prostate cancer, the C57BL/6 genome delays cancer progression relative to an accelerated rate of carcinogenesis in other strains, including FVB/N [14]. We also focused on transcript differences between the C57BL/6 and BALB/c strains due to a recent report describing a reduced incidence of prostate adenocarcinomas in *Pten* deficient mice of a 129/C57 background relative to high rates of prostate carcinomas, up to 90% by 6 months, in *Pten* deficient mice of a 129/BALB/c background. These studies suggest the hypothesis that genes expressed highly in C57BL/6 prostates might function as inhibitors of carcinogenesis whereas genes expressed highly in other strains - relative to C57BL/6 - could function to promote or permit carcinogenesis. Direct comparisons of transcript abundance levels from prostates of the C57BL/6 strain against FVB/N and C57BL/6 against BALB/c identified 237 and 173 genes with significant differences, respectively (Table 1; Figures 5a and 6a).

We next measured the transcript abundance levels of these variable murine prostate genes in human prostate tissues. Based on the TRAMP mouse model data, we hypothesized that if genes expressed highly in C57BL/6 relative to FVB/N prostates (designated C57-High) retard aspects of carcinogenesis, they would be down-regulated in the prostates of those individuals shown to have aggressive prostate cancers, and if genes expressed highly in FVB/N relative to C57BL/6 prostates (designated C57-Low) promote aspects of carcinogenesis, they would be elevated in the prostates of individuals with aggressive prostate cancers. Similar reasoning was applied to genes differentially expressed between BALB/c and C57BL/6 prostates.

We analyzed data reported by Lapointe *et al*. [26] that generated independent gene expression profiles from matched pairs of benign and neoplastic human prostate tissues accompanied by pathological criteria of tumor aggressiveness according to the Gleason grading system. This human dataset contained orthologs for 113 of the 237 genes with differential expression in C57BL/6 relative to FVB/N prostates, and 91 of the 173 genes with differential expression in C57BL/6 relative to BALB/c prostates. We specifically focused on gene expression in the benign tissue of each human prostate sample as a potential measure of an underlying predisposition to cancer phenotypes reflected by cancer grade: low pathological grade (Gleason ≤6) versus cancers of higher grade (Gleason 7-10).

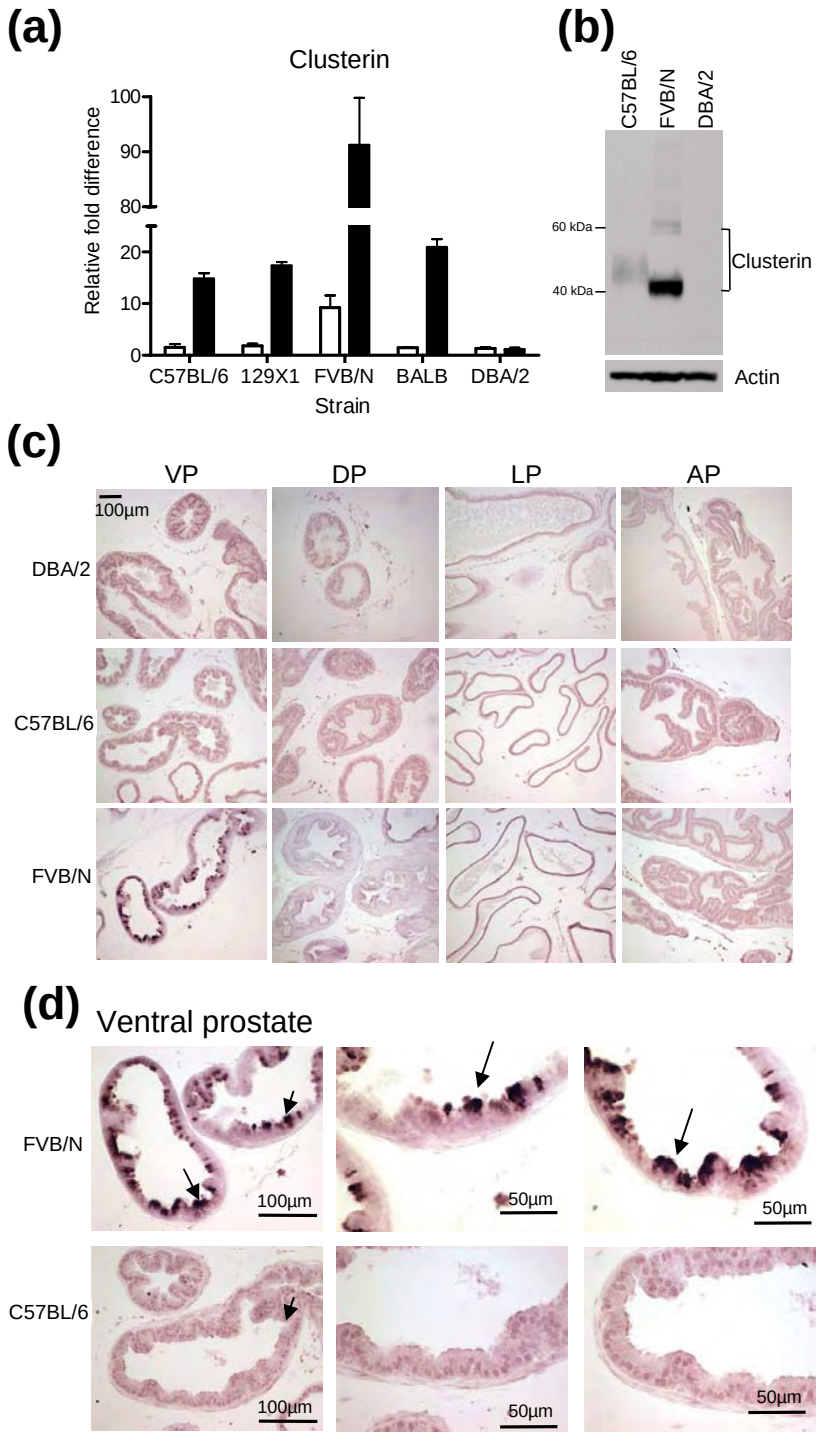

Figure 4

Clusterin is highly expressed in the FVB/N strain. **(a)** qRT-PCR measurement of *Clusterin* RNA in prostate preparations used in microarray analysis. White bars are the data from the microarray experiments and black bars are values generated by qRT-PCR. **(b)** Western blot analysis of clusterin in the ventral prostates of FVB/N, DBA/2 and C57BL/6 mouse strains. Ventral prostate tissue (pool of three ventral prostates per lane/strain) was prepared and equal amounts of protein were resolved by SDS-PAGE and probed with anti-clusterin antibody. Antibody against β-actin was used as a loading control. **(c, d)** Immunohistochemical analysis of paraffin sections from dorsal prostate (DP), lateral prostate (LP), anterior prostate (AP) (c) and ventral prostate (VP) lobes (c, d) of 8-9 week old mice from FVB/N, DBA/2 and C57BL/6 strains. Sections were stained with anti-clusterin antibody. Clusterin immunoreactivity is most intense in the apical region of the secretory epithelial cells from the ventral prostate (arrow).

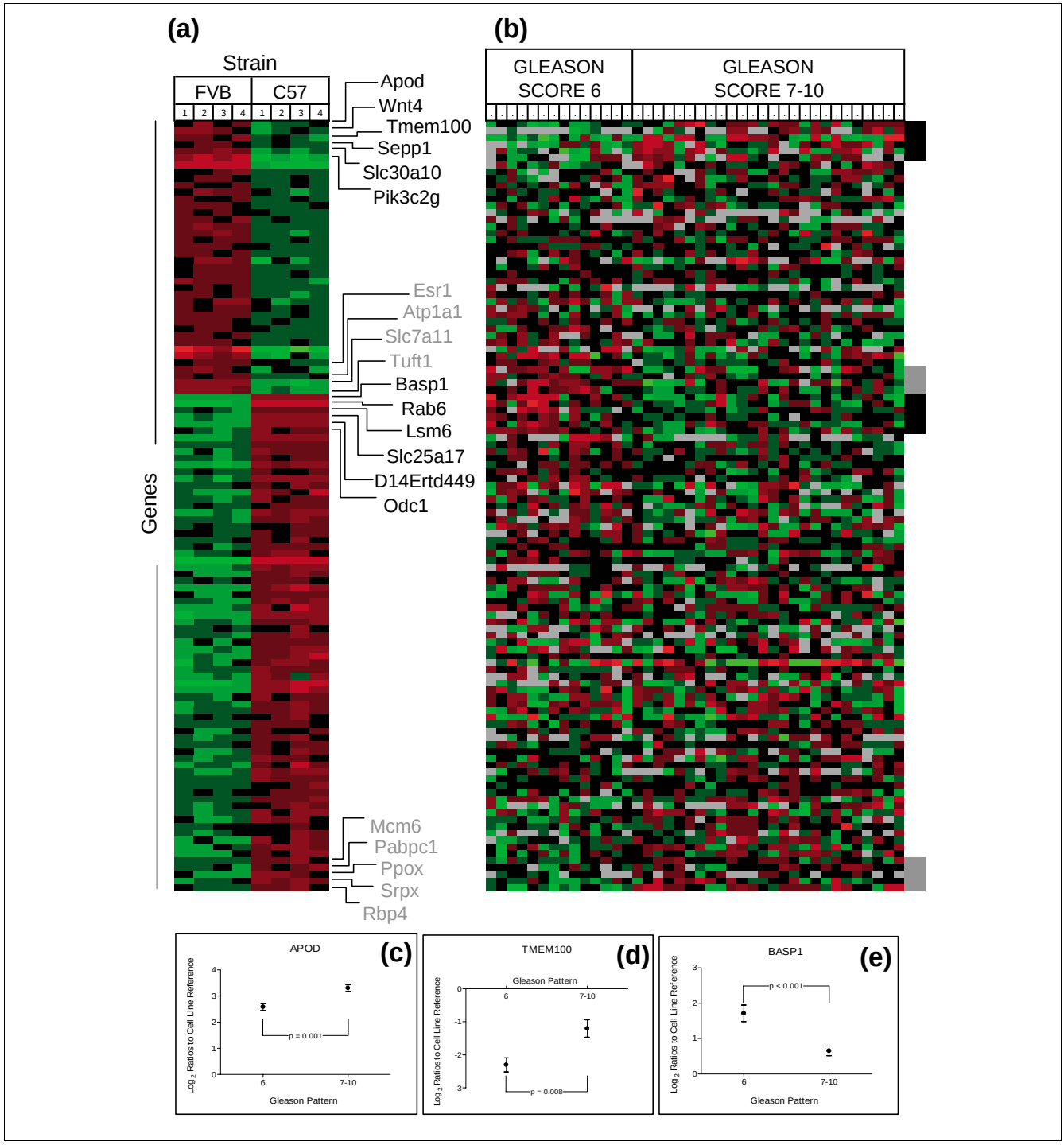

Figure 5
Mouse prostate strain-associated gene expression and analysis in human prostate tissues: FVB/N and C57BL/6. **(a)** Genes differentially expressed in prostates of FVB/N and C57BL/6 strains. Heat map colors reflect fold ratio values between sample and reference pool. Columns 1-4 represent biological replicates for each strain. Rows represent individual genes. Values shown in red are relatively larger than the overall mean; values shown in green are relatively smaller than the overall mean. **(b)** Transcript abundance levels in benign human prostate tissues associated with high grade (7-10) or low grade (≤6) adenocarcinomas for each gene determined to be altered in mouse strain comparisons where a corresponding ortholog was identified. Genes depected in (a) and (b) are in identical order. Black box (b) and text (a) represent genes with significant differential expression in the human datasets altered in the expected orientation. Gray box (b) and text (a) represent genes with significant differential expression in the human datasets altered in the opposite orientation. **(c-e)** Transcript alterations for selected genes in benign tissue samples associating with high (Gleason 7-10) and low (Gleason ≤6) prostate cancers. Plots represent the 95% confidence intervals of $\log_2$ expression ratios of tissues samples relative to a cell line reference.

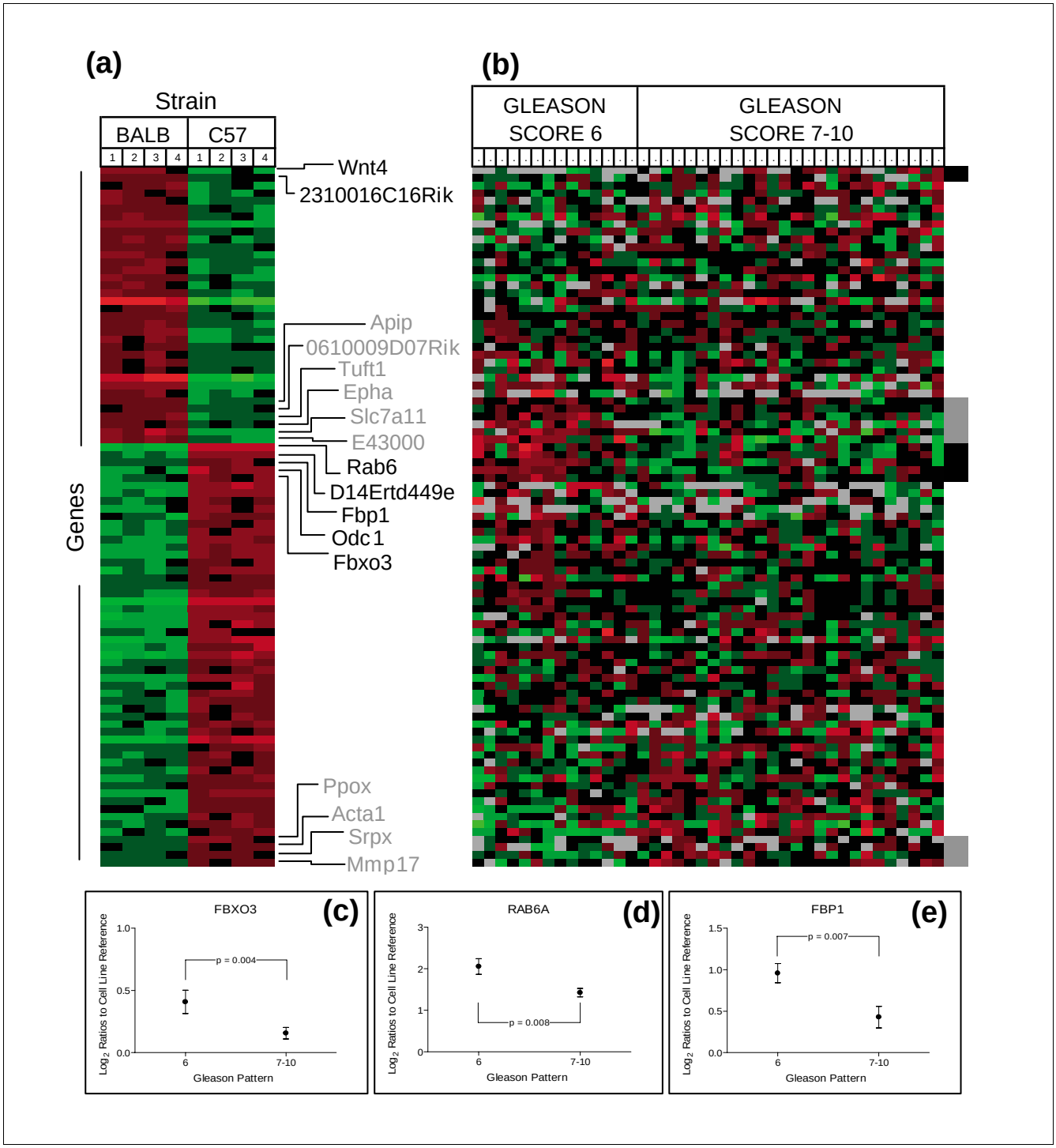

Figure 6

Mouse prostate strain-associated gene expression and analysis in human prostate tissues: BALB/c and C57BL/6. **(a)** Genes differentially expressed in prostates of BALB/c (BALB) and C57BL/6 (C57) strains. Heat map colors reflect fold ratio values between sample and reference pool. Columns 1-4 represent biological replicates for each strain. Rows represent individual genes. Values shown in red are relatively larger than the overall mean; values shown in green are relatively smaller than the overall mean. **(b)** Transcript abundance levels in benign human prostate tissues associated with high grade (7-10) or low grade (≤6) adenocarcinomas for each gene determined to be altered in mouse strain comparisons where a corresponding ortholog was identified. Genes depicted in (a) and (b) are in identical order. Black box (b) and text (a) represent genes with significant differential expression in the human datasets altered in the expected orientation. Gray box (b) and text (a) represent genes with significant differential expression in the human datasets altered in the opposite orientation. **(c-e)** Transcript alterations for selected genes in benign tissue samples associating with high (Gleason 7-10) and low (Gleason ≤6) prostate cancers. Plots represent the 95% confidence intervals of $\log_2$ expression ratios of tissues samples relative to a cell line reference.

In agreement with this hypothesis, seven genes expressed highly in C57BL/6 prostates were measured at significantly lower levels in prostates with high-grade cancers relative to prostates with low-grade cancers (for example, *BASP1*) (Figure 5b-e).

Six genes expressed relatively highly in FVB/N prostates (for example, *ApoD*) exhibited significantly higher transcript levels in the prostates containing high-grade cancers relative to prostates with low-grade cancer (Figure 5). Apolipoprotein D (*APOD*) is a member of the lipocalin superfamily of protein transporters that is implicated in the pathogenesis of neurodegenerative diseases and is regulated by androgens in both breast and prostate cells [27,28]. Studies of prostate cancer have demonstrated elevated APOD protein levels in prostate intraepithelial neoplasia and prostate carcinoma [29], but associations between *APOD* polymorphisms, or APOD expression in benign epithelium in the context of cancer phenotypes have not been reported. Two recent studies of the *Drosophila* ApoD ortholog, *GLaz*, provide context for the potential influence of ApoD expression on cytoprotection and cell survival [30,31]. Overexpression of Glaz increased resistance to stresses that included starvation, hyperoxia and hypoxia, and resulted in the extension of organismal lifespan [30]. Conversely, loss of *GLaz* resulted in the reduction of *Drosophila* stress resistance and lifespan, consistent with APOD being part of a defense system that is activated in the setting of oxidative stress, or incited by exogenous environmental factors or intrinsic events such as aging or neoplasia [31].

Counter to our hypothesis, several genes exhibited significant expression differences inversely associated with the human prostate cancer grade-status predicted by the mouse phenotypes. For example, transcript levels of four C57-Low genes (for example, *Esr1*) in benign prostate tissues were significantly associated with low-grade cancers and five C57-High genes (for example, *Rbp4*) were expressed at greater levels in benign tissue associated with high-grade relative to low-grade prostate cancers (Figure 5b). Similar results were observed for genes differentially expressed between BALB/c and C57BL/6 prostates when evaluated in benign tissues from prostates with high-grade cancers relative to prostates with low-grade cancers (Figure 6).

One possible explanation for these findings centers on different tumor initiating mechanisms (and pathways) that subsequently interact with different intrinsic intracellular and extracellular 'host' gene expression programs. For example, although studies of mouse prostate tumorigenesis demonstrate that the C57 strain appears to reduce tumorigenesis caused by *p53/Rb* (TRAMP model) or *Pten* alterations, the C57 background increases the development of prostate intraepithelial neoplasia lesions in mice with targeted deletions of the *Nkx3.1* homeobox gene [32], and increases tumorigenesis in the setting of *ras+myc* expression, relative to other strains [33]. Thus, the complexities of the interactions between different tumor initiating events and host genomes are likely to be quite complex, a factor that could certainly influence the interpretation of human data where initiating events for any particular primary tumor are poorly defined. As heritable differences provide ample opportunities for mutations in growth control genes to exert differential effects depending upon the inherent wiring of the altered cell or the surrounding micro- and macroenvironment, improved subclassifications of human prostate tumors that associate with specific oncogenenic events, such as the recently reported TMPRSS2-ERG fusions [34], may assist in defining consistent associations. In support of this concept are data demonstrating that a polymorphism in the promoter region of the *MDM2* gene enhances MDM2 expression, attenuates p53 tumor suppressor function and accelerates tumor progression rates of both hereditary and sporadic human cancers arising in the context of p53 alterations [35].

Conclusion

The quantification of tissue gene expression represents a measure of phenotypic variation at the molecular level that can be ascertained as comprehensive profiles reflecting active biological pathways. Exploiting gene expression information as quantitative traits (QTL) has facilitated large-scale efforts to identify genomic loci that contribute to complex phenotypes and diseases [36]. In this study we have found substantial reproducible gene expression differences in the murine prostate that associate with genetic background. Large strain-specific differences in tissue gene expression are not unique to the prostate. We have previously demonstrated that transcript abundance levels in the liver differ between mice of different strains [37]. Studies of strain-dependent differences in the development and progression of murine breast carcinoma have delineated gene expression differences in tumors arising in the context of genetic background [8], but it is likely that many of these differences were present in the breast tissues prior to cancer development. Indeed, mouse strains with high- or low-metastatic genotypes are reportedly distinguishable using gene expression measurements from benign breast tissue [38].

These data emphasize that, in addition to the initiating incident, context may be important for the process of carcinogenesis. Importantly, the predisposition to a detrimental sequence of events leading to pathology might be determined through assessments of the expression program operative in the normal state between different individuals. Thus, as with studies associating disease predisposition with variations in DNA polymorphisms, copy numbers, and epigenetic marks, studies of variation in gene expression in benign tissues, optimally with a tissue or cell type-specific focus, could provide insights into cancer predisposition and gene-environment interactions.

Materials and methods

Animal work and RNA preparation

Male mice 7 weeks of age were purchased from the Jackson Laboratory (C57BL/6J, 129X1/SvJ and FVB/NJ) or the Charles River Laboratories (BALB/cAnNCrl and DBA/2NCrl), maintained in a barrier facility and cared for in accordance with approved IACUC protocols. Following shipment, mice were acclimated to a common temperature, day-night cycle, and diet for 12 days to minimize environmental differences. Twelve mice from each of five strains, C57BL/6J, 129X1/SvJ, FVB/NJ, BALB/cAnNCrl and DBA/2NCrl (abbreviated C57BL/6, 129X1/Sv, BALB/c, FVB/N and DBA/2, respectively), were randomized for the day and time of sacrifice. Following halothane anesthesia, mice were sacrificed by cervical dislocation. Prostates were rapidly excised, and dorsal, lateral, ventral and anterior lobes were separately dissected and snap-frozen in liquid nitrogen and stored at -80°C. To control for individual variability [39], the dissected prostate lobes from mice of each strain were divided into four pools of three mice each and combined for total RNA isolation. Prostate tissues were homogenized using a Polytron and total RNA was isolated using the RNeasy extraction kit (Qiagen, Valencia, CA). Due to the limited concentration of total RNA obtained, specifically from the lateral lobe, equal amounts of total RNA (0.7 μg) from each of the four pooled lobes/strain were combined to produce secondary pools, and amplified with the MessageAmp™ aRNA kit (Ambion, Austin, TX). Amplified RNA from each secondary pool (four pools per strain) was hybridized separately to cDNA microarrays for a total of 4 independent biological replicates per strain (12 mice, 4 pools of 3 mice per strain for a total of 4 microarray experiments per strain; Figure 1). A common reference sample was created by combining equal amounts of RNA from all the samples from all strains.

Probe construction, microarray hybridization and data acquisition

The amplified RNA was used as template for cDNA probe synthesis followed by hybridization to a custom mouse prostate cDNA array (mPEDB array) composed of approximately 8,300 genes expressed in the developing and adult mouse prostate [40]. The 20 microarrays used for the experiment were all from the same printing batch. cDNA probes were made from 2 μg of amplified RNA in a reaction volume of 30 μl containing 170 ng random hexamer primers, 0.2 mM 5-(3-aminoallyl)-2-deoxyuridine-5-triphosphate (amino acid-dUTP; Sigma-Aldrich, St. Louis, MO), 0.3 mM dTTP, 0.5 mM each dATP, dCTP, and dGTP, and 380 units of Superscript II reverse transcriptase (Invitrogen, Carlsbad, CA) incubated at 42°C for 120 minutes. After RNA hydrolysis, purified cDNA was combined with either Cy3 or Cy5 monoreactive fluors (Amersham Pharmacia, Piscataway, NJ) that covalently couple to the cDNA incorporated aminoallyl linker in the presence of 50 mM NaHCO3 (pH 9.0). The coupling reaction was quenched with hydroxylamine and reference and experimental probes were combined, filtered, and competitively hybridized to microarrays under a coverslip for 16 h at 63°C. Slides were washed sequentially with 1× saline sodium citrate (SSC)/0.03% sodium dodecyl sulfate (SDS), 1× SSC, 0.2× SSC, 0.05× SSC, and spun dry. To account for dye bias, half of the biological experimental samples per strain were labeled with Cy3 dye and the reference with Cy5 dye, and in the other half the labeling was inversed.

Microarray data collection and analysis

Fluorescent array images were collected for both Cy3 and Cy5 using a GenePix 4000B fluorescent scanner (Axon Instruments, Foster City, CA, USA). The image intensity data were gridded and extracted using GenePix Pro 4.1 software. For each array spot, the expression levels of the two fluorophores were obtained by subtracting median background intensity from median foreground intensity. A gene was only considered expressed if the fluorescence intensity of the corresponding spot was at least six foreground pixels greater than four standard deviations above background in at least half of the arrays per strain. Array spots not meeting these criteria were designated NA. For each gene, the logarithm base 2 ratios (referred henceforth as log ratios) of the two channels were calculated to quantify the relative expression levels of genes between the experimental and reference samples.

To allow for inter-array comparisons, each array was normalized to remove systematic sources of variation. This was accomplished by means of a print-tip-specific intensity-based normalization method [41]. A scatter-plot smoother, which uses robust locally linear fits, was applied to capture the dependence of the log ratios on overall log-spot intensities. The log ratios were normalized by subtracting the fitted values based on the print-tip-specific scatter-plot smoother from the log ratios of experimental and control channels. After normalization, spots were removed from further analysis if they had more then 3 NA values or if they were in the lower third quantile of abundance across all 20 arrays.

To identify genes that varied among strains of mice, $\log_2$ ratio measurements were statistically analyzed using the SAM procedure [42]. A multiclass response *t*-test was used to determine whether the gene expression of one strain significantly differed from the other strains giving a moderate estimate of false positive genes of 10% (FDR). When differences in the expression of genes were examined using SAM software, 932 genes were statistically differentially expressed across the five strains of mice. Transcriptional profiles of the five mouse strains were also compared with average-linkage hierarchical clustering and Principle Components Analysis (PCA.) Average linkage hierarchical clustering was used to cluster the samples using all the genes or only those that were differentially expressed. To further characterize the relationships between the strains, we performed PCA on the 932 differentially expressed genes. All analyses were done using Bioconductor software [43].

Comparisons of mouse prostate and human prostate gene expression for association with tumor phenotypes

To evaluate transcript abundance levels in benign human prostate epithelium that associated with cancer grade or stage, we focused on genes that were differentially expressed between prostates of C57BL/6 and FVB/N, and between C57BL/6 and BALB/c mouse strains. Based on studies of the TRAMP and *Pten* prostate cancer models, we designated the C57BL/6 strain as 'prostate cancer-inhibiting' and the FVB/N and BALB/c strains as 'prostate cancer-permitting'. The SAM algorithm was used to identify the 237 genes differentially expressed between C57BL/6-FVB/N and the 173 genes between C57BL/6-BALB/c strains using a FDR of <5%.

We next investigated whether differences in gene expression patterns of benign prostate tissues adjacent to prostate cancers were associated with Gleason pattern or patient outcomes. We evaluated a study by Lapointe *et al*. [26] that profiled benign tissues matched with prostate adenocarcinomas of defined Gleason grades. The data were derived from spotted cDNA microarrays and we normalized the data by fitting a print-tip specific Lowess curve to the log-intensity versus log-ratio plot. Normalized $\log_2$ ratio data were filtered to include clones with orthologs to the Mouse Prostate Expression Database (MPEDB) array. Out of the 237 and 173 genes that were identified as differentially expressed (q-value of <5%) between C57BL/6 and FVB/N, and between C57BL/6 and BALB/c, respectively, 113 and 91 had sufficient information to test in the Lapointe *et al*. data. An unpaired two-sample *t*-test was used to determine the association between expression level in the benign tissue and the corresponding Gleason pattern cancers adjacent to the normal samples. The R-code for this analysis can be found online at the MPEDB website in the supplementary data section [44].

Biological pathway analysis

In order to identify specific biological pathways that exhibit strain specific variation, we utilized the GST method available in BioConductor, an algorithm similar to the GSEA method reported by Subramanian *et al*. [25]. Briefly, t-statistics comparing the expression levels of genes between the C57BL/6 and all other strains were used as input to the GST algorithm. All other settings were kept at their default status and the pathways were obtained from the GO database [45]. We defined a pathway as showing strain-specific variation if its corresponding FDR was less than 25%.

Microdissection of luminal epithelium

Frozen sections (7 μm) were cut from snap-frozen mouse prostate glands and immediately fixed in cold 95% ethanol. After fixing, the slides were washed in deionized RNase-free water, stained with Mayer's hematoxylin for 30 seconds, followed by another water wash. The sections were then dehydrated with two one-minute washes in 100% followed by two five-minute changes in Xylene. Approximately 4,000 luminal epithelial cells were captured from the ventral, dorsal, lateral and anterior prostate lobes from 3 independent animals for a total of 12,000 cells per lobe using the Arcturus PixCell II instrument (Arcturus, Mountain View, CA, USA). Digital photos were taken of tissue sections before, during, and after LCM and assessed independently to confirm the cell type-specificity of the captured cells. Total RNA was extracted using the Picopure RNA isolation kit (Arcturus) according to the manufacturer's specifications. The extracted RNA was subjected to two rounds of amplification using the MessageAmpTM aRNA kit (Ambion).

Quantitative RT-PCR

RNA from microdissected epithelium and from preparations used in the microarray analysis were used as template for qRT-PCR. We used 200 ng of amplified RNAs or 20 ug of total RNAs to generate cDNAs. SYBR GREEN real-time PCR was performed as previously described [39]. Primers to ribosomal protein S16 were used to normalize cDNA loading. The sequences of the primers used in this study were: *S16* forward, 5'-AGGAGCGATTTGCTGGTGTGGA-3', *S16* reverse, 5'-GCTACCAGGCCTTTGAGATGGA-3'; *Psca* forward, 5'-GCCTGGTAGAGGCTGAGATG-3', *Psca* reverse, 5'-ATCATCTCCTGGGACTCCTG-3'; *Clusterin* forward, 5'-TTTATGGACACAGTGGCGGA-3', *Clusterin* reverse, 5'-GCTTTTCCTGCGGTATTCCTG-3'; *Mmp7* forward, 5'-CTGATGATGAGGACGCAGGA-3', *Mmp7* reverse, 5'-ATTCATGGGTGGCAGCAAAC-3'; *Svs2* forward, 5'-TCAGAAAGGCCGTCTCAGTT-3', *Svs2* reverse, 5'-AGCTGCTTCGTCACTTCCTC-3'; *Sbp* forward, 5'-TGGAAACGATGATGATGACC-3', *Sbp* reverse, 5'-TGTGGAGATGCAGGACTGAG-3'.

Western blot analysis

Prostates from three animals per strain were rapidly excised, and ventral lobes were separately dissected. Protein extracts were prepared by homogenizing and sonicating each ventral prostate lobe in 500 μl of T-PER buffer (Pierce Biotechnology, Rockford, IL, USA) and a cocktail of protease inhibitors (Roche, Indianapolis, IN, USA). Pooled ventral lobe lysates (50 μg) were separated by SDS-PAGE followed by western blot analysis using antibodies recognizing clusterin (M-18, Santa Cruz Biotechnology, Santa Cruz, CA, USA) and actin (I-19, Santa Cruz) at 1:200 and 1:400 dilutions, respectively.

Immunohistochemistry

Formalin-fixed, paraffin-embedded mouse prostate tissue sections were deparaffinized, and endogenous peroxidase activity was blocked with 3% H_2O_2 for 5 minutes. Antigen was retrieved by steam heating with 10 mM citrate buffer (pH 6.0) for 20 minutes. For the detection of clusterin, a rabbit polyclonal anti-clusterin antibody (H330; Santa Cruz Biotechnology) was used at 1:1,000 dilution in blocking solution, and the sections were incubated for 1 h at room temperature. After washing, the slides were incubated for 30 minutes with biotinylated species-specific secondary antibody diluted 1:500 (Vector Laboratories, Burlingame, CA, USA), washed, then

incubated with avidin-peroxidase complex (ABC, Vector Laboratories) for 30 minutes and visualized using VIP peroxidase substrate (Vector Laboratories). The sections were dehydrated, and permanently mounted. Species-specific IgG isotypes were added in lieu of primary antibody as controls, and these sections demonstrated no detectable staining. The expression of clusterin was assessed in four independent animals per strain.

Tissue morphometry

To evaluate the percentage of each prostate lobe occupied by stroma, two formalin-fixed, paraffin-embedded prostates per strain were serially cut to generate 5 μm sections spaced 30 μm apart. Sections were stained with hematoxylin and eosin and the total tissue areas and stroma areas were separately calculated from each prostate lobe using ImageJ image analysis software [46]. Six measurements were taken from each of the four lobes for each of the five strains. To determine overall differences between strains, we fit the following model:

$$Y_{ijk} = \mu + \text{Strain}_i + \text{Lobe}_j + \varepsilon_k$$

where Y_{ijk} is the percentage of stroma area observed from mouse K, lobe j, strain i.

Data

Microarray data for this study have been deposited in the Gene Expression Omnibus [47] under accession GSE5962.

Acknowledgements

We thank members of the Nelson laboratory for helpful discussions. We thank Barbara Trask for critical review of the manuscript and helpful discussions. We thank Sarah Hawley for assistance with statistical analyses. This work was supported by grants from the National Institutes of Health (R01CA078836, U01CA84294, P01CA85859) and the Department of Defense (PC041158).

References

1. Lichtenstein P, Holm NV, Verkasalo PK, Iliadou A, Kaprio J, Koskenvuo M, Pukkala E, Skytthe A, Hemminki K: **Environmental and heritable factors in the causation of cancer - analyses of cohorts of twins from Sweden, Denmark, and Finland.** *N Engl J Med* 2000, **343:**78-85.
2. Hsing AW, Tsao L, Devesa SS: **International trends and patterns of prostate cancer incidence and mortality.** *Int J Cancer* 2000, **85:**60-67.
3. Emery J, Lucassen A, Murphy M: **Common hereditary cancers and implications for primary care.** *Lancet* 2001, **358:**56-63.
4. Kattan MW, Stapleton AM, Wheeler TM, Scardino PT: **Evaluation of a nomogram used to predict the pathologic stage of clinically localized prostate carcinoma.** *Cancer* 1997, **79:**528-537.
5. Partin AW, Yoo J, Carter HB, Pearson JD, Chan DW, Epstein JI, Walsh PC: **The use of prostate specific antigen, clinical stage and Gleason score to predict pathological stage in men with localized prostate cancer [see comments].** *J Urol* 1993, **150:**110-114.
6. Balmain A: **Cancer as a complex genetic trait: tumor susceptibility in humans and mouse models.** *Cell* 2002, **108:**145-152.
7. Tripodis N, Hart AA, Fijneman RJ, Demant P: **Complexity of lung cancer modifiers: mapping of thirty genes and twenty-five interactions in half of the mouse genome.** *J Natl Cancer Inst* 2001, **93:**1484-1491.
8. Qiu TH, Chandramouli GV, Hunter KW, Alkharouf NW, Green JE, Liu ET: **Global expression profiling identifies signatures of tumor virulence in MMTV-PyMT-transgenic mice: correlation to human disease.** *Cancer Res* 2004, **64:**5973-5981.
9. Nagase H, Mao JH, Balmain A: **A subset of skin tumor modifier loci determines survival time of tumor-bearing mice.** *Proc Natl Acad Sci USA* 1999, **96:**15032-15037.
10. Koratkar R, Silverman KA, Pequignot E, Hauck WW, Buchberg AM, Siracusa LD: **Analysis of reciprocal congenic lines reveals the C3H/HeJ genome to be highly resistant to ApcMin intestinal tumorigenesis.** *Genomics* 2004, **84:**844-852.
11. Asamoto M, Hokaiwado N, Cho YM, Shirai T: **Effects of genetic background on prostate and taste bud carcinogenesis due to SV40 T antigen expression under probasin gene promoter control.** *Carcinogenesis* 2002, **23:**463-467.
12. Demant P: **Cancer susceptibility in the mouse: genetics, biology and implications for human cancer.** *Nat Rev Genet* 2003, **4:**721-734.
13. Hunter K, Welch DR, Liu ET: **Genetic background is an important determinant of metastatic potential.** *Nat Genet* 2003, **34:**23-24. author reply 25
14. Gingrich JR, Barrios RJ, Foster BA, Greenberg NM: **Pathologic progression of autochthonous prostate cancer in the TRAMP model.** *Prostate Cancer Prostatic Dis* 1999, **2:**70-75.
15. Freeman D, Lesche R, Kertesz N, Wang S, Li G, Gao J, Groszer M, Martinez-Diaz H, Rozengurt N, Thomas G, *et al.*: **Genetic background controls tumor development in pten-deficient mice.** *Cancer Res* 2006, **66:**6492-6496.
16. Sandberg R, Yasuda R, Pankratz DG, Carter TA, Del Rio JA, Wodicka L, Mayford M, Lockhart DJ, Barlow C: **Regional and strain-specific gene expression mapping in the adult mouse brain.** *Proc Natl Acad Sci USA* 2000, **97:**11038-11043.
17. Fernandes C, Paya-Cano JL, Sluyter F, D'Souza U, Plomin R, Schalkwyk LC: **Hippocampal gene expression profiling across eight mouse inbred strains: towards understanding the molecular basis for behaviour.** *Eur J Neurosci* 2004, **19:**2576-2582.
18. Bhatia-Gaur R, Donjacour AA, Sciavolino PJ, Kim M, Desai N, Young P, Norton CR, Gridley T, Cardiff RD, Cunha GR, *et al.*: **Roles for Nkx3.1 in prostate development and cancer.** *Genes Dev* 1999, **13:**966-977.
19. Mills JS, Needham M, Parker MG: **Androgen regulated expression of a spermine binding protein gene in mouse ventral prostate.** *Nucleic Acids Res* 1987, **15:**7709-7724.
20. Gleave ME, Miyake H, Zellweger T, Chi K, July L, Nelson C, Rennie P: **Use of antisense oligonucleotides targeting the antiapoptotic gene, clusterin/testosterone-repressed prostate message 2, to enhance androgen sensitivity and chemosensitivity in prostate cancer.** *Urology* 2001, **58:**39-49.
21. July LV, Akbari M, Zellweger T, Jones EC, Goldenberg SL, Gleave ME: **Clusterin expression is significantly enhanced in prostate cancer cells following androgen withdrawal therapy.** *Prostate* 2002, **50:**179-188.
22. Zhang H, Kim JK, Edwards CA, Xu Z, Taichman R, Wang CY: **Clusterin inhibits apoptosis by interacting with activated Bax.** *Nat Cell Biol* 2005, **7:**909-915.
23. Wang S, Gao J, Lei Q, Rozengurt N, Pritchard C, Jiao J, Thomas GV, Li G, Roy-Burman P, Nelson PS, *et al.*: **Prostate-specific deletion of the murine Pten tumor suppressor gene leads to metastatic prostate cancer.** *Cancer Cell* 2003, **4:**209-221.
24. Kim MJ, Cardiff RD, Desai N, Banach-Petrosky WA, Parsons R, Shen MM, Abate-Shen C: **Cooperativity of Nkx3.1 and Pten loss of function in a mouse model of prostate carcinogenesis.** *Proc Natl Acad Sci USA* 2002, **99:**2884-2889.
25. Subramanian A, Tamayo P, Mootha VK, Mukherjee S, Ebert BL, Gillette MA, Paulovich A, Pomeroy SL, Golub TR, Lander ES, Mesirov JP: **Gene set enrichment analysis: a knowledge-based approach for interpreting genome-wide expression profiles.** *Proc Natl Acad Sci USA* 2005, **102:**15545-15550.
26. Lapointe J, Li C, Higgins JP, van de Rijn M, Bair E, Montgomery K, Ferrari M, Egevad L, Rayford W, Bergerheim U, *et al.*: **Gene expression profiling identifies clinically relevant subtypes of prostate cancer.** *Proc Natl Acad Sci USA* 2004, **101:**811-816.
27. Simard J, Veilleux R, de Launoit Y, Haagensen DE, Labrie F: **Stimulation of apolipoprotein D secretion by steroids coincides with inhibition of cell proliferation in human LNCaP prostate cancer cells.** *Cancer Res* 1991, **51:**4336-4341.
28. Haagensen DE, Stewart P, Dilley WG, Wells SA: **Secretion of breast gross cystic disease fluid proteins by T47D breast cancer cells in culture - modulation by steroid hormones.** *Breast*

Cancer Res Treat 1992, **23:**77-86.
29. Hall RE, Horsfall DJ, Stahl J, Vivekanandan S, Ricciardelli C, Stapleton AM, Scardino PT, Neufing P, Tilley WD: **Apolipoprotein-D: a novel cellular marker for HGPIN and prostate cancer.** *Prostate* 2004, **58:**103-108.
30. Walker DW, Muffat J, Rundel C, Benzer S: **Overexpression of a Drosophila homolog of apolipoprotein D leads to increased stress resistance and extended lifespan.** *Curr Biol* 2006, **16:**674-679.
31. Sanchez D, Lopez-Arias B, Torroja L, Canal I, Wang X, Bastiani MJ, Ganfornina MD: **Loss of glial lazarillo, a homolog of apolipoprotein D, reduces lifespan and stress resistance in Drosophila.** *Curr Biol* 2006, **16:**680-686.
32. Kim MJ, Cardiff RD, Desai N, Banach-Petrosky WA, Parsons R, Shen MM, Abate-Shen C: **Cooperativity of Nkx3.1 and Pten loss of function in a mouse model of prostate carcinogenesis.** *Proc Natl Acad Sci USA* 2002, **99:**2884-2889.
33. Thompson TC, Timme TL, Kadmon D, Park SH, Egawa S, Yoshida K: **Genetic predisposition and mesenchymal-epithelial interactions in ras+myc-induced carcinogenesis in reconstituted mouse prostate.** *Mol Carcinog* 1993, **7:**165-179.
34. Tomlins SA, Rhodes DR, Perner S, Dhanasekaran SM, Mehra R, Sun XW, Varambally S, Cao X, Tchinda J, Kuefer R, *et al.*: **Recurrent fusion of TMPRSS2 and ETS transcription factor genes in prostate cancer.** *Science* 2005, **310:**644-648.
35. Bond GL, Hu W, Bond EE, Robins H, Lutzker SG, Arva NC, Bargonetti J, Bartel F, Taubert H, Wuerl P, *et al.*: **A single nucleotide polymorphism in the MDM2 promoter attenuates the p53 tumor suppressor pathway and accelerates tumor formation in humans.** *Cell* 2004, **119:**591-602.
36. Schadt EE, Monks SA, Drake TA, Lusis AJ, Che N, Colinayo V, Ruff TG, Milligan SB, Lamb JR, Cavet G, *et al.*: **Genetics of gene expression surveyed in maize, mouse and man.** *Nature* 2003, **422:**297-302.
37. Pritchard C, Coil D, Hawley S, Hsu L, Nelson PS: **The contributions of normal variation and genetic background to mammalian gene expression.** *Genome Biol* 2006, **7:**R26.
38. Yang H, Crawford N, Lukes L, Finney R, Lancaster M, Hunter KW: **Metastasis predictive signature profiles pre-exist in normal tissues.** *Clin Exp Metastasis* 2005, **22:**593-603.
39. Pritchard CC, Hsu L, Delrow J, Nelson PS: **Project normal: defining normal variance in mouse gene expression.** *Proc Natl Acad Sci USA* 2001, **98:**13266-13271.
40. Abbott DE, Pritchard C, Clegg NJ, Ferguson C, Dumpit R, Sikes RA, Nelson PS: **Expressed sequence tag profiling identifies developmental and anatomic partitioning of gene expression in the mouse prostate.** *Genome Biol* 2003, **4:**R79.
41. Dudoit S, Yang Y, Callow M, Speed T: *Technical Report* Berkeley, CA: Department of Statistics, University of California at Berkeley; 2000.
42. Tusher VG, Tibshirani R, Chu G: **Significance analysis of microarrays applied to the ionizing radiation response.** *Proc Natl Acad Sci USA* 2001, **98:**5116-5121.
43. Gentleman RC, Carey VJ, Bates DM, Bolstad B, Dettling M, Dudoit S, Ellis B, Gautier L, Ge Y, Gentry J, *et al.*: **Bioconductor: open software development for computational biology and bioinformatics.** *Genome Biol* 2004, **5:**R80.
44. **The Mouse Prostate Expression Database** [http://www.mpedb.org]
45. **The Gene Ontology Database** [http://www.geneontology.org]
46. **Image J Software** [http://rsb.info.nih.gov/ij/]
47. **Gene Expression Omnibus** [http://www.ncbi.nlm.nih.gov/geo/]

Tissue-Specific Consequences of Cyclin D1 Overexpression in Prostate Cancer Progression

Yue He,[1] Omar E. Franco,[2] Ming Jiang,[2] Karin Williams,[2] Harold D. Love,[2] Ilsa M. Coleman,[4] Peter S. Nelson,[4] and Simon W. Hayward[1,2,3]

Departments of [1]Cancer Biology and [2]Urologic Surgery, [3]Vanderbilt-Ingram Cancer Center, Vanderbilt University Medical Center, Nashville, Tennessee and [4]Divisions of Human Biology and Clinical Research, Fred Hutchinson Cancer Research Center, Seattle, Washington

Abstract

The cyclin D1 oncogene encodes the regulatory subunit of a holoenzyme that phosphorylates and inactivates the Rb protein and promotes progression through G_1 to S phase of the cell cycle. Several prostate cancer cell lines and a subset of primary prostate cancer samples have increased cyclin D1 protein expression. However, the relationship between cyclin D1 expression and prostate tumor progression has yet to be clearly characterized. This study examined the effects of manipulating cyclin D1 expression in either human prostatic epithelial or stromal cells using a tissue recombination model. The data showed that overexpression of cyclin D1 in the initiated BPH-1 cell line increased cell proliferation rate but did not elicit tumorigenicity *in vivo*. However, overexpression of cyclin D1 in normal prostate fibroblasts (NPF) that were subsequently recombined with BPH-1 did induce malignant transformation of the epithelial cells. The present study also showed that recombination of BPH-1 + cyclin D1–overexpressing fibroblasts ($NPF^{cyclin\ D1}$) resulted in permanent malignant transformation of epithelial cells ($BPH\text{-}1^{NPF\text{-}cyclin\ D1}$ cells) similar to that seen with carcinoma-associated fibroblasts (CAF). Microarray analysis showed that the expression profiles between CAFs and $NPF^{cyclin\ D1}$ cells were highly concordant including cyclin D1 up-regulation. These data indicated that the tumor-promoting activity of cyclin D1 may be tissue specific. [Cancer Res 2007;67(17):8188–97]

Introduction

Prostate development is controlled by steroid hormones that induce and maintain a complex cross-talk between the stromal and epithelial cells (1). The result of this intercellular communication depends on the context and differentiation status of the cell type being stimulated (2, 3). The process of prostatic carcinogenesis includes aberrations in the interactions of the prostatic epithelium and its local microenvironment resulting in reciprocal dedifferentiation of both the emerging carcinoma cells and the prostatic smooth muscle.

The vast majority of human prostatic cancers arise as adenocarcinomas, which, by definition, are derived from the epithelial cells that form the glands and ducts of the prostate. As the carcinoma evolves, phenotypic changes and alterations in gene expression also occur in the adjacent stroma. These "changes" may enhance the invasive potential of the epithelial tumor (4–6). Chung et al. (7) reported that coinoculation of tumorigenic Nbf-1 fibroblasts with human PC-3 cells accelerated tumor growth. Human prostatic carcinoma-associated fibroblasts (CAF) have also been shown to be capable of stimulating carcinogenesis and inducing the progression of an initiated epithelium (the SV40 immortalized BPH-1 cell line), whereas normal prostate fibroblasts (NPF) were incapable of stimulating such progression (8). The mechanistic basis by which stromal-epithelial interactions enhance the process of prostatic carcinogenesis and tumor invasion is beginning to be dissected (6, 9).

The cells in the tumor microenvironment supporting and nurturing the developing tumor include stromal fibroblasts, infiltrating immune cells, blood, and lymphatic vascular networks (10). A detailed understanding of the changes occurring within tumor stroma and to the signaling mechanisms acting between stroma and epithelium will allow for the rational design of therapies aimed at inhibiting prostate tumor growth.

Cyclin D1 encodes the regulatory subunit of a holoenzyme that phosphorylates and inactivates the retinoblastoma protein and promotes progression through G_1 to S phase of the cell cycle (11, 12). Overexpression of cyclin D1 plays important roles in the development of human cancers, including breast, colon, and melanoma (11, 13–17). Increased cyclin D1 expression occurs relatively early during tumorigenesis; however, its role in prostate cancer is not well understood. Studies have shown that mouse prostatic normal and $Rb^{-/-}$ epithelial cells have elevated cyclin D1 expression as they enter the cell cycle (18). Human prostate carcinoma cell lines frequently express elevated levels of cyclin D1 protein, although the gene is not amplified in these cells (18). This situation is analogous to that seen in a subset of human breast cancer cell lines and tumors (19, 20). Overexpression of cyclin D1 can increase tumorigenicity of LNCaP cell lines. Additionally, androgen ablation has a smaller inhibitory effect on tumors formed by cyclin D1–overexpressing LNCaP cells compared with tumors formed by parental LNCaP cells, which regress after castration. This phenomenon suggests that cyclin D1 overexpression might be related to the evolution of androgen-independent prostate cancer (21). Immunostaining studies indicated that primary prostate carcinoma samples displayed moderate or strong expression of cyclin D1 protein in the epithelial compartment compared with normal epithelium. Little is known about the role of cyclin D1 in the stromal compartment of tumors, especially in adenocarcinomas. One study of cyclin D1 expression in esophageal carcinomas indicated that cyclin D1 is strongly expressed in stromal fibroblasts (22).

In this study, we examined the consequences of targeted regulation of cyclin D1 expression in epithelial or stromal cells to investigate the effects of cyclin D1 in prostate cancer progression.

Note: Supplementary data for this article are available at Cancer Research Online (http://cancerres.aacrjournals.org/).

Requests for reprints: Simon W. Hayward, Department of Urologic Surgery, Vanderbilt University Medical Center, A1302 MCN, Nashville, TN 37232-2765. Phone: 615-322-5823; Fax: 615-322-8990; E-mail: simon.hayward@vanderbilt.edu.

doi:10.1158/0008-5472.CAN-07-0418

Materials and Methods

Cells. BPH-1 (a nontumorigenic prostate epithelial cell) and its tumorigenic derivatives BPH^{CAFTD1} and BPH^{CAFTD2} were from our own stocks (23, 24). DU145, LNCaP, and PC-3 cells were obtained from American Type Culture Collection (ATCC). NPF, BPH fibroblasts, and CAFs were isolated and bioassayed as described previously (8). Prostatic epithelial cell (PrE) 1 cells were isolated from human benign prostate tissue. 957E/hTERT cells were generously supplied by Dr. John Isaacs (Johns Hopkins Oncology Center, Baltimore, MD). PrE3 cells were kindly provided by Dr. Dean Tang (The University of Texas M. D. Anderson Cancer Center, Houston, TX). BPH-1$^{C7\text{-}cyclin\ D1}$, BPH-1$^{C7\text{-}\Delta}$, BPH-1^{NPF}, NPF$^{cyclin\ D1}$, and BPH-1$^{NPF\text{-}cyclin\ D1}$ cells were generated as described below. All of the epithelial cells were maintained in RPMI 1640 (Life Technologies) with 1% antibiotic/antimycotic (Life Technologies) and 5% cosmic calf serum (CCS; HyClone). All of the stromal cells were maintained in the same condition except that 5% fetal bovine serum (Atlanta Biologicals) was used in place of CCS.

Construction of cyclin D1 expression vector. The plasmid C7-cyclin D1 was constructed using the LZRS-EGFP backbone (Nolan Laboratory, Stanford University, CA). The cytomegalovirus promoter was cut from pIRES-EGFP (Clontech) as a *Bgl*II/*Bam*HI fragment. The fragment was then ligated into the *Bam*HI site of the LZRS-EGFP backbone to produce C7-Δ. The human cyclin D1 cDNA clone was obtained from ATCC and amplified by PCR using a 5′ primer specific to translational start site and a 3′ primer containing an *Xho*I restriction site and the consensus sequence for the translational stop site. After PCR amplification, the product was gel purified and cloned into pGemT-Easy (Promega). Following DNA sequence verification, the cyclin D1 coding region was cut using *Eco*RI/*Xho*I and subcloned into the *Eco*RI/*Xho*I sites of pLZRS-EGFP to obtain C7-cyclin D1 construct.

Generation of a stable cyclin D1–overexpressing BPH-1 cell line. Viral particles were prepared as described previously and used to infect BPH-1 cells (25). Fresh virus was placed onto target cells every 24 h until green fluorescent protein (GFP) expression was observed. Cell sorting was done to select the GFP-expressing BPH-1 cells. Two stable cell lines were generated: C7-cyclin D1–overexpressing BPH-1 cell line and C7-Δ control BPH-1 cell line, which were designated as BPH-1$^{C7\text{-}cyclin\ D1}$ and BPH-1$^{C7\text{-}\Delta}$, respectively.

Generation of NPF$^{cyclin\ D1}$ cells. Human prostatic cells were prepared as described previously (25). Cyclin D1 virus was generated using phoenix A cells, and the prostatic cells were infected as described (25). After 1 week of successive rounds of infection, some cells expressed enhanced GFP (EGFP) when monitored by fluorescence microscopy. Differential trypsinization was used to separate fibroblasts from the epithelial cells. The resulting colonies were characterized by phenotype and their nature was confirmed using immunocytochemical staining against keratin and vimentin. After 12 passages, EGFP-expressing cells self-sorted as all unstained cells became senescent and died.

Western blotting analysis. Cell lysates were prepared and Western blotting was done as described previously (25). Membranes were incubated with mouse monoclonal antibody to cyclin D1 (1:1,000 dilution; BD Biosciences PharMingen) or α-tubulin (1:1,000 dilution; Santa Cruz Biotechnology) overnight, washed with PBS-Tween 20 for 1 h, and incubated with horseradish peroxidase (HRP)–linked antimouse or antirabbit secondary antibody (1:1,000 dilution; Amersham Biosciences) for 1 h. Bound antibodies were visualized using enhanced chemiluminescence Western blotting detection reagents (Amersham Bioscences). Cyclin D1 expression levels were normalized to β-actin and quantitated using Image J software from the NIH.[5]

Growth curves. BPH-1$^{C7\text{-}\Delta}$ and BPH-1$^{C7\text{-}cyclin\ D1}$ cells were plated in a 24-well plate (1,000 cells per well) in RPMI 1640 supplemented with 5% CCS. After the cells had attached overnight, 300 μL of CellTiter 96 Aqueous One Solution (Promega) were added at indicated times (1–5 days) to each well and the absorbance was measured at 490 nm after 3 h of incubation at 37°C. Experiments were done in triplicate.

Wound healing assays. Confluent monolayers of BPH-1$^{C7\text{-}\Delta}$ and BPH-1$^{C7\text{-}cyclin\ D1}$ cells were grown in six-well plates. An even line of cells was displaced by scratching through the layer using a pipette tip. Specific points on the wounds were identified and marked. These open areas were then inspected microscopically over time as the cells move in and fill the damaged area. Wounds were imaged at 0, 3, 6, and 8 h postwounding and the cell migration rate into the wound was calculated. Experiments were done in triplicate.

Transwell migration assay. One hundred thousand BPH-1$^{C7\text{-}\Delta}$ or BPH-1$^{C7\text{-}cyclin\ D1}$ cells were plated on top of the 8-μm pore polycarbonate culture inserts (Becton Dickinson Labware), which were situated in wells of a 24-well culture plate and immersed in RPMI 1640 supplemented with 5% CCS. The cells were incubated at 37°C for 12 h. The cells on the upper surface of the inserts were removed using cotton swabs and those that had migrated to the bottom side were fixed with 11% glutaraldehyde (Sigma) for 20 min and stained with 0.1% crystal violet (Sigma) for 20 min. Inserts were then washed with water three times. The number of cells that had migrated was counted using a microscope. The filters were viewed under bright-field optics to count stained cells in eight fields (with a 20× objective) for the two types of cells. The mean number of cells per field was determined, and results from at least three experiments were expressed as the mean relative cell migration ± SD, with that of BPH-1$^{C7\text{-}\Delta}$ cells set at 1.

Boyden chamber assay. Polycarbonate culture inserts with 8-μm pores were coated with 20 μL of 2.5 mg/mL Matrigel (BD Biosciences). After the gel solidified, the chambers were equilibrated with RPMI 1640 with 5% CCS for 2 h in a humidified tissue culture incubator at 37°C with 5% CO_2 atmosphere. More media were then added to the lower compartment, and 100k BPH-1$^{C7\text{-}\Delta}$ and BPH-1$^{C7\text{-}cyclin\ D1}$ cells were seeded in the upper compartment of the chamber. Each cell group was plated in three duplicate wells. After 12 h of incubation, the Matrigel was removed using a cotton swab. The number of cells that had migrated to the lower sides of the membrane was then determined as described for the Transwell migration assay.

Tissue recombination and xenografting. One hundred thousand epithelial cells and 300k stromal cells were recombined to make the BPH-1$^{C7\text{-}\Delta}$ + rat urogenital mesenchyme (rUGM), BPH-1$^{C7\text{-}cyclin\ D1}$ + rUGM, BPH-1 + NPF, and BPH-1 + NPF$^{cyclin\ D1}$ tissue recombinants as described previously (26). After incubating overnight at 37°C, the tissue recombinants were grafted under the kidney capsule of adult male severe combined immunodeficient (SCID) mice (Harlan). All the experiments were repeated six times. Mice were sacrificed after 4 weeks and grafts were harvested, fixed, and embedded.

Immunohistochemical staining. Immunohistochemical staining was done following a protocol that was described previously (25). Tissue slides were incubated with the primary antibody against SV40 (1:1,000 dilution; Santa Cruz Biotechnology), E-cadherin (1:1,000; BD Biosciences PharMingen), or anti–phospho-histone H3 (1:200; Upstate) overnight. The polyclonal rabbit or mouse immunoglobulins/biotinylated antimouse secondary antibody (DAKO) was incubated for 60 min after the slides were washed with PBS buffer for 1 h. After washing the slides in PBS extensively, slides were incubated in ABC-HRP complex (Vector Laboratories) for 30 min. Bound antibodies were then visualized by incubation with liquid 3,3′-diaminobenzidine tetrahydrochloride (DAKO). Slides were then rinsed extensively in tap water, counterstained with hematoxylin, and mounted.

Isolation of cell strains and regrafting. BPH-1^{NPF} and BPH-1$^{NPF\text{-}cyclin\ D1}$ cells were isolated and selected with 50 μg/mL G418 (Clontech) from BPH-1 + NPF and BPH-1 + NPF$^{cyclin\ D1}$ grafts and regrafted without stromal cells to SCID mice as described previously (27). Four to 14 weeks after grafting, the hosts were sacrificed. The harvested grafts were removed from the kidney and formalin fixed for immunohistochemical analysis.

Cell cycle analysis. BPH-1^{NPF} cells and BPH-1$^{NPF\text{-}cyclin\ D1}$ cells were harvested from monolayer culture. The cell pellets were washed, counted, and resuspended in PBS and fixed with 80% ethanol with vortexing. Cells were then pelleted and resuspended with PBS containing 1% CCS for cell counting after storing at −20°C for 4 h. One hundred thousand cells were

[5] http://rsb.info.nih.gov/ij/

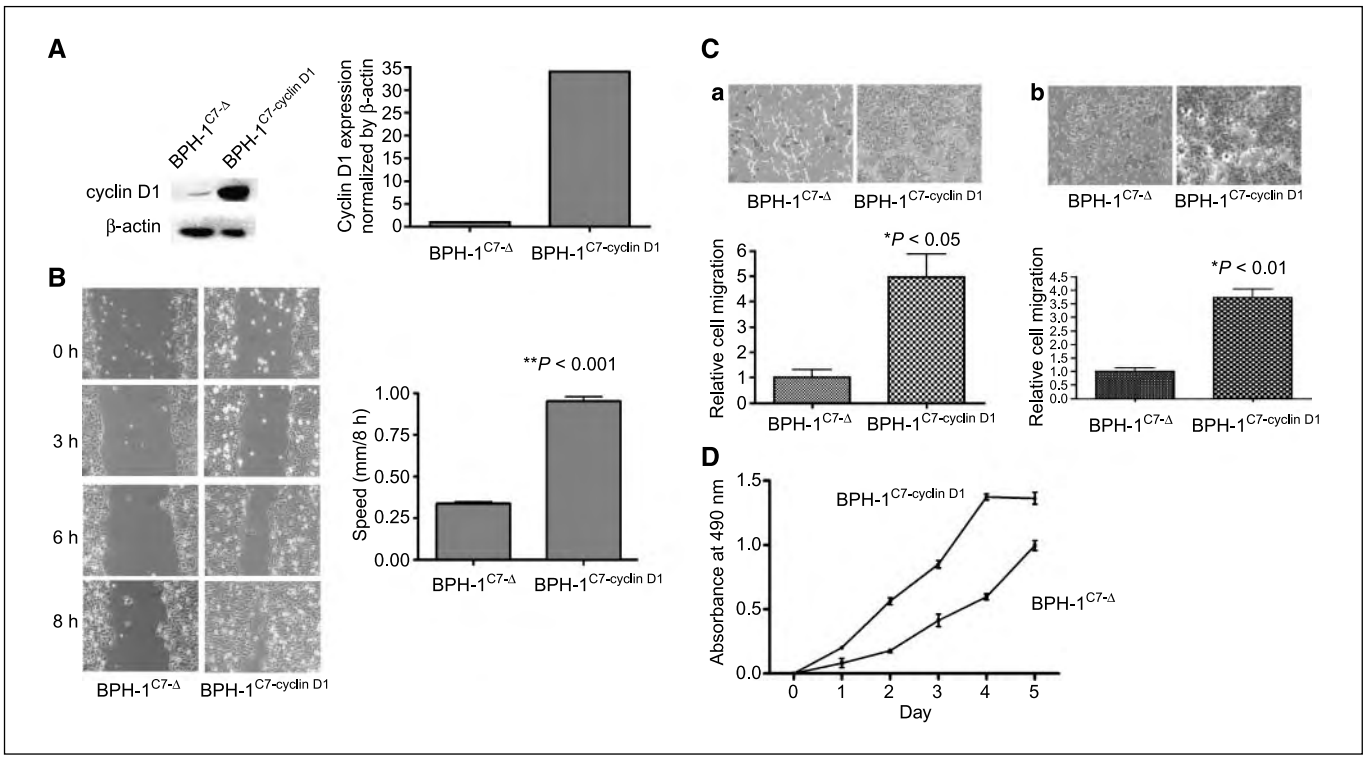

Figure 1. *In vitro* comparison of BPH-1$^{C7\text{-}\Delta}$ and BPH-1$^{C7\text{-cyclin D1}}$ cells. *A,* to examine the role of cyclin D1 in prostate cancer progression, C7-Δ (control – BPH-1$^{C7\text{-}\Delta}$) and cyclin D1–overexpressing (BPH-1$^{C7\text{-cyclin D1}}$) BPH-1 cell lines were generated by stable retroviral infection. Cyclin D1 overexpression in BPH-1$^{C7\text{-cyclin D1}}$ was confirmed by Western blotting and band intensity was quantitated. *B,* wound healing assay. BPH-1$^{C7\text{-cyclin D1}}$ closed wounds in the confluent monolayer were significantly faster than BPH-1$^{C7\text{-}\Delta}$ cells. Images (*left*) and quantitation (*right*). $P < 0.001$, Student's *t* test. *C,* Transwell migration study and invasion assay. BPH-1$^{C7\text{-cyclin D1}}$ migrated through the uncoated Boyden chamber significantly faster than BPH-1$^{C7\text{-}\Delta}$. Representative phase-contrast optical photomicrographs after overnight culture were shown (*a, top*) and quantitated (*a, bottom*). $P < 0.05$, Student's *t* test. BPH-1$^{C7\text{-cyclin D1}}$ cells had increased invasive ability in a Matrigel-coated Boyden chamber invasion assay compared with BPH-1$^{C7\text{-}\Delta}$. Representative phase-contrast optical photomicrographs after overnight culture were shown (*b, top*) and quantitated (*b, bottom*). $P < 0.01$, Student's *t* test. *D,* proliferation assay. Cyclin D1 overexpression promoted BPH-1 cell proliferation significantly over control growth rate. $P < 0.001$, Student's *t* test.

resuspended in propidium iodide/RNase/1% CCS/PBS. Propidium iodide was used to stain double-stranded nucleic acids stoichiometrically. Cells were treated with RNase A to stain only the DNA. Cell cycle distribution was analyzed on the flow cytometer after at least 30 min.

Microarray analysis. NPF$^{\text{cyclin D1}}$ cells were generated from NPFs, which were isolated from two different patient samples; CAFs were isolated from two different patient samples as well. RNA was isolated from NPFs, CAFs, and NPF$^{\text{cyclin D1}}$ cells using total RNA isolation kit (Qiagen). Custom spotted cDNA microarrays were constructed as described previously (28) using a nonredundant set of 6,700 prostate-derived cDNA clones identified from the prostate expression data base, a public sequence repository of expressed sequence tag data derived from human prostate cDNA libraries. Total RNA was amplified through one round of linear amplification using the MessageAmp aRNA kit (Ambion). Sample quality and quantification was assessed by agarose gel electrophoresis and absorbance at A_{260}. Cy3-labeled and Cy5-labeled cDNA probes were made from 4 μg of amplified RNA. Two NPF$^{\text{cyclin D1}}$ and two CAF samples (labeled with Cy3) were hybridized head-to-head with a NPF control sample labeled with Cy5. Probes were hybridized competitively to microarrays under a coverslip for 16 h at 63°C. Fluorescent array images were collected for both Cy3 and Cy5 by using a GenePix 4000B fluorescent scanner, and image intensity data were gridded and extracted using GenePix Pro 4.1 software. Differences in gene expression between NPF$^{\text{cyclin D1}}$/NPF and CAF/NPF groups were determined using a two-sample *t* test with Significance Analysis of Microarrays (SAM) software[6] with a false discovery rate (FDR) of ≤10% considered significant (Tusher, 2001). Similarities in gene expression between NPF$^{\text{cyclin D1}}$/NPF and CAF/NPF groups were determined using a one-sample *t* test in SAM with a FDR of ≤0.1% considered significant. These results were reduced to unique genes by eliminating all but the highest scoring clones for each gene. A Pearson correlation coefficient was calculated in Excel to assess the strength of the linear relationship between NPF$^{\text{cyclin D1}}$/NPF and CAF/NPF average log 2 ratios.

[6] http://www-stat.stanford.edu/_tibs/SAM/

Results

Cyclin D1 expression levels are elevated in malignant human prostatic epithelial cell lines. Cyclin D1 expression was examined by Western blotting in the prostate cancer cell lines, DU145, LNCaP, BPH$^{\text{CAFTD1}}$, and BPH$^{\text{CAFTD2}}$, and in a subset of nontumorigenic prostatic cells, PrE1, 957E/hTERT (27, 29), PrE3, and BPH-1 cell line. Cyclin D1 expression was found to be higher in all of the cancer cells compared with the nontumorigenic prostatic cells. A representative Western blot is shown in Supplementary Fig. S1. Primary epithelial cells had the lowest cyclin D1 expression. The SV40 T-antigen immortalized BPH-1 cells had higher cyclin D1 expression compared with PrE, 957E/hTERT and PrE, but lower expression level than that in malignant cell lines. These data crudely correlate cyclin D1 with tumorigenicity but, as with similar correlations seen in patient samples, do not address whether cyclin D1 overexpression is a cause or an effect of malignant change. To address this question, we tested the consequences of overexpressing cyclin D1 in nontumorigenic prostatic epithelial cells.

Cyclin D1 overexpression in BPH-1 cells can increase cell proliferation rate, migration, and invasive ability *in vitro*. Western blotting showed that the BPH-1$^{cyclin\ D1}$ cells have a 34-fold elevation in cyclin D1 expression compared with control BPH-1$^{C7\text{-}\Delta}$ cells (Fig. 1*A*). BPH-1$^{C7\text{-}cyclin\ D1}$ cells showed enhanced motile ability in wound healing, Transwell migration, and Boyden chamber assays. Wound healing assays showed that BPH-1$^{C7\text{-}cyclin\ D1}$ cells were significantly more motile than BPH-1$^{C7\text{-}\Delta}$ cells. This difference was clear after 3 h and was very marked after 8 h ($P < 0.001$, Student's *t* test; Fig. 1*B*). In a Transwell migration study, the BPH-1$^{C7\text{-}cyclin\ D1}$ cells migrated through the uncoated Boyden chambers to the underside of the insert in greater numbers in a 12-h response to conditional medium containing 1% CCS in the lower chamber than BPH-1$^{C7\text{-}\Delta}$ cells ($P < 0.05$, Student's *t* test; Fig. 1*C*). These data confirmed the elevated motility of BPH-1$^{C7\text{-}cycin\ D1}$ cells, as seen in the wound healing assay. An invasion assay, in which the inside chamber was coated with Matrigel to mimic the *in vivo* extracellular matrix (ECM), showed that BPH-1$^{C7\text{-}cyclin\ D1}$ cells had significantly increased invasive activity *in vitro* ($P < 0.01$, Student's *t* test; Fig. 1*D*). We used a 3-(4,5-dimethylthiazol-2-yl)-2,5-diphenyltetrazolium bromide assay to assess the effect of cyclin D1 overexpression on the growth rate of BPH-1 cells. Our results showed that the cyclin D1–overexpressing cells proliferated faster than control cells. The difference was observed even after 24 h of incubation (Fig. 1*E*). Collectively, the assays showed that when cyclin D1 is forcibly overexpressed, BPH-1 cells acquired an enhanced proliferation rate, motility, and invasive ability *in vitro*.

Cyclin D1–overexpressing BPH-1 cells are not tumorigenic in tissue recombinants with rUGM. To determine whether cyclin D1 could exert a tumorigenic effect on prostate cells *in vivo*, 100k BPH-1$^{C7\text{-}cyclin\ D1}$ cells or control cells were recombined with 300k rUGM and grafted under the kidney capsule of SCID mice. The grafts were harvested after 4, 8, 12, and 16 weeks. The results showed that BPH-1$^{C7\text{-}cyclin\ D1}$ cells formed significantly larger and

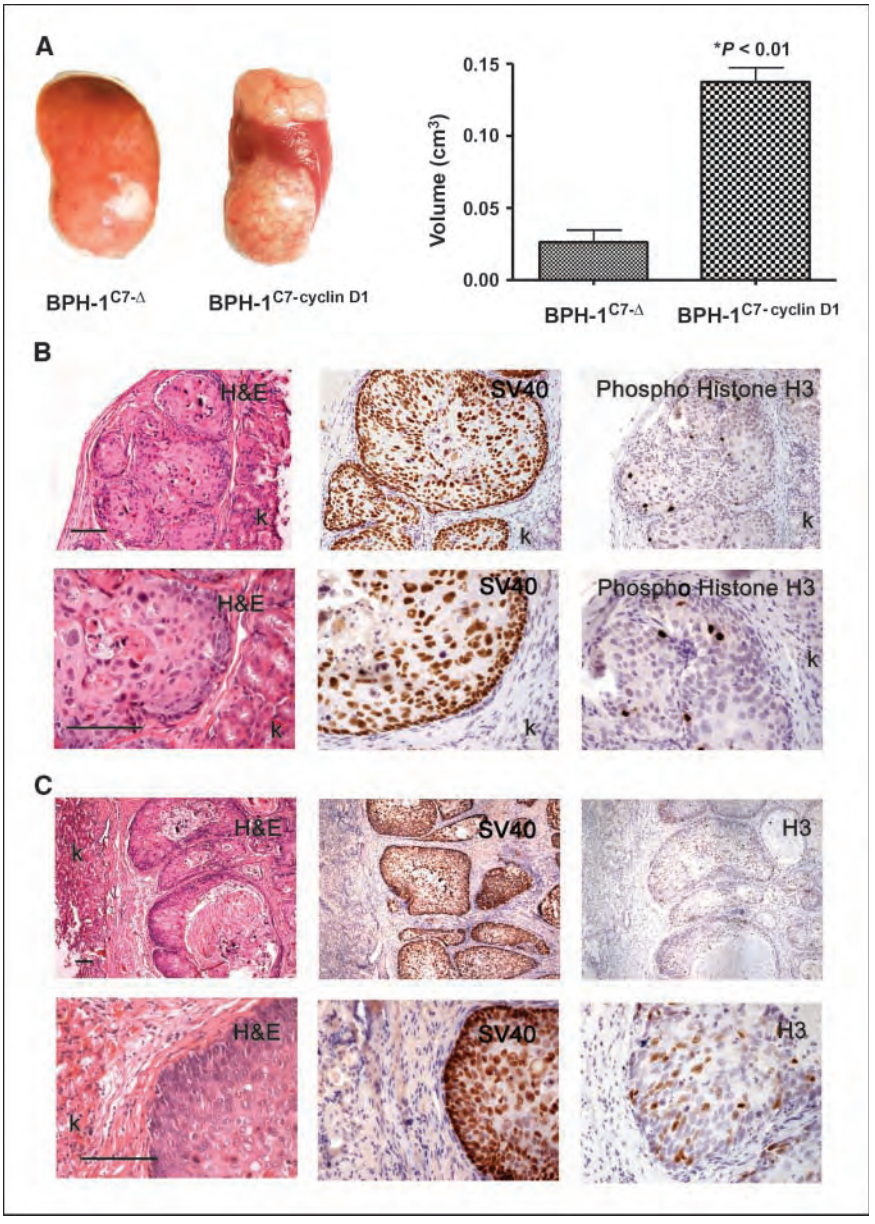

Figure 2. Overexpression of cyclin D1 in epithelium was insufficient to induce malignant transformation in BPH-1 cells as determined by *in vivo* assays. *A,* BPH-1$^{C7\text{-}cyclin\ D1}$ cells were not tumorigenic under the influence of the inductive rUGM in the tissue recombination model. Gross morphology of 2-month grafts of BPH-1$^{C7\text{-}\Delta}$ + UGM (*left*) and BPH-1$^{C7\text{-}cyclin\ D1}$ + UGM (*right*). The volume of grafts containing BPH-1$^{C7\text{-}cyclin\ D1}$ was significantly larger than controls. $P < 0.01$, Student's *t* test. *B,* H&E staining of BPH-1$^{C7\text{-}\Delta}$ + UGM grafts showed that the recombinants formed solid cord structures with no sign of invasion to the host kidney. SV40 T-antigen staining confirmed the cell origin of the epithelium. Phospho-histone H3 staining identified few positive cells in the solid cords. Higher magnification pictures (*bottom*). *Bar*, 50 μm. *C,* H&E and SV40 T-antigen staining of BPH-1$^{C7\text{-}cyclin\ D1}$ + UGM grafts. Histology is similar to that seen in the control groups. The basement membrane between kidney and graft was intact and no sign of invasion into the host kidney was seen. Phospho-histone H3 staining identified significantly more positive cells in the solid cords compared in (*B*). Higher-magnification images (*bottom*). *Bar*, 50 μm. *k,* host kidney.

more vascularized grafts under the induction of rUGM compared with BPH-1$^{C7\text{-}\Delta}$ cells. An example of the gross morphology of grafts at 8 weeks is shown in Fig. 2*A*. These results are consistent with our *in vitro* experiments, which showed that BPH-1$^{C7\text{-cyclin D1}}$ cells proliferate faster than controls. Histologically, both experimental and control grafts exhibited the formation of solid epithelial cords surrounded by a muscular stroma. SV40 T-antigen staining confirmed the origin of BPH-1 cells in both control and cyclin D1–overexpressing groups and showed that there were sharp delineations from the host kidney with no sign of invasion (Fig. 2*B* and *C*). It was noteworthy that a clear layer of stromal cells was always seen between the graft and host kidney under both control and test conditions. In the control grafts, few epithelial cells were phospho-histone H3 positive (indicating low proliferation rates). However, there were significantly more histone H3–positive cells in BPH-1$^{\text{cyclin D1}}$ cords ($P < 0.01$, Student's t test; data not shown). These data indicated that BPH-1$^{\text{cyclin D1}}$ cells proliferated much faster than control cells (Fig. 2*B* and *C*). To assess whether cyclin D1 can transform BPH-1 cells in a longer period *in vivo*, we sacrificed mice every month for up to 4 months. The histologic appearance of the grafts at 4 months was similar to the earlier grafts with solid cord structures and no invasion of the kidney (date not shown). Therefore, although cyclin D1 can increase BPH-1 cell motility and promote cell proliferation *in vitro*, overexpression of the gene did not induce BPH-1 cells to undergo malignant transformation with associated invasion.

NPF$^{\text{cyclin D1}}$ cells have increased life span compared with NPFs and CAF cells have up-regulated cyclin D1 expression. Because the stroma is viewed as an important active contributor to tumor growth and to understand whether cyclin D1 does different functions in stromal and epithelial tissues, we generated NPF$^{\text{cyclin D1}}$ cells by overexpressing cyclin D1 in primary cultures of normal prostate stromal cells. To investigate whether the cyclin D1–overexpressing fibroblasts have an increased life span compared with control or noninfected cells, we passaged the cell mixtures 12 times. The uninfected cells underwent spontaneous senescence and died within 12 passages. The EGFP-expressing cells still looked healthy and grew well after 11 more passages (total of 23 passages; Fig. 3*A*). Western blot analysis showed that EGFP-positive cells also overexpressed cyclin D1 (Fig. 3*B*). This result indicated that NPFs acquired a prolonged life span as a consequence of up-regulated cyclin D1.

It has been shown previously that CAF cells can induce BPH-1 cells to undergo malignant transformation, whereas NPFs cannot (8). Cyclin D1 is strongly expressed in stromal fibroblasts in carcinoma and adenocarcinoma (22). We were interested to determine whether human prostatic CAFs have elevated cyclin D1 expression and if so whether CAFs and NPF$^{\text{cyclin D1}}$ cells share common functional sequelae. Therefore, we examined the expression level of cyclin D1 in NPFs, BPH fibroblasts, and CAF cells. These experiments showed that CAFs expressed a much higher level of cyclin D1 protein than either NPFs or fibroblasts isolated from BPH patients (Fig. 3*B*).

NPF$^{\text{cyclin D1}}$ cells elicit CAF-like effects promoting tumorigenesis. To investigate the *in vivo* consequences of overexpression of cyclin D1 in NPFs, 100k BPH-1 cells were recombined with either 300k NPF$^{\text{cyclin D1}}$ or NPF cells. Grafts were harvested after 1 month. Tissue recombinants composed of BPH-1 + NPF$^{\text{cyclin D1}}$ exhibited moderate growth; in contrast, consistent with previously published data, control recombinants composed of BPH-1 + NPFs showed minimal growth. Control grafts of NPF and NPF$^{\text{cyclin D1}}$ were likewise

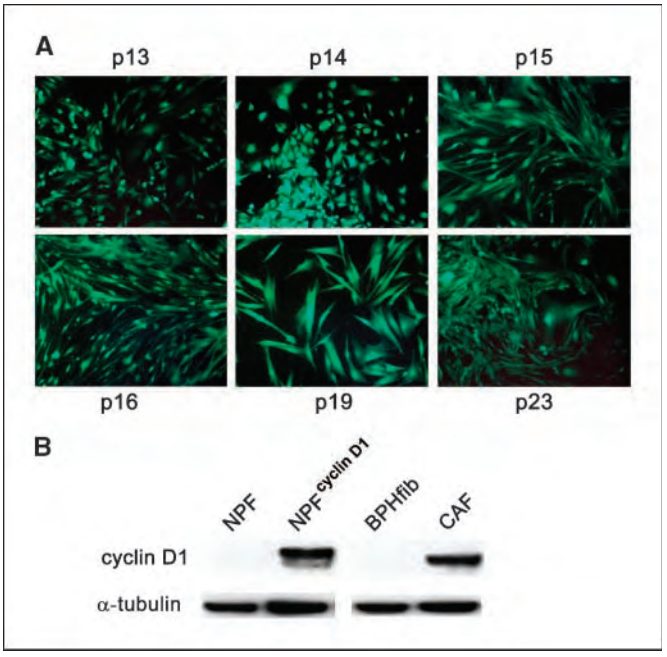

Figure 3. Expression of cyclin D1 in human prostatic fibroblasts. *A,* NPF$^{\text{cyclin D1}}$ cells have increased life span compared with NPF cells. Control cells were all dead within 12 passages. The NPF$^{\text{cyclin D1}}$ cells seemed healthy after 23 passages (passage number shown adjacent to illustration) after infection by C7-cyclin D1–overexpressing retroviral vector (total of 23 passages). *B,* Western blotting results confirmed that cyclin D1 was overexpressed in NPF$^{\text{cyclin D1}}$ cells. Human prostatic CAF cells also expressed elevated levels of cyclin D1 protein compared with NPF or with BPH-derived fibroblasts.

small and flattened (Fig. 4*A, a* and *b*). Comparison between the volume of the control and test recombinants showed that the test samples were significantly larger ($P < 0.01$, Student's t test). The histologic appearance of the BPH-1 + NPF$^{\text{C7-cyclin D1}}$ grafts, as assessed by H&E staining, resembled a poorly differentiated carcinoma with areas of squamous differentiation (Fig. 4*B, a* and *b*). Instead of forming solid cord structures, some epithelium fused to form large nests with keratinization and a broad pushing margin against the host kidney (Fig. 4*B, a* and *b*). Tumors also contained irregular epithelial cords intermingled within a fibrous stroma [Fig. 4*B, e* and *f* (*right arrow*)]. In other areas, single epithelial cells were intermixed with fibrous stroma [Fig. 4*B, c* (*arrow*) and *f* (*left arrow*)]. SV40 T-antigen staining confirmed the origin of the epithelial component of the tumors as being from the BPH-1 cells (Fig. 4*B, c* and *f*). E-cadherin expression was patchy, with positive expression in cell-cell junctions in some areas but weak or absent in many areas (Fig. 4*B, d*). The histology of recombinants of BPH-1 + NPF$^{\text{cyclin D1}}$ was similar to that previously described for BPH-1 + CAF recombinants (8, 30), although the overall tumor size was smaller. After 5 months of incubation in the kidney capsule, BPH-1 cells formed larger tumors with clear kidney invasion (Fig. 4*B, g* and *i*). Small kidney tubes intermingled with tumor cells [Fig. 4*B, g* (*arrows*) and *h* (*arrow*)] and there were no clear margins between the kidney and grafts.

In contrast to the malignant histologic appearance of the BPH-1 + NPF$^{\text{cyclin D1}}$ recombinants, the BPH-1 + NPF recombinants appeared benign and, as described previously, the bulk of the grafts were composed of stromal cells. Occasional small epithelial cords were found (Fig. 4*B, k* and *l*). This confirmed previous observations that stromal cells from normal peripheral zone recombined with BPH-1 cells produced benign or no visible grafts (8, 30).

To examine if NPF$^{\text{cyclin D1}}$ cells are tumorigenic, we grafted either NPF or NPF$^{\text{cyclin D1}}$ cells alone to SCID mice. Both control groups formed flattened grafts (Fig. 4*A, c* and *d, arrows*). H&E staining showed that both grafts were present as a thin layer of fibrous tissue (data not shown).

Epithelial cells isolated from BPH-1 + NPF$^{\text{cyclin D1}}$ grafts (BPH-1$^{\text{NPF-cyclin D1}}$) are tumorigenic. After cell culture and G418 selection, two cell strains were derived from BPH-1 + NPF and BPH-1 + NPF$^{\text{cyclin D1}}$ grafts, designated BPH-1$^{\text{NPF}}$ and BPH-1$^{\text{NPF-cyclin D1}}$. The two strains were grafted in collagen gels beneath the renal capsule of male SCID mice. Grossly, after 3 months, the BPH-1$^{\text{NPF-cyclin D1}}$ cells formed significantly larger grafts than the control group (Fig. 5*A, right*). The control group formed small flattened grafts (Fig. 5*A, left*). Histologically, the BPH-1$^{\text{NPF}}$ cells grew to form occasional small cords, which were SV40 positive, similar to the grafts reported previously for BPH-1 cells grafted alone (Fig. 5*B*). The BPH-1$^{\text{NPF-cyclin D1}}$ cells, in contrast, formed large fused nests generally with a broad pushing margin to the host kidney (Fig. 5*C, a, arrow*). Many smaller nests with irregular shapes were scattered throughout the tumor and intermingled with

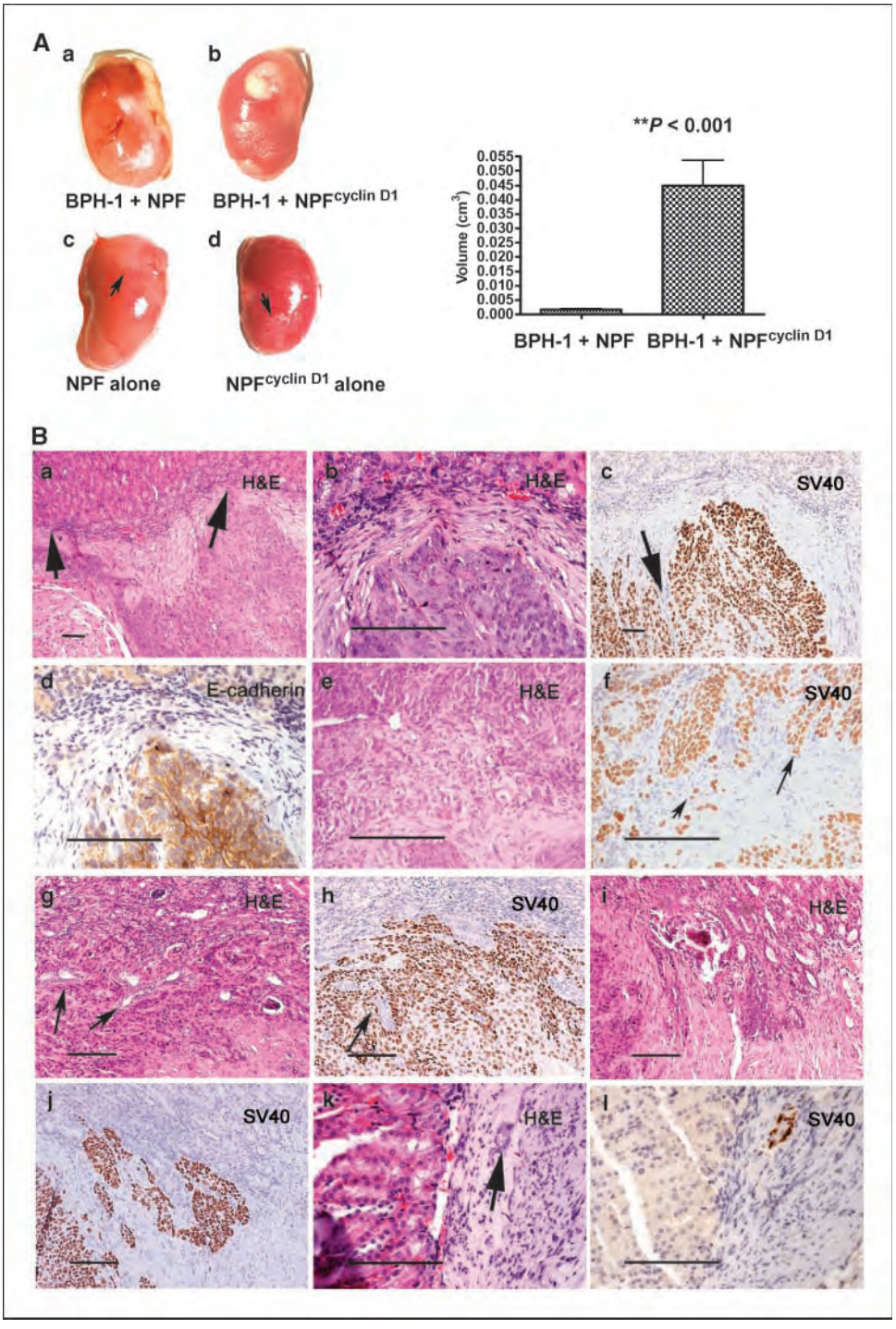

Figure 4. Effects of NPF$^{\text{cyclin D1}}$ cells on BPH-1 epithelium *in vivo. A,* gross morphology of 1-month grafts of tissue recombinants composed of BPH-1 + NPF (*a*), BPH-1 + NPF$^{\text{cyclin D1}}$ cells (*b*), NPF alone (*c*), and NPF$^{\text{cyclin D1}}$ alone (*d*). The graft volume of BPH-1 + NPF$^{\text{cyclin D1}}$ was significantly larger than that of BPH-1 + NPF. $P < 0.001$, Student's *t* test (*right*). *B,* staining of BPH-1 + NPF$^{\text{cyclin D1}}$ recombinants revealed organization resembling a poorly differentiated carcinoma. Some epithelium fused to form large nests (*a* and *b*) with keratinization and a broad pushing margin to kidney (*a, arrow*). Tumors contained irregular epithelial cords and epithelial cells intermingled within a fibrous stroma [*c, e*, and *f* (*right arrow*)]. Single epithelial cells were intermixed with fibrous stroma in other areas [*c* (*arrow*) and *f* (*left arrow*)]. Immunohistochemical localization of SV40 T antigen confirmed the origin of the tumors (*c* and *f*). E-cadherin staining was patchy (*d*). After 5 mo of incubation in kidney capsule, BPH-1 cells formed larger tumors and invaded the host kidney (*g–j*). Tumor cells surrounded and intermingled with kidney tubes [*g* and *h* (*arrow*)]. There were no clear margins between kidney and grafts. H&E staining of BPH-1 + NPF grafts revealed small grafts with minimal epithelial growth consistent with previous observations [*k* (*arrow*) and *l*]. *Bar*, 50 μm.

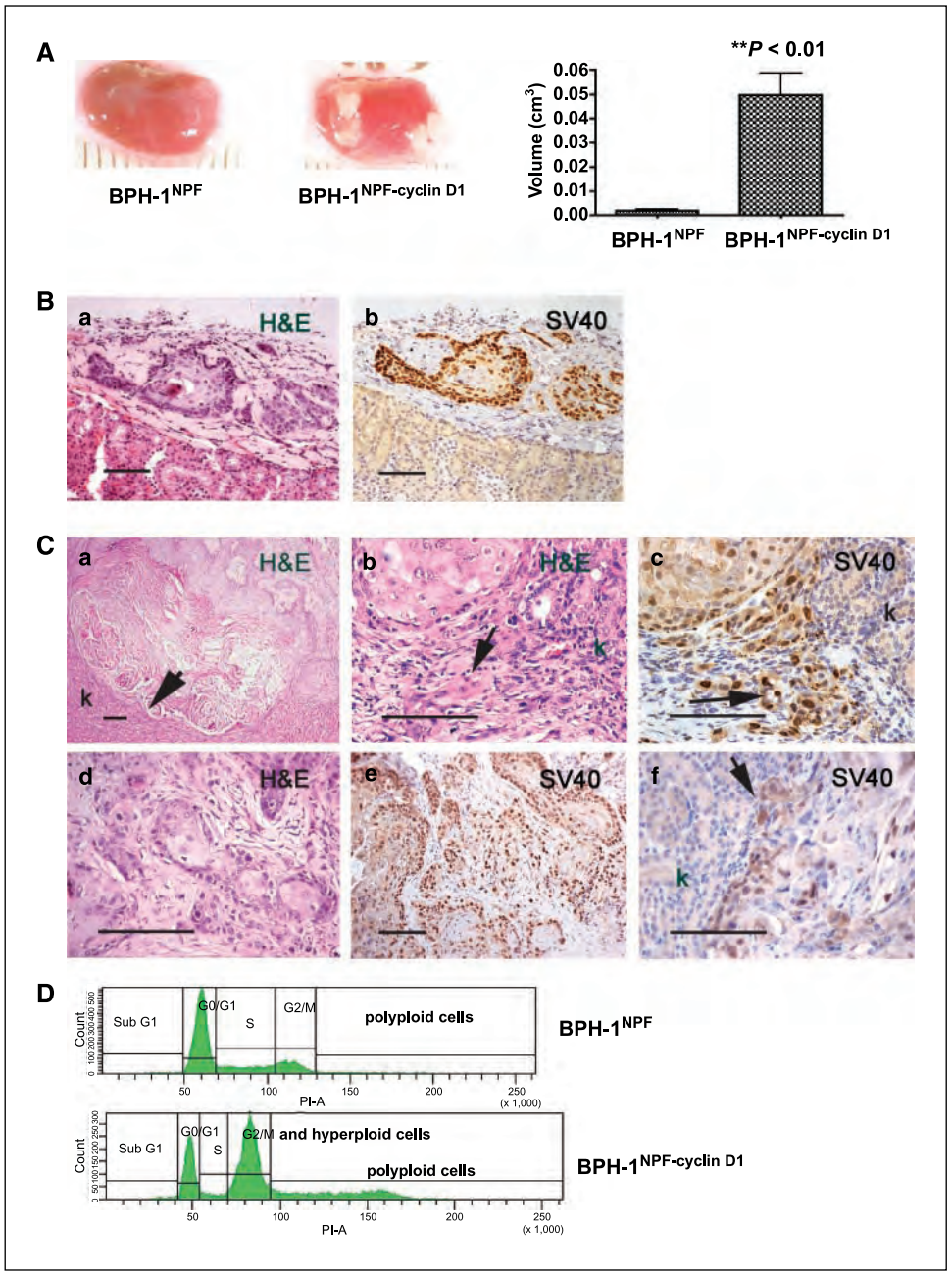

Figure 5. The BPH-1$^{\text{NPF-cyclin D1}}$ cells, which were isolated from BPH-1 + NPF$^{\text{cyclin D1}}$ grafts, exhibited a transformed phenotype. *A,* gross morphology of 3-month grafts of BPH-1$^{\text{NPF}}$ (*left*) and BPH-1$^{\text{NPF-cyclin D1}}$ (*right*). The volume of the BPH-1$^{\text{NPF-cyclin D1}}$ grafts was significantly larger than the control grafts. $P < 0.01$, Student's *t* test. *B,* in grafts of BPH-1$^{\text{NPF}}$ cells, occasionally, epithelial cords were seen (*a*) and their origin was confirmed by SV40 staining (*b*). No evidence of malignant growth or invasion was seen in these grafts. *Bar*, 50 μm. *C,* BPH-1$^{\text{NPF-cyclin D1}}$ tumors were larger than controls with areas of keratinization (*a*). The grafts formed a pushing margin directly touching the host kidney (*a, arrow*). Small nests of epithelial cells with irregular shapes intermingled with stroma (*d* and *e*). Some infiltrative areas (*b, arrow*) were found to be composed of bubbly cytoplasm and indistinct cells borders (*c, arrow*). Minimally invasive growth into the kidney was seen in a few areas. The invading cells expressed SV40 T antigen (*f, arrow*). *Bar*, 50 μm. *D,* fluorescence-activated cell sorting analysis showed striking differences in cell population distribution between BPH-1$^{\text{NPF}}$ and BPH-1$^{\text{NPF-cyclin D1}}$ cells. The majority (64%) of the BPH-1$^{\text{NPF}}$ cells were in the G_1-G_0 phase of cell cycle. In contrast, in BPH-1$^{\text{NPF-cyclin D1}}$ cells, an abnormal peak that contains 55% of the total cell population is located close to but somewhat below where the G_2-M peak would be expected. Additionally, polyploid cells are composed of 23.1% of the total population in the BPH-1$^{\text{NPF-cyclin D1}}$ cells.

stroma (Fig. 5*C, d* and *e*). Some infiltrative areas recapitulated prostatic carcinoma (Fig. 5*C, b, arrow*). Cells contained a foamy cytoplasm and their borders were indistinct (Fig. 5*C, c, arrow*). Minimally invasive growth was found in some areas (Fig. 5*C, f*). Tumors continued to express SV40 T-antigen confirming the BPH-1 origin of the malignant epithelium.

DNA flow cytometry analysis showed that stromal cyclin D1 caused a shift of the cell cycle distribution of BPH-1$^{\text{NPF-cyclin D1}}$ cells. An abnormal wider peak that contains 55% of the cell population is located close to where the G_2-M peak (which has twice the normal copies of DNA) is supposed to be, but its position is below the G_2-M peak position. It was reported that a wide peak may represent two populations of cells with different quantities of DNA (31). Given that the original BPH-1 population has been described previously to have an abnormal chromosomal make up and further that this can be altered by exposure to cancer stroma, it is possible that BPH-1$^{\text{NPF-cyclin D1}}$ cells became hyperdiploid or nearly tetraploid, and the hyperdiploid cell population mixed with the tetraploid G_2-M population to produce this abnormal peak. A large proportion (23.1%) of BPH-1$^{\text{NPF-cyclin D1}}$ cells also appear to be polyploid with varying but high DNA content. In marked contrast, only 0.9% of BPH-1$^{\text{NPF}}$ cells were found to be polyploid and BPH-1$^{\text{NPF}}$ cells showed a normal distribution of cell populations with 64% cells in the G_1 phase of cell cycle. (Fig. 5*D*).

Gene expression profiles were highly concordant between CAFs and NPF$^{\text{cyclin D1}}$ cells. The gene expression patterns of NPFs, CAFs, and NPF$^{\text{cyclin D1}}$ cells were compared by cDNA microarray analysis (Gene Expression Omnibus submission GSE6936; National Center for Biotechnology Information tracking system 15248638). NPF$^{\text{cyclin D1}}$ cells and CAFs showed a high level of gene expression

correlations when compared with NPFs (Pearson $r = 0.65$ across all 5,652 clones returning data in all four samples.) A one-sample t test in SAM identified 118 unique genes up-regulated and 51 unique genes down-regulated ($q \leq 0.1\%$) commonly expressed between $NPF^{cyclin\ D1}$ cells and CAFs when compared with NPFs. (Supplementary Figs. S2 and S3). Relatively few significant differences in transcript abundance measurements between $NPF^{cyclin\ D1}$ cells and CAFs were identified: a two-sample t test in SAM identified 6 unique genes up-regulated and 20 unique genes down-regulated ($q \leq 10\%$) in CAFs when compared with cyclin D1–overexpressing fibroblasts (Supplementary Fig. S4).

Discussion

The concept of stroma as a contributor to, and potentially an initiator of, carcinogenesis have led to altered perceptions of the development and progression of epithelial malignancies. Histopathologic examination has shown clear differences in gene expression patterns between the reactive stroma of tumors and normal stroma; additionally, these differences have clinical prognostic value (32–34). The importance of stromal-epithelial interactions in tumorigenesis has been shown in many malignancies, including, carcinoma of the skin, colon, breast, and prostate (35–38). Not only stromal-epithelial interactions play an important role in normal development and adult growth quiescence of the prostate (39) but also changes in these interactions can promote a malignant progression of initiated epithelium and result in tumorigenesis (2, 4, 32, 40, 41).

There are cases in which addition of a single dominant-acting oncogene is sufficient to transform a nontumorigenic cell. For example, massive overexpression of c-*myc* converted normal prostatic epithelial cells to rapidly become an invasive prostate carcinoma cell (25), whereas lower levels of c-myc expression had similar but slower effects (42). Similarly loss of genes with tumor suppressor function can also contribute to malignancy (43). These observations emphasize the importance of genetic changes as key factors in malignancy. Alterations in the microenvironment adjacent to the epithelial cells can drive nontumorigenic cells to become malignant both *in vivo* and *in vitro* (8, 44, 45). Stromal factors can also elicit reversion of a malignant teratocarcinoma to a benign phenotype despite genetic changes within the epithelial cells (46–48). The growth and differentiation of epithelial cells from R3327 Dunning prostatic adenocarcinoma (DT) were modified when reassociated with normal stromal environment. The epithelial cells were induced to differentiate to tall columnar secretory epithelial cells and tumorigenesis was remarkably diminished (48, 49). Experiments in mice suggested that genetic inactivation of the stromal transforming growth factor-β receptor II resulted in the transformation of normal epithelial cells (50). Bissell's group showed that by manipulating ECM proteins, human breast cancer cells reverted to normal functional cells in culture and tumorigenicity was reduced dramatically in mice (51).

Cyclin D1 is an important oncogene in many human cancers, but its function in prostate cancer is not clear (21, 52–55). We show here that cyclin D1 is up-regulated in prostate cancer cell lines, indicating that it might be associated with prostate tumorigenicity. Overexpression of cyclin D1 can increase tumorigenicity of LNCaP cell lines (21). We have observed that BPH-1 cells, in which cyclin D1 was overexpressed, did not become tumorigenic under the influence of inductive rUGM in the tissue recombination model when grafted to SCID mice. However, the cyclin D1–overexpressing cells did have a higher proliferation rate *in vitro* and *in vivo* and motility *in vitro*. Such observations indicated that this single gene is not enough to transform BPH-1 cells even in the face of SV40 large T antigen, which is expressed in these cells. This underlines the important point that increased proliferation per se is insufficient for malignant transformation.

In marked contrast to the effects in epithelial cells, overexpression of cyclin D1 in primary cultures of benign human prostatic fibroblasts extended the life span and altered the behavior of the stromal cells, nonetheless falling short of directly inducing malignant transformation. Cyclin D1 induced these cells to behave in a manner similar to CAFs, imparting an ability to elicit malignant transformation in BPH-1 epithelial cells in a tissue recombination model. The cyclin D1–overexpressing fibroblasts have increased life span compared with NPFs. NPFs were all dead within 12 passages. However, the $NPF^{cyclin\ D1}$ cells seemed healthy after an additional 11 passages. NPFs overexpressing cyclin D1 may be selectively advantageous for the proliferation and survival characteristics often associated with oncogenesis compared with noninfected cells in the same mixture. However, it should be noted that, as when expressed in epithelial cells, expression of cyclin D1 did not result in transformation of the stromal cell population. As a result of *in vitro* adaptation, cells may pick up generic alterations such as the mRNA changes we have seen in microarray data. However, $NPF^{cyclin\ D1}$ cells are not fully immortal and are not tumorigenic by themselves. This is consistent with observations that CAFs are also not immortal and not tumorigenic per se but have the ability to transform adjacent BPH-1 cells.

By expressing cyclin D1 in stromal cells, we showed that benign stromal cell behavior can be modified to mimic that of cancer stromal cells. $NPF^{cyclin\ D1}$ cells have a potential to transform BPH-1 cells similar to that seen with CAFs although with a reduced intensity. Tissue architecture in recombinants showed irregular epithelial cords and epithelium infiltrating into the stroma. This observation indicated that the presence of altered stromal cells in proximity to an initiated epithelium has an important biological effect on prostatic carcinogenesis. Expression of this single oncogene in the stroma may mimic the effects of CAFs on epithelium by modifying the local microenvironment. Specifically altering the expression of growth factors and ECM proteinases results in expansion and malignant progression of the initiated epithelial cells.

BPH-1 cells form tumors after recombination with CAFs and epithelial cells derived from these tumors ($BPH\text{-}1^{CAFTD}$) are tumorigenic without the stimulation of stromal cells when regrafted to mice (23). The present study shows that the tumorigenic behavior of $BPH\text{-}1^{NPF\text{-}cyclin\ D1}$ cells (derived from recombination of BPH-1 + $NPF^{cyclin\ D1}$ cells) also resulted in a permanent malignant transformation of epithelial cells similar to that seen with CAF.

Cell cycle analyses of cells from malignant tissues have shown the presence of aneuploid cells as well as normal diploid cells (56). In the present study, an abnormal peak in cell cycle histogram of $BPH\text{-}1^{NPF\text{-}cyclin\ D1}$ likely represented hyperdiploid cells. Many of these cells had multiple nuclei. It has been shown that aneuploidy is the possible underlying mechanism and potential consequences in the pathogenesis of human lung cancer (57). Clinical progression of prostate cancer is also associated with formation of DNA aneuploidy (58). These data suggested that $BPH\text{-}1^{NPF\text{-}cyclin\ D1}$ cells might be transformed through chromosomal changes (aneuploidy).

The histologic appearance of $BPH\text{-}1^{NPF\text{-}cyclin\ D1}$ tumors was consistent with poorly differentiated carcinoma. It is important to

note that CAFs have elevated expression levels of cyclin D1 protein; therefore, many of their characteristics could be linked to the downstream consequences of this change. Microarray comparison of the $NPF^{cyclin\ D1}$ and CAFs versus NPF showed highly concordant gene expression profiles. The same 118 unique genes were up-regulated and 51 unique genes were down-regulated in $NPF^{cyclin\ D1}$ cells and CAFs when compared with NPFs. Relatively few significant differences in transcript abundance measurements between $NPF^{cyclin\ D1}$ cells and CAFs were identified. These data indicate that cyclin D1 expression in stroma can critically affect paracrine interactions with adjacent epithelial cells in a manner resembling CAFs.

In summary, the present study showed for the first time the importance of cyclin D1 as a potential regulator of paracrine interactions in prostate cancer progression. The cyclin D1–overexpressing fibroblasts have an increased life span and share many commonalities with CAFs making them a potentially useful research tool. Traditional therapy for all epithelial malignancies, including prostate cancer, has been targeted at the epithelial cells that progressively acquire genetic changes. The stroma may provide a more stable target at which to direct treatment because the gene expression profile differs from that seen in normal tissues. We should also bear in mind that the tumor stromal compartment is heterogeneous and that CAFs are a mixed population of fibroblastic cells. Juxtacrine signaling between fibroblastic cells of different types may contribute to changes in overall paracrine signaling, which boosts the growth of epithelial cells. Interactions with other stromal cell types, including inflammatory cells or nerve cells, also turn out to be of critical importance. A better understanding of these complex interactions within the stroma and between stroma and epithelium, and the manner in which these are influenced by gene expression in stromal cells will allow for the rational design of therapies aimed at inhibiting prostate tumor growth.

Acknowledgments

Received 2/5/2007; revised 5/3/2007; accepted 6/12/2007.

Grant support: The taxpayers of the United States via NIH and Department of Defense-Prostate Cancer Research Program (DOD-PCRP) grants CA96403 and U54CA126505-01 (S.W. Hayward) and PC041158 and U54CA126540-01 (P.S. Nelson) and DOD-PCRP predoctoral fellowship W81XWH-07-1-0139 (Y. He). The Vanderbilt University Medical Center Institutional Flow Cytometry Core was supported by the Vanderbilt Ingram Cancer Center grant P30CA68485.

The costs of publication of this article were defrayed in part by the payment of page charges. This article must therefore be hereby marked *advertisement* in accordance with 18 U.S.C. Section 1734 solely to indicate this fact.

We thank the Frances Williams Preston Laboratories of the TJ Martell Foundation for their generous support.

References

1. Cunha GR, Alarid ET, Turner T, Donjacour AA, Boutin EL, Foster BA. Normal and abnormal development of the male urogenital tract: role of androgens, mesenchymal-epithelial interactions, and growth factors. J Androl 1992;13:465–75.
2. Hayward SW, Haughney PC, Rosen MA, et al. Interactions between adult human prostatic epithelium and rat urogenital sinus mesenchyme in a tissue recombination model. Differentiation 1998;63:131–40.
3. Hayward SW, Cunha GR. The prostate: development and physiology. Radiol Clin North Am 2000;38:1–14.
4. Grossfeld G, Hayward S, Tlsty T, Cunha G. The role of stroma in prostatic carcinogenesis. Endocr Relat Cancer 1998;5:253–70.
5. Joesting MS, Perrin S, Elenbaas B, et al. Identification of SFRP1 as a candidate mediator of stromal-to-epithelial signaling in prostate cancer. Cancer Res 2005;65:10423–30.
6. Ao M, Franco OE, Park D, Raman D, Williams K, Hayward SW. Cross talk between paracrine-acting cytokine and chemokine pathways promotes malignancy in benign human prostatic epithelium. Cancer Res 2007; 67:4244–53.
7. Chung LW. Fibroblasts are critical determinants in prostatic cancer growth and dissemination. Cancer Metastasis Rev 1991;10:263–74.
8. Olumi AF, Grossfeld GD, Hayward SW, Carroll PR, Tlsty TD, Cunha GR. Carcinoma-associated fibroblasts direct tumor progression of initiated human prostatic epithelium. Cancer Res 1999;59:5002–11.
9. Ayala GE, Dai H, Tahir SA, et al. Stromal antiapoptotic paracrine loop in perineural invasion of prostatic carcinoma. Cancer Res 2006;66:5159–64.
10. Mueller MM, Fusenig NE. Friends or foes—bipolar effects of the tumour stroma in cancer. Nat Rev Cancer 2004;4:839–49.
11. Fu M, Wang C, Li Z, Sakamaki T, Pestell RG. Minireview: cyclin D1: normal and abnormal functions. Endocrinology 2004;145:5439–47.
12. Petty WJ, Dragnev KH, Dmitrovsky E. Cyclin D1 as a target for chemoprevention. Lung Cancer 2003;41 Suppl 1:S155–61.
13. Polsky D, Cordon-Cardo C. Oncogenes in melanoma. Oncogene 2003;22:3087–91.
14. Hunter T, Pines J. Cyclins and cancer. II: cyclin D and CDK inhibitors come of age. Cell 1994;79:573–82.
15. Sherr CJ. Mammalian G_1 cyclins. Cell 1993;73: 1059–65.
16. Bartkova J, Lukas J, Strauss M, Bartek J. Cyclin D1 oncoprotein aberrantly accumulates in malignancies of diverse histogenesis. Oncogene 1995;10:775–8.
17. Roy PG, Thompson AM. Cyclin D1 and breast cancer. Breast 2006;15:718–27.
18. Day KC, McCabe MT, Zhao X, et al. Rescue of embryonic epithelium reveals that the homozygous deletion of the retinoblastoma gene confers growth factor independence and immortality but does not influence epithelial differentiation or tissue morphogenesis. J Biol Chem 2002;277:44475–84.
19. Caldon CE, Daly RJ, Sutherland RL, Musgrove EA. Cell cycle control in breast cancer cells. J Cell Biochem 2006;97:261–74.
20. Arnold A, Papanikolaou A. Cyclin D1 in breast cancer pathogenesis. J Clin Oncol 2005;23:4215–24.
21. Chen Y, Martinez LA, LaCava M, Coghlan L, Conti CJ. Increased cell growth and tumorigenicity in human prostate LNCaP cells by overexpression to cyclin D1. Oncogene 1998;16:1913–20.
22. Pera M, Fernandez PL, Palacin A, et al. Expression of cyclin D1 and p53 and its correlation with proliferative activity in the spectrum of esophageal carcinomas induced after duodenal content reflux and 2,6-dimethylnitrosomorpholine administration in rats. Carcinogenesis 2001;22:271–7.
23. Hayward SW, Wang Y, Cao M, et al. Malignant transformation in a nontumorigenic human prostatic epithelial cell line. Cancer Res 2001;61:8135–42.
24. Hayward SW, Dahiya R, Cunha GR, Bartek J, Despande N, Narayan P. Establishment and characterization of an immortalized but non-tumorigenic human prostate epithelial cell line: BPH-1. In Vitro 1995;31A: 14–24.
25. Williams K, Fernandez S, Stien X, et al. Unopposed c-MYC expression in benign prostatic epithelium causes a cancer phenotype. Prostate 2005;63:369–84.
26. Hayward SW, Haughney PC, Lopes ES, Danielpour D, Cunha GR. The rat prostatic epithelial cell line NRP-152 can differentiate *in vivo* in response to its stromal environment. Prostate 1999;39:205–12.
27. Dalrymple S, Antony L, Xu Y, et al. Role of notch-1 and E-cadherin in the differential response to calcium in culturing normal versus malignant prostate cells. Cancer Res 2005;65:9269–79.
28. True L, Coleman I, Hawley S, et al. A molecular correlate to the Gleason grading system for prostate adenocarcinoma. Proc Natl Acad Sci U S A 2006;103: 10991–6.
29. Yasunaga Y, Nakamura K, Ewing CM, Isaacs WB, Hukku B, Rhim JS. A novel human cell culture model for the study of familial prostate cancer. Cancer Res 2001; 61:5969–73.
30. Barclay WW, Woodruff RD, Hall MC, Cramer SD. A system for studying epithelial-stromal interactions reveals distinct inductive abilities of stromal cells from benign prostatic hyperplasia and prostate cancer. Endocrinology 2005;146:13–8.
31. Seidman JD, Berman JJ, Moore GW, Yetter RA. Multiparameter DNA flow cytometry of keratoacanthoma. Anal Quant Cytol Histol 1992;14:113–9.
32. Tuxhorn JA, Ayala GE, Smith MJ, Smith VC, Dang TD, Rowley DR. Reactive stroma in human prostate cancer: induction of myofibroblast phenotype and extracellular matrix remodeling. Clin Cancer Res 2002;8:2912–23.
33. Bosman FT, de Bruine A, Flohil C, van der Wurff A, ten Kate J, Dinjens WW. Epithelial-stromal interactions in colon cancer. Int J Dev Biol 1993;37:203–11.
34. Seljelid R, Jozefowski S, Sveinbjornsson B. Tumor stroma. Anticancer Res 1999;19:4809–22.
35. De Cosse J, Gossens CL, Kuzma JF. Breast cancer: induction of differentiation by embryonic tissue. Science 1973;181:1057–8.
36. Fukamachi H, Mizuno T, Kim YS. Morphogenesis of human colon cancer cells with fetal rat mesenchymes in organ culture. Experientia 1986;42:312–5.
37. Singer C, Rasmussen A, Smith HS, Lippman ME, Lynch HT, Cullen KJ. Malignant breast epithelium selects for insulin-like growth factor II expression in breast stroma: evidence for paracrine function. Cancer Res 1995;55:2448–54.
38. Wright JH, McDonnell S, Portella G, Bowden GT, Balmain A, Matrisian LM. A switch from stromal to tumor cell expression of stromelysin-1 mRNA associated with the conversion of squamous to spindle carcinomas during mouse skin tumor progression. Mol Carcinog 1994;10:207–15.
39. Cunha GR, Ricke W, Thomson A, et al. Hormonal,

cellular, and molecular regulation of normal and neoplastic prostatic development. J Steroid Biochem Mol Biol 2004;92:221–36.
40. Hayward SW, Olumi AF, Haughney PC, Dahiya R, Cunha GR. Prostate adenocarcinoma causes dedifferentiation of its surrounding smooth muscle. Proc Am Urol Assoc 1996;155:605A.
41. Hayward SW, Rosen MA, Cunha GR. Stromal-epithelial interactions in normal and neoplastic prostate. Br J Urol 1997;79 Suppl 2:18–26.
42. Ellwood-Yen K, Graeber TG, Wongvipat J, et al. Myc-driven murine prostate cancer shares molecular features with human prostate tumors. Cancer Cell 2003;4:223–38.
43. Wang S, Gao J, Lei Q, et al. Prostate-specific deletion of the murine Pten tumor suppressor gene leads to metastatic prostate cancer. Cancer Cell 2003;4:209–21.
44. Hayward SW, Wang Y, Cao M, et al. Malignant transformation in a non-tumorigenic human prostatic epithelial cell line. Cancer Res 2001;61:8135–42.
45. Maffini MV, Soto AM, Calabro JM, Ucci AA, Sonnenschein C. The stroma as a crucial target in rat mammary gland carcinogenesis. J Cell Sci 2004;117:1495–502.
46. Pierce G. The benign cells of malignant tumors. In: King T, editor. Developmental aspects of carcinogenesis and immunity. New York: Academic Press, Inc.; 1974. p. 3–22.
47. Mintz B. Genetic mosaicism and *in vivo* analyses of neoplasia and differentiation. In: Saunders G, editor. Cell differentiation and neoplasia. New York: Raven Press; 1978. p. 27–56.
48. Hayashi N, Cunha GR. Mesenchyme-induced changes in neoplastic characteristics of the Dunning prostatic adenocarcinoma. Cancer Res 1991;51:4924–30.
49. Hayashi N, Cunha GR, Wong YC. Influence of male genital tract mesenchymes on differentiation of Dunning prostatic adenocarcinoma. Cancer Res 1990;50:4747–54.
50. Bhowmick NA, Chytil A, Plieth D, et al. TGF-β signaling in fibroblasts modulates the oncogenic potential of adjacent epithelia. Science 2004;303:848–51.
51. Weaver VM, Petersen OW, Wang F, et al. Reversion of the malignant phenotype of human breast cells in three-dimensional culture and *in vivo* by integrin blocking antibodies. J Cell Biol 1997;137:231–45.
52. Kallakury BV, Sheehan CE, Ambros RA, Fisher HA, Kaufman RP, Jr., Ross JS. The prognostic significance of p34cdc2 and cyclin D1 protein expression in prostate adenocarcinoma. Cancer 1997;80:753–63.
53. Bubendorf L, Kononen J, Koivisto P, et al. Survey of gene amplifications during prostate cancer progression by high-throughout fluorescence *in situ* hybridization on tissue microarrays. Cancer Res 1999;59:803–6.
54. Gumbiner LM, Gumerlock PH, Mack PC, et al. Overexpression of cyclin D1 is rare in human prostate carcinoma. Prostate 1999;38:40–5.
55. Han EK, Lim JT, Arber N, Rubin MA, Xing WQ, Weinstein IB. Cyclin D1 expression in human prostate carcinoma cell lines and primary tumors. Prostate 1998;35:95–101.
56. Givan AL. Cells from within: DNA in life and death. In: Flow Cytometry: First Principles (Second Edition). New York: Wiley-Liss, Inc.; 2001. p. 123–58.
57. Masuda A, Takahashi T. Chromosome instability in human lung cancers: possible underlying mechanisms and potential consequences in the pathogenesis. Oncogene 2002;21:6884–97.
58. Koivisto P. Aneuploidy and rapid cell proliferation in recurrent prostate cancers with androgen receptor gene amplification. Prostate Cancer Prostatic Dis 1997;1:21–5.